

State-of-the-Art Infrared Applications in Drugs, Dietary Supplements, and Nutraceuticals

Lead Guest Editor: Alessandra Durazzo

Guest Editors: Massimo Lucarini, Johannes Kiefer, and Sarfaraz Ahmed Mahesar





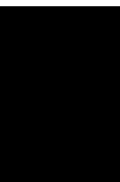
**State-of-the-Art Infrared Applications
in Drugs, Dietary Supplements, and
Nutraceuticals**

Journal of Spectroscopy

**State-of-the-Art Infrared Applications
in Drugs, Dietary Supplements, and
Nutraceuticals**

Lead Guest Editor: Alessandra Durazzo

Guest Editors: Massimo Lucarini, Johannes Kiefer, and
Sarfaraz Ahmed Mahesar



Copyright © 2020 Hindawi Limited. All rights reserved.

This is a special issue published in "Journal of Spectroscopy." All articles are open access articles distributed under the Creative Commons Attribution License, which permits unrestricted use, distribution, and reproduction in any medium, provided the original work is properly cited.





Editorial Board

Khaliq Ahmed, USA
Wagner A. Alves, Brazil
Hakan Arslan, Turkey
Luciano Bachmann, Brazil
Mark Baker, United Kingdom
Malgorzata Baranska, Poland
Dhananjay Bodas, India
Damien Boyer, France
Jose S. Camara, Portugal
Elizabeth A. Carter, Australia
Wee Chew, Singapore
Jau-Wern Chiou, Taiwan
Stephen Cooke, USA
Daniel Cozzolino, Australia
Vincenza Crupi, Italy
Arnaud Cuisset, France
Eugen Culea, Romania
Alessandro De Giacomo, Italy
Renata Diniz, Brazil
Ana Dominguez-Vidal, Spain
Alessandra Durazzo, Italy
Michele Fedel, Italy
Hicham Fenniri, Canada
Nives Galic#, Croatia
Javier Garcia-Guinea, Spain
Andras Gorzsas, Sweden
Tino Hofmann, USA
Rodolphe Jaffiol, France
Christopher K. Jankowski, Canada
Rizwan Hasan Khan, India
Jeongkwon Kim, Republic of Korea
K.S.V. Krishna Rao, India
Nikša Krstulović, Croatia
Violeta Lazic, Italy
Young Jong Lee, USA
Nicolae Leopold, Romania
Alessandro Longo, Italy
Massimo Lucarini, Italy
Paola Luches, Italy
Sarfraz Ahmed Mahesar, Pakistan
Petre Makreski, Macedonia
Artem E. Masunov, USA




Li-June Ming, USA
Austin Nevin, Italy
Carlos Palacio, Colombia
Jose M. Pedrosa, Spain
Simona C. Pinzaru, Romania
Piotr Przybylski, Poland
Davidson Sajan, India
Stephane Schilt, Switzerland
Feride Severcan, Turkey
Zhifeng Shao, USA
Rafal Sitko, Poland
Veronica Vaida, USA
Pedro D. Vaz, Portugal
Stéphane Viel, France
Thomas Walther, United Kingdom
Chuji Wang, USA
Maria C. Yebra-Biurrun, Spain
Guoqiang Yu, USA

Contents




State-of-the-Art Infrared Applications in Drugs, Dietary Supplements, and Nutraceuticals

Alessandra Durazzo , Massimo Lucarini , Johannes Kiefer , and Sarfaraz Ahmed Mahesar 
Editorial (2 pages), Article ID 1397275, Volume 2020 (2020)




Application of Infrared Spectroscopy for Functional Compounds Evaluation in Olive Oil: A Current Snapshot

Sarfaraz Ahmed Mahesar , Massimo Lucarini, Alessandra Durazzo , Antonello Santini, Anja I. Lampe, and Johannes Kiefer 
Review Article (11 pages), Article ID 5319024, Volume 2019 (2019)




Rapid Recognition of Geothermalism and Authenticity of a Chinese Herb by Data Fusion of Near-Infrared Spectroscopy (NIR) and Mid-Infrared (MIR) Spectroscopy Combined with Chemometrics

Haiyan Fu, Qiong Shi , Liuna Wei, Lu Xu , Xiaoming Guo, Ou Hu, Wei Lan, Shunping Xie, and Tianming Yang 
Research Article (9 pages), Article ID 2467185, Volume 2019 (2019)



Real-Time Release Testing of Herbal Extract Powder by Near-Infrared Spectroscopy considering the Uncertainty around Specification Limits

Guolin Shi , Bing Xu , Xin Wang, Zhong Xue, Xinyuan Shi, and Yanjiang Qiao 
Research Article (10 pages), Article ID 4139762, Volume 2019 (2019)




FT-IR Spectroscopy Applied for Identification of a Mineral Drug Substance in Drug Products: Application to Bentonite

H. Ouhaddouch , A. Cheikh , M. O. B. Idrissi, M. Draoui, and M. Bouatia 
Research Article (6 pages), Article ID 2960845, Volume 2019 (2019)

Photoacoustic Spectroscopy in the Optical Characterization of Foodstuff: A Review

Claudia Hernández-Aguilar , Arturo Domínguez-Pacheco, Alfredo Cruz-Orea , and Rumen Ivanov
Review Article (34 pages), Article ID 5920948, Volume 2019 (2019)

The Quality Control of Tea by Near-Infrared Reflectance (NIR) Spectroscopy and Chemometrics

Ming-Zhi Zhu , Beibei Wen, Hao Wu, Juan Li, Haiyan Lin, Qin Li, Yinhua Li, Jianan Huang , and Zhonghua Liu 
Review Article (11 pages), Article ID 8129648, Volume 2019 (2019)

Editorial

State-of-the-Art Infrared Applications in Drugs, Dietary Supplements, and Nutraceuticals

Alessandra Durazzo ¹, **Massimo Lucarini** ¹, **Johannes Kiefer** ²,
and Sarfaraz Ahmed Mahesar ³

¹CREA-Research Centre for Food and Nutrition, Via Ardeatina 546, Rome 00178, Italy

²Technische Thermodynamik, Universität Bremen, Badgasteiner Str. 1, Bremen 28359, Germany

³National Centre of Excellence in Analytical Chemistry, University of Sindh, Jamshoro-76080, Pakistan

Correspondence should be addressed to Alessandra Durazzo; alessandra.durazzo@crea.gov.it

Received 7 July 2019; Accepted 9 July 2019; Published 3 February 2020

Copyright © 2020 Alessandra Durazzo et al. This is an open access article distributed under the Creative Commons Attribution License, which permits unrestricted use, distribution, and reproduction in any medium, provided the original work is properly cited.

Infrared spectroscopy, including near-infrared (NIR) and mid-infrared (MIR), is an example of a green, fast, and environment-friendly technique. It is considered as an innovative and rapid analytical method for “fingerprinting” of organic compounds.

Over the past few decades, the application of this technique has opened up for new directions in analytical science and technology. Its use in combination with chemometrics led to new approaches in quality control and assurance, safety, and traceability as well as tackling challenges for analyzing innovative and established model systems in their totality.

This special issue aims at providing an overview of the latest developments in the field of mid- and near-infrared spectroscopy using ATR and transmission modes. A particular focus lies on applications in the design and development of new drugs, dietary supplements, botanicals, and nutraceuticals as well as in process development for production and quality assurance and in potential uses for labelling.

All articles, which are part of this special issue, reflect modern trends and outline new ideas for future applications of spectroscopic technologies combined with chemometric data analysis in the food and pharmaceutical sectors.

The special issue contains three review articles and three regular papers. The paper of M. Zhu et al. reviews the quality control of tea by near-infrared (NIR) reflectance spectroscopy

and chemometrics. Tea is one of the most popular beverages around the world. The wide variety of tea quality, however, calls for measures of control quality for commercialized tea products. NIR reflectance spectroscopy is a rapid, noninvasive, and nondestructive tool that required minimal sample preparation. The article gives an overview of recent advances and applications in this field. The review by C. Hernández-Aguilar et al. addresses the application of the photoacoustic spectroscopy (PAS) to evaluate of the quality of food. The PAS technique is based upon photothermal phenomena, which allow spectroscopic studies. An overview is given on PAS applications in the food industry, for example, to analyse fruit, vegetables, condiments, grains, milk, water, eggs, and so on. It was concluded that the method is capable of detecting adulteration and contamination of food samples. The third review article by S.A. Mahesar et al. is concerned with the applications of NIR and MIR spectroscopic techniques to olive oils. A special focus of the paper is the detection and determination of functional compounds such as fatty acids and phenols. It is demonstrated that MIR spectroscopy is particularly well suited to distinguish olive oils from potential adulterants. The contributed regular papers demonstrate cutting-edge advancements of the field. G. Shi et al. described real-time release testing of herbal extract powder by near-infrared spectroscopy considering the uncertainty around specification limits. For two active pharmaceutical ingredients (APIs), they show that the reliable concentration ranges covering the specification limits can be verified by the accuracy

profile (AP) methodology. The method was tested in the estimation of the β -content and γ -confidence tolerance intervals (β -CTIs) around the specification limits. H. Ouhadouch et al. applied FT-IR spectroscopy for the identification of a mineral drug substance in drug products using a case study on bentonite. For this purpose, they carefully characterized purified bentonite, bentonite in organic mixtures and organic excipients, and mineralized organic mixtures containing bentonite. They observed distinct changes and variations in the spectra, which could be attributed to the properties of the samples. H. Fu et al. reported the use of an NIR-MIR data fusion technique and evaluated the spectra via a moving window partial least-squares discriminant analysis for authenticity and adulteration discrimination of herbs. They concluded that their approach is a promising tool for the rapid discrimination of geoherbalism and authenticity of Chinese herbs. We hope that the readers will find this special issue interesting and inspiring.

Conflicts of Interest

The editors declare no conflicts of interest.




Acknowledgments

We would like to thank the authors and the reviewers of the publications in this special issue for their invaluable contribution and effort. We are also grateful to the editorial board members and support staff of the journal for their kind support during the preparation of this special issue.

*Alessandra Durazzo
Massimo Lucarini
Johannes Kiefer
Sarfaraz Ahmed Mahesar*

Review Article

Application of Infrared Spectroscopy for Functional Compounds Evaluation in Olive Oil: A Current Snapshot

Sarfaraz Ahmed Mahesar ¹, Massimo Lucarini,² Alessandra Durazzo ²,
Antonello Santini,³ Anja I. Lampe,⁴ and Johannes Kiefer ⁴

¹National Centre of Excellence in Analytical Chemistry, University of Sindh, Jamshoro-76080, Pakistan

²CREA-Research Centre for Food and Nutrition, Via Ardeatina 546, Rome 00178, Italy

³Department of Pharmacy, University of Napoli Federico II, Via D. Montesano 49, 80131 Napoli, Italy

⁴Technische Thermodynamik, Universität Bremen, Badgasteiner Str. 1, 28359 Bremen, Germany

Correspondence should be addressed to Sarfaraz Ahmed Mahesar; sarfaraz.mahesar@usindh.edu.pk

Received 29 April 2019; Accepted 27 June 2019; Published 17 July 2019

Academic Editor: Jose S. Camara

Copyright © 2019 Sarfaraz Ahmed Mahesar et al. This is an open access article distributed under the Creative Commons Attribution License, which permits unrestricted use, distribution, and reproduction in any medium, provided the original work is properly cited.

Olive oil is a liquid fat obtained from the fruit of *Olea europaea*, a plant belonging to the *Oleaceae* family, which is widely cultivated and diffused in the Mediterranean area. It is largely produced and used since antiquity. It is mainly used and consumed as food but also as key ingredient in a wide variety of cosmetic products, e.g., to moisturize and nourish dry skin. In the last few decades, olive oil has received much attention as compared to the other seed-obtained oils as well as to the animal fats due to many functional compounds with positive effects on health. To maintain the genuine picture of olive oil, it is essential to assure its authenticity and quality. The presence of bioactive compounds, which characterize the olive oil owing to their antioxidant properties, can be assessed by spectroscopic and chromatographic methods. Currently, spectroscopic techniques combined with chemometric data analysis represent one of the most promising detection methods in the food sector. They offer rapid, versatile, and inexpensive data collection and analyses. The main advantages include the limited and simple sample preparation and the possibility to get spectra directly from the production line. Infrared spectroscopy (mid- and near-infrared) coupled to chemometrics is considered as powerful, fast, accurate, and nondestructive analytical tool for rapid and precise determination of the bioactive compounds content, as well of their bioactivities, i.e., antioxidant properties. These techniques represent a valid alternative to the existing conventional methods of analysis, e.g., based on chromatography and mass spectrometry. Indeed, the present review focuses on the application of infrared spectroscopy for functional compounds evaluation in olive oil.

1. Introduction

Olive oil is a high-quality natural product, typical from the Mediterranean area, where it has been produced for millennia, and it is obtained from the fruits of *Olea europaea* L, [1–4]. The quality of the starting matrix, i.e., the olives, is a crucial parameter to obtain a high-quality product [5]. The quality can be affected, for example, by fungal occurrence and mycotoxin contamination. In particular, the contamination with microfungi capable of producing secondary metabolites (mycotoxins) that potentially affect health is a growing source of concern [6–12]. Consequently, considerable research interest towards more environmentally compatible,

field-deployable, and sustainable fungi control systems was prompted over the last couple of years [13–15].

The process of extracting the oil from the seeds is a crucial step as well. There are various methods for this purpose and they can give different yield and quality grades [16]. As an example, extra-virgin olive oil (EVOO) is obtained using mechanical pressure devices. The lower-grade products are typically obtained from a variety of extraction methods including high-pressure extraction, solvent extraction, heat treatment, esterification, and refining. The lower-grade olive oils (e.g., lampante olive oil, pomace oil, refined pomace oil, and refined olive oil) are often characterized by a comparatively high acidity. For instance,

according to the current regulations, the acidity of extra-virgin olive oil must not exceed 0.8%, while olive oil and lampante olive oil contain 2% and >2%, respectively. Refining processes lower the acidity to about 0.3%. In blends of virgin and refined olive oils the free acidity is typically about 1%. Olive pomace oil obtained by extraction with a solvent also has acidity around 1%, while the refined olive pomace oil can have an acidity of only 0.3%.

EEC Regulation 29/2012 determines the compulsory and optional information to include on olive oil labels, supplementing the general rules relating to foodstuffs and their marketing in EEC Regulation 2000/2013. The chemical composition of olive oil is characterized mainly by triacylglycerols, monoacylglycerols, diacylglycerols, and free fatty acids [17, 18], as well as fatty acid derivatives (i.e., phospholipids and waxes) [19, 20]. Moreover, there is a diverse group of compounds such as sterols, aliphatic alcohols, chlorophylls, carotenoids, and hydrocarbons [21–23]. The bioactive compounds in olive oil play an imperative role in the authentication and genuineness, quality and purity, traceability, and more importantly to the health point of view [24–33].

Olive oil is a highly interesting product from the nutraceutical perspective [34–42]. It exhibits sensory properties due to the presence of substances with functional activity, such as carotenoids, chlorophylls, tocopherols, and phenolic compounds. These substances are often missing in other common seed-based oils [43]. Moreover, olive oil is characterized by high levels of natural antioxidants, which are associated to potential beneficial properties to humans [44–49]. Phenolic compounds are the main bioactive compounds in olive oil and can be divided into lipophilic and hydrophilic phenols. As reported by El Riachy et al. [50], lipophilic phenols such as tocopherols [51] can be commonly found in other vegetable oils. On the contrary, most hydrophilic phenols found in olive oil are exclusive and/or characteristic of the *Olea europaea* species giving rise to a chemotaxonomic peculiarity [52].

A recent work by Garcia and co-workers [53] divided the phenolic compounds with biological activity into four groups: simple phenols, secoiridoid derivatives, lignans, and flavones. Oleuropein, hydroxytyrosol, tyrosol, and ligstroside are examples of specific phenols, which are usually present in olive oil. In addition, caffeic acid, vanillic acid, and syringic acid are characteristic components of olive oil [54, 55]. The phenolic composition and its total concentration in olive oil have an impact on the characteristic taste, which is bitter and pungent. It depends on different factors, mainly on the degree of ripening of the fruit, the cultivar, the geographic origin [56–61], and the processing [62, 63]. Phenolic compounds are important antioxidants and act as radical scavengers in biological systems, consequently diminishing the lipid oxidation rate [64]. Phenolic compounds are also responsible for the olive oil stability during storage because of their antioxidant activity. With reference to the tocopherols in olive oil, α -tocopherol is the major constituent while β - and γ -tocopherols are present in minor quantities [65, 66]. Figure 1 shows the chemical structure of α -tocopherol.

The greenish color of virgin olive oil is due to the presence of chlorophyll pigments. Amongst the chlorophyll

compounds, pheophytin A is found in high amounts in olive oils. On the contrary, lutein and β -carotene are the major “yellow” coloring pigments responsible for the yellowish color of virgin olive oil. Due to the antioxidant nature and pro-oxidant activity of carotenoids and chlorophylls, respectively, they both play a crucial role in the oxidative stability during storage [67]. Moreover, phenols and tocopherols, together with carotenoids, provide excellent oxidative stability to olive oils and have a synergic anticarcinogenic and antioxidant activity.

The main lipid components of olive oil are unsaturated fatty acids such as mono-(oleic) and di-glycerides (linoleic acid). Both are bioactive compounds and play a major role in human health [68]. Besides this, triterpene squalene is also considered as a functional compound in the unsaponifiable fraction of olive oil. The content of such functional compounds is contributing to or even determining the quality and positive sensory properties especially in extra-virgin olive oil.

Many instrumental analytical methods have been developed for the determination of functional compounds in olive oil, mainly using mass spectrometry and chromatography. However, most of these methods are expensive, time-consuming, nonenvironmentally friendly and also may require highly qualified staff for the instrumental analyses. On the contrary, spectroscopic methods such as ultraviolet, visible, near-infrared, and mid-infrared spectroscopy have been successfully employed as rapid, nondestructive, real-time techniques capable of on/offline monitoring of various quality parameters of olive oil. Their benefits include minimum sample preparation and good measurement accuracy with less or no waste generation. This review article presents an updated overview of the infrared spectroscopic methods in combination with chemometric data analysis to determine the functional compounds in olive oil.

2. Basics of Infrared Spectroscopy (Theory and Instrumentation)

2.1. Theoretical Principles. Infrared (IR) and near-infrared (NIR) spectroscopy are based on the absorption of photons by molecules. Absorption can take place when the energy of the photon to be absorbed matches the energy difference between two molecular rotovibrational energy levels. The mid-infrared spectral range is normally specified as 2.5–50 μm (200–4000 cm^{-1}), where the fundamental vibrational modes are located. On the contrary, the near-infrared covers the range 0.75–2.5 μm (4000 to 13333 cm^{-1}) containing overtone and combination bands. A general requirement for allowing the absorption of a photon is that an oscillating dipole moment be produced during the vibrational motion of the molecule. This prerequisite can be expressed mathematically by the following equation:

$$\left(\frac{\partial\mu}{\partial q}\right) \neq 0, \quad (1)$$

where μ is the dipole moment and q is the normal coordinate. When this equation is fulfilled, the molecule or a specific vibrational mode is called IR-active.

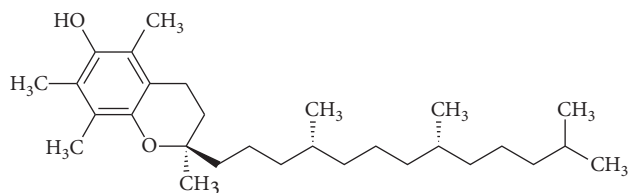


FIGURE 1: The structure of α -tocopherol.

The observed absorbance A , i.e., negative logarithmic transmission (intensity I of the light transmitted divided by the incident intensity I_0) of a sample of thickness d is given by the Beer–Lambert law:

$$A = -\log\left(\frac{I}{I_0}\right) = \varepsilon_\lambda cd, \quad (2)$$

with the extinction coefficient ε , which depends on the wavelength λ , and the concentration c of absorbing molecules. The IR spectrum eventually comprises the individual contributions from all the different vibrations originating from all the molecules in the sample. Consequently, it represents a true molecular fingerprint [69–71].

2.2. Instrumentation. As mentioned above, IR and NIR spectroscopy are absorption-based methods and hence the radiation needs to match the energy difference of the molecular transitions of interest. In other words, sources and detectors in the mid- and near-infrared are required. In the near-IR, Xenon and tungsten lamps are typically used as light sources and the detectors are commonly based on indium gallium arsenide (InGaAs) semiconductor materials. This allows us to perform spectroscopic analysis at wavelengths up to about $2.5 \mu\text{m}$. The common silicon-based detectors that can be found in digital cameras are not suitable at wavelengths longer than $1.1 \mu\text{m}$. Typical sources of mid-infrared radiation are glowing black-body radiators. Thermal detectors as well as semiconductors based on MCT and LiTaO₃ are suitable for detecting the radiation.

Spectral dispersion of the signal is normally achieved by an interferometric analysis employing a Michelson interferometer. The obtained interferogram is then Fourier transformed to yield the spectrum in the frequency domain giving rise to the common name Fourier-transform infrared (FTIR) spectroscopy. Most commercial instruments are FTIR spectrometers.

There is a variety of approaches to achieve an interaction between the radiation and the sample. The most common method is the transmission measurement. The sample is placed in-between two transmissive plates, and the transmitted intensity in the infrared region is recorded as a function of wavelength. Choosing the appropriate sample thickness, however, is crucial in this approach. A very thick sample will result in strong lines being saturated since almost all the photons around the peak center wavelength are absorbed. Such peaks manifest as broadened bands without

the typical Gaussian or Lorentzian shape. This may affect the data evaluation. For liquids, typical sample thicknesses lie in the range $25\text{--}500 \mu\text{m}$. Therefore, it is needless to say that the preparation of the sample is crucial as even dust particles may have significant influence. Common window materials include KBr, CaF₂, ZnSe, and NaCl, which are transmissive for the IR radiation. Conventional borosilicate or fused silica quartz glasses cannot be employed.

The method referred to as attenuated total reflection (ATR) FTIR spectroscopy is easier to use. In such an experiment, the IR radiation is propagating in a transmissive high-refractive-index material (often ZnSe or a diamond crystal), called the internal reflection element (IRE). The sample has a lower refractive index and is in contact with the surface of the crystal. The radiation undergoes total internal reflection at the angle α at this surface, so that the evanescent field can interact with the sample. As a consequence, the reflected beam is attenuated and carries the spectroscopic information.

Both approaches are illustrated schematically in Figure 2. An advantage of the transmission arrangement lays in the well-defined sample thickness, which is given simply by the distance between the plates where the sample is placed. On the opposite, in ATR experiments, the effective path length depends on the penetration depth, d_p , of the evanescent wave. This is a complex function of the wavelength and must be taken into account when ATR FTIR spectra are interpreted quantitatively [72]. The penetration depth is approximately $1/5$ of the wavelength and thus consists on order of a few micrometers in the mid-infrared wavelength spectrum. The resulting effective path length, d_{eff} , is usually the actual parameter of interest. It represents the corresponding sample thickness that would lead to the same absorption in a transmission experiment [73]. It is not a physical quantity and therefore it cannot be determined in a straightforward manner [72–74].

In the analysis of food and food products like olive oil, the ATR approach is highly beneficial since it does not require sample preparation and hence the measurements can be performed very quickly. The measurement time per sample is typically significantly below one minute. The data analysis depends on the information desired. Chemometric approaches are the methods of choice when the aim is to quantify constituents such as unsaturated fatty acids or other bioactive compounds. Cross-correlation techniques can be applied to compare the recorded spectrum with a library in order to find out whether or not the sample is genuine. This is often sufficient in order to identify adulterated and counterfeit products. Example applications will be discussed in more detail in the following. In order to give an impression, the FTIR spectra of 17 different olive oil samples from a local supermarket in Bremen, Germany, are displayed in Figure 3. The individual spectra are very similar to each other. This highlights the potential of FTIR spectroscopy for the authentication of olive oils. The most prominent signature at 1745 cm^{-1} is the characteristic C=O stretching vibration, which can be assigned to the fatty acids and ester groups.

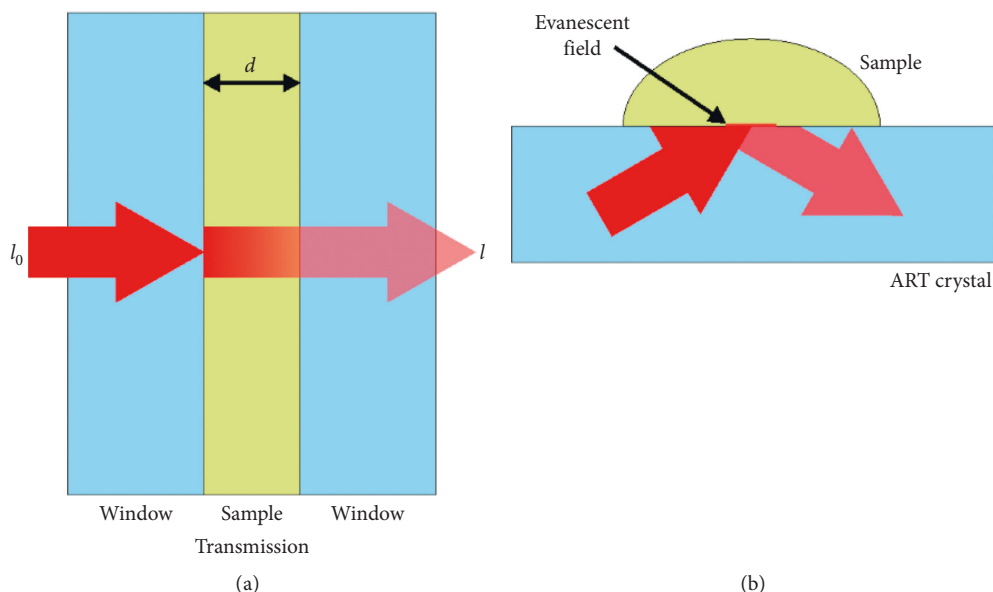


FIGURE 2: Schematic concepts of transmission and ATR spectroscopy. (a) Transmission. (b) ATR.

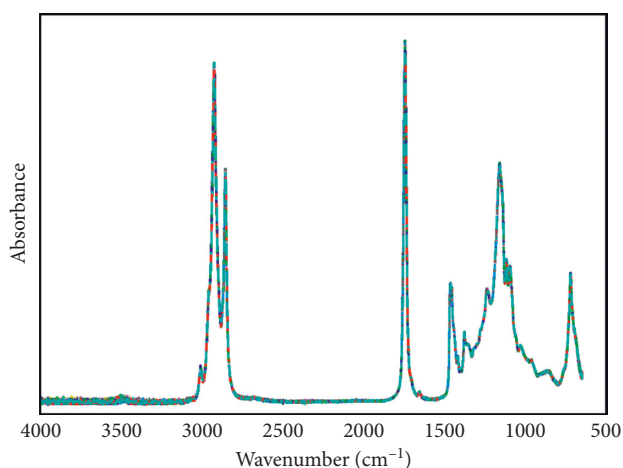


FIGURE 3: FTIR spectra of 17 different olive oil samples.

3. Application of Infrared Spectroscopy to Olive Oil: Focus on Functional Compounds Evaluation

For many years, analytical methods such as TLC, HPLC, GC-MS, and LC-MS/MS were the gold standard to identify and quantify the bioactive compounds (phenols, squalene, tocopherol, and fatty acids) in olive oils [75, 76]. Nowadays, as pointed out previously, the evaluation of bioactive compounds should be integrated in a multidisciplinary study approach for food research. This calls for the combination of advanced and innovative analytical techniques and sophisticated statistical methods for the data analysis in food science [77–79]. NIR and MIR techniques are rapidly emerging in this field. The bioactive compounds and antioxidant properties can be predicted by the spectroscopic methods. In particular, infrared spectroscopy coupled to chemometrics is considered as a powerful, fast, accurate, and

nondestructive analytical tool for rapid and precise determination of the content of bioactive compounds as well as their bioactivities, i.e., antioxidant properties. It represents a versatile alternative to the conventional methods. Further advantages in the context of food analysis include the rapid and inexpensive acquisition of data with nil or minimal sample preparation and the possibility to record spectra at or even in the production line. Besides a lot of studies on adulteration and discrimination of olive oil as well as monitoring contaminations, process or recovery by infrared spectroscopy [80–90], the focus here is on the evaluation of functional components.

3.1. Fatty Acids. Being the main constituents of olive oils, fatty acids and their triglycerides dominate the spectra of olive oils. Mailer [91] collected 216 olive oil samples throughout the Australian olive-growing areas to develop a NIR spectroscopy calibration for a range of quality parameters including the major fatty acids in olive oil. Multiple correlation coefficients squared (R^2) for minor fatty acids such as stearic acid (0.86) and linolenic acid (0.85) were reported relatively low because of the very narrow concentration range, while the major fatty acids oleic (0.99) and linoleic (1.00) provided high levels of accuracy compared with the reproducibility of the reference method.

It has been reported that authentication of virgin olive oil is time-consuming and requires expertise in the use of sophisticated instruments. To overcome this issue, Galtier et al. [92] evaluated the chemometric treatment of NIR spectra for the assessment of fatty acids and triacylglycerols in French virgin olive oil samples ($n=125$) for their classification (PLS1-DA) into geographically closed registered designations of origin (RDOs). The chemometric treatments of NIR spectra revealed that regression vectors of each RDO were correlated to one or more specific components with similar results obtained by conventional techniques according to

their cultivar compositions. For the very first time, Maggio et al. [93] reported a rapid method to determine the fatty acid profile of olive oils using FTIR spectroscopy with the ATR sampling technique as described in Section 2. Calibration models were built using PLS regression. The fatty acid calibration models (oleic acid, linoleic acid, SFA, MUFA, and PUFA) were constructed in the spectral range from 3033 to 700 cm^{-1} using PLS. The values obtained for the correlation coefficient for all models were in the range of 0.96–0.99. The LODs of the FTIR-chemometry methods were reported for oleic acid 3.0%, linoleic acid 0.5%, saturated fatty acids 1.3%, monounsaturated fatty acids 0.3%, and polyunsaturated fatty acids 0.3%, with recovery rates in the range 98–103%. The proposed method showed results comparable to the one obtainable by using the official method, but with the advantage of being more rapid and less expensive. Another study by Gurdeniz et al. described the classification and quantification of Turkish extra-virgin olive oil on the basis of fatty acids by using mid-infrared spectroscopy in combination with chemometric methods [94]. The PCA successfully distinguished the southern olive oil samples from the northern samples, while PLS detected a correlation between the spectral data and the fatty acid profile. The values obtained for the correlation coefficient were 0.83, 0.97, 0.97, 0.83, and 0.69 for stearic, oleic, linoleic, arachidic, and linolenic acids, respectively. Dupuy et al. [95] investigated the potential use of NIR and MIR spectroscopy for the quantitative analysis of triacylglycerols and fatty acids for the identification of the RDO of extra-virgin olive oils. PLS and PLS-DA regressions were separately applied to the two spectral ranges. MIR spectroscopy was found to perform better. It was further reported that RDO identification by DA using a multiblock method showed proficiency.

The quantification of oxidized fatty acids in virgin olive oil using mid-infrared spectroscopy coupled with multiple linear regression has been described by Lerma-García et al. [96]. For the prediction of oxidized fatty acid, the entire mid-infrared region was divided into 25 subregions. The subregions affected by oxidation were identified using multiple linear regression with a cube root data transformation that successfully predicted oxidized fatty acids. The value obtained for correlation coefficient was 0.944 with a prediction error of 17%. Uncu and Ozen [97] studied some important quality parameters (oxidative stability, color pigments, fatty acid profile, and phenolic composition) of olive oils by FTIR spectroscopy as one of the vibrational spectroscopic methods: it is possible to predict successfully the oxidative stability, the major fatty acids (palmitic (0.87), oleic (0.94), and linoleic acid (0.97), saturated (0.91), monounsaturated (0.94), and polyunsaturated fatty acids (0.97)), and the chlorophyll content and some phenolic compounds of the samples.

Casale et al. [98] authenticated the Italian protected designation of origin (PDO) extra-virgin olive oil Chianti Classico using UV-vis, NIR and MIR spectroscopy coupled with a chemometric data analysis. Unequal class models (UNEQ) and soft independent modelling of class analogy (SIMCA) along with PLS were employed individually and jointly on the fatty acid composition data. PLS successfully

predicted the oleic and linoleic acid content in the extra-virgin olive oils. Similarly, Inarejos-García et al. [99] investigated the degree of unsaturation of virgin olive oil by NIR spectroscopy. They reported an excellent performance of the multivariate algorithms in particular for the fatty acid profile (r -multiple coefficient of determination = 0.84–0.96). In a different approach, Valli et al. [100] pointed out new parameters for the detection of low quality of extra-virgin olive oil. These parameters were based on the total amount of fatty acids methyl and ethyl esters Σ (FAMEs + FAEEs) and their ratio (FAEEs/FAMEs) applying PLS to MIR spectra. The spectroscopic data showed a good agreement between predicted and actual reference values of calibration data sets. The limit of detection and quantification was reported to be 8.8 and 29.3 $\text{mg}\cdot\text{kg}^{-1}$ for Σ (FAMEs + FAEEs) with R^2 (0.98). On the contrary, the ratio of FAEEs/FAMEs showed R^2 (0.83).

Recently, the European Union regulation for olive oil set a value of fatty acids ethyl ester contents ($35\text{ mg}\cdot\text{kg}^{-1}$) in extra-virgin olive oils. To evaluate the fatty acid alkyl esters in extra-virgin olive oil, Cayuela [101] recently developed predictive models for the determination of total fatty acid alkyl esters based on NIR spectroscopy. The external validation exercise of FAAEs, FAEEs, and FAMEs using the NIR spectrometer showed SEP values of 33.6 and 54.5, 25.6, and 67.2, 18.7 with $r = 0.91$ and 0.93, 0.89, and 0.88, 0.92, respectively, for two validation sets.

3.2. Phenolic Compounds, Tocopherols, and Squalenes.

Several studies applied chemometrics to spectroscopic data in order to develop models and predict the content of minor components/functional compounds such as phenolic compounds and tocopherols in olive oils [1, 102, 103]. The recent chapter of Lagouri et al. [102] summarizes the optical UV-Vis-NIR-MIR spectroscopic tools and chemometrics used for the monitoring of olive oil functional compounds. Fatty acids, phenols, tocopherols, carotenoids, and squalene were considered with a focus on the bioactivity, chemistry, and processing. Inarejos-García et al. [99] investigated minor components, sensory characteristics, and quality of virgin olive oil by NIR spectroscopy. Their multivariate algorithms allowed reasonably accurate measurements, in particular of hydroxytyrosol derivatives (r -multiple coefficient of determination = 0.86–0.88) and C6 alcohols (r -multiple coefficient of determination = 0.69–0.80). FTIR spectroscopy, on the contrary, was used by Gouvinhas et al. [104]. They carried out a chemometric analysis of FTIR spectra from extra-virgin olive oils of three cultivars from Portugal (cultivars “Cobranco,” “Galega,” and “Picual”) at different maturation stages. To create a model for the discrimination of the olive oil samples, principal component analysis and discriminant analysis were utilised. The need for such sophisticated data analysis can also be seen in Figure 3, which shows that the spectra of olive oils are very similar. For the quantification of individual compounds, Gouvinhas et al. [104] developed regression-based calibration and validation models. This allowed the determination of the total phenolic content, *ortho*-diphenols, flavonoids, and

antioxidant activity during the ripening process. For *ortho*-diphenols and flavonoids, the slope R^2 and the RMSE were higher than 0.98 and lower than 0.03, respectively, whereas the phenolic content had the lowest multiple coefficient of determination in the calibration model ($R^2 = 0.94$). The same authors reported a slope R^2 and the RMSE of 0.93 and 0.04, respectively, for the determination of the antioxidant activity. Their quality measures became worse when data were cross validated ($R^2 = 0.86$, RMSECV = 0.05).

Mora-Ruiz et al. [105] applied NIR and MIR spectroscopy to study polar phenolic compounds of virgin olive oil and their impact on the oil quality. They obtained satisfactory multivariate test set validation algorithms for total polar phenolic (TPP) compounds (r -coefficient of determination = 0.91), hydroxytyrosol and tyrosol secoiridoid derivatives (HtyrSec, TyrSec; $r = 0.91$ and 0.92, respectively) by NIR spectroscopy. Moreover, the authors pointed out that, in contrast to the NIR data, the chemometric analysis of the MIR spectra gave no satisfactory validation models ($r = 0.43$, 0.54, and 0.66 for HtyrSec, TyrSec, and TPP). This was unexpected as the calibration algorithms for MIR actually gave an even better correlation than NIR ($r > 0.96$ for all the polar phenolics studied). On the contrary, the optimization of phenolic compounds extraction from EVOO was achieved applying a response surface methodology as proposed by Fratoddi et al. [106].

Also, very good MIR results for the quantification of virgin olive oil phenolic compounds were reported by Hirri et al. [107]. They obtained values for the correlation coefficient and the root mean square errors of prediction of 0.99 and 0.11, respectively. This study underlined also that the spectral region in the range 3050–600 cm^{-1} was useful for predicting the total polyphenol content. Bellincontro et al. [108] also focused on the total phenols. They developed a portable NIR-AOTF tool for the on-field and non-destructive measurement of specific and total phenols in olives for oil production. Models were developed for the main phenolic compounds (e.g., oleuropein, verbascoside, and 3,4-DHPEA-EDA) and total phenols by PLS. The results in terms of R^2 for the calibration, prediction, and cross validation ranged between 0.930 and 0.998, 0.874 and 0.942, and 0.837 and 0.992, respectively. A recent preliminary study of Trapani et al. [109] applied cost-saving NIR based on a discrete filter system for the rapid measurement of total phenolic content and oleuropein of olive fruits, in addition to the moisture, oil, and sugar. Although PLS models built for the latter ones were satisfactory, the instrument did not prove itself suitable for obtaining predictive models for phenolic compound contents. This is probably because the necessary wavelengths in the section of absorbance from 1100 to 1400 nm were not covered. Further studies in this direction are necessary and requested for enabling the possible application and use.

Concerning tocopherols, Cayuela and García [110] recently reported the classification of olive oils based on α -tocopherol and total tocopherol content using NIR spectroscopy. Other studies utilised pigments such as carotenoids and chlorophyll derivatives in extra-virgin olive oil as parameters/index of authenticity and quality. Pigments in oil

matrices can be identified and quantified by chromatographic techniques after a pretreatment of the samples such as extraction and/or saponification, or by spectroscopic techniques without pretreatment of the samples [111]. Another work by the same authors quantified the main pigments, i.e., β -carotene, lutein, pheophytin A, and pheophytin B, in several extra-virgin olive oils produced from a blend of three cultivars (Moraiolo, Frantoio, and Leccino) typical of Tuscany (Italy) in three different years. For this purpose, they employed a method based on the mathematical analysis of the near-ultraviolet-visible absorption spectra of the oils [112]. Besides a good prediction of fatty acid ethyl ester and wax, Uncu et al. [113] quantified lutein, pheophytin A, and their derivatives and total xanthophylls by FTIR + UV/vis with a range of R_{cv}^2 of 0.71–0.85, R_{pred}^2 of 0.70–0.84, and RPD = 1.5–2.5 values but the prediction of the rest of the pigments were poor ($R_{\text{cv}}^2 = 0.60$ –0.76, R_{pred}^2 : 0.42–0.62, and RPD = 1.2–1.5). Along the same line, Borello and Domenici [114] compared two near-UV/vis spectroscopic techniques for the determination of pigments, i.e., total carotenoids, and total chlorophyll derivatives in virgin and extra-virgin olive oils. Although UV/vis spectroscopy is very tempting for analysing the pigments, NIR and MIR spectroscopy typically gives a more specific molecular fingerprint of oil. Cayuela and García [115] developed rapid NIR techniques using PLS analysis for measuring the squalene content of olive oil. The external validation exercise for estimating squalene was performed with the squared validation regression coefficient (r^2) 0.83 and residual predictive deviation of 2.31.

3.3. Antioxidants. The assessment of interactions between natural active compounds and other food matrix components represent the bioactivity of a food. The first indicator of potential health benefits is commonly given by the antioxidant properties. The comprehension of concerted and synergistic actions, of antagonist interactions, or of no effect of biologically active compounds should be considered in this context. The same is true for the factors influencing the overall effects such as the peculiar combination of antioxidants and the structure of the food matrix [77]. Lu and Rasco [116] reviewed and summarized the recent applications of infrared spectroscopy for the development of models for the prediction of antioxidant properties in food, in addition to qualitative and quantitative analysis of antioxidant compounds. It is also worthy of mentioning the review article of Cozzolino [117], who concluded that infrared spectroscopy is a versatile analytical tool for the quantitative determination of antioxidant properties in agricultural products, foods, and plants.

Carretani et al. [118] reported the rapid FTIR determination of phenolics and antioxidant activity of olive oil, in addition to water. For total phenols, good results were obtained considering the spectrum from 3610 to 816 cm^{-1} , while the range from 3707 to 1105 cm^{-1} was most suitable for ABTS+. Satisfactory LOD values were achieved by the FTIR-chemometry approach: 12.5 (mg gallic acid/kg oil) for total phenols and 0.76 (mmol Trolox/kg oil) for ABTS+. The authors concluded that the results obtained with the

chemometric data analysis are comparable to those obtained using the official reference method. This highlights the potential of the spectroscopic technique as an alternative to the standard procedure for routine analysis or control at-line of production processes.

4. Conclusion

NIR and MIR spectroscopy coupled with chemometric data analysis has shown considerable potential for the determination of functional compounds present in olive oil. Recent applications have demonstrated to perform the assay of antioxidant activity (tocopherols, phenols, and squalene), to allow the discrimination of geographical origins, to facilitate the assessment of sensory attributes, and to determine the fatty acid profile, which is characteristic of the oil matrix. IR spectroscopic methods represent an interesting alternative to the conventional analytical methods as they do not require a pretreatment of the samples. Moreover, they offer a high sample throughput and significant time saving. In addition, these techniques are considerably more environmentally friendly since no solvents or carrier gases are used. These new approaches based on mid- and near-IR absorption spectroscopy are therefore interesting alternatives, for example, for rapid screening purposes.

In the future, IR spectroscopic methodology in combination with chemometric data evaluation will possibly overtake the conventional methodologies. In some cases, this may require the change of the regulatory frameworks, which are currently naming only conventional analytical tools for certain official purposes. However, the convincing performance of the spectroscopic approaches with respect to authentication and comprehensive quantitative analysis will certainly make a strong case in the regulatory and political processes. Without a doubt, the methods reviewed in this paper will soon be extensively used in the oil processing industries as a routine method to evaluate the characteristic parameters of olive oil.

Conflicts of Interest

The authors declare that they have no conflicts of interest.

References

- [1] M. Casale and R. Simonetti, "Review: near infrared spectroscopy for analysing olive oils," *Journal of Near Infrared Spectroscopy*, vol. 22, no. 2, pp. 59–80, 2014.
- [2] D. Boskou, "Olive fruits, table olives, and olive oil bioactive constituents," in *Olive and Olive Oil Bioactive Constituents*, D. Boskou, Ed., pp. 1–30, AOCS Press, Urbana, IL, USA, 1st edition, 2015.
- [3] F. P. Zito, B. Polese, L. Vozzella et al., "Good adherence to mediterranean diet can prevent gastrointestinal symptoms: a survey from Southern Italy," *World Journal of Gastrointestinal Pharmacology and Therapeutics*, vol. 7, no. 4, pp. 564–571, 2016.
- [4] C. M. Lăcătușu, E. D. Grigorescu, M. Floria, A. Onofriescu, and B. M. Mihai, "The mediterranean diet: from an environment-driven food culture to an emerging medical prescription," *International Journal of Environmental Research and Public Health*, vol. 16, no. 6, p. 942, 2019.
- [5] L. Conte, A. Bendini, E. Valli et al., "Olive oil quality and authenticity: a review of current EU legislation, standards, relevant methods of analyses, their drawbacks and recommendations for the future," *Trends in Food Science & Technology*, 2019, In press.
- [6] A. Srobarova, J. A. Teixeira da Silva, G. Kogan, A. Ritieni, and A. Santini, "Beauvericin decreases cell viability of wheat," *Chemistry and Biodiversity*, vol. 6, pp. 1208–1215, 2009.
- [7] P. Mikušová, A. Šrobárová, M. Sulyok, and A. Santini, "Fusarium fungi and associated metabolites presence on grapes from Slovakia," *Mycotoxin Research*, vol. 29, no. 2, pp. 97–102, 2013.
- [8] R. Bhat and K. R. N. Reddy, "Challenges and issues concerning mycotoxins contamination in oil seeds and their edible oils: updates from last decade," *Food Chemistry*, vol. 215, pp. 425–437, 2017.
- [9] K. Otto, A. Santini, and S. Oancea, "Recent aflatoxin survey data in milk and milk products: a review," *International Journal of Dairy Technology*, vol. 70, no. 3, pp. 320–331, 2017.
- [10] P. Mikušová, A. Ritieni, A. Santini, G. Juhasová, and A. Šrobárová, "Contamination by moulds of grape berries in Slovakia," *Food Additives & Contaminants Part A*, vol. 27, no. 5, pp. 738–747, 2010.
- [11] A. Santini, G. Meca, S. Uhlig, and A. Ritieni, "Fusaproliferin, beauvericin and enniatins: occurrence in food—a review," *World Mycotoxin Journal*, vol. 5, no. 1, pp. 71–81, 2012.
- [12] P. Mikušová, A. Santini, A. Ritieni, J. Pavlokin, and A. Šrobárová, "Berries contamination by microfungi in Slovakia vineyard regions: impact of climate conditions on microfungi biodiversity," *Revista Iberoamericana de Micología*, vol. 29, no. 3, pp. 126–131, 2012.
- [13] A. Cimmino, A. Andolfi, M. C. Zonno et al., "Chenopodolin: a phytotoxic unrearranged ent-pimaradiene diterpene produced by phoma chenopodicola, a fungal pathogen for *Chenopodium album* biocontrol," *Journal of Natural Products*, vol. 76, no. 7, pp. 1291–1297, 2013.
- [14] A. Medina, S. Mohale, N. I. P. Samsudin, A. Rodriguez-Sixtos, A. Rodriguez, and N. Magan, "Biocontrol of mycotoxins: dynamics and mechanisms of action," *Current Opinion in Food Science*, vol. 17, pp. 41–48, 2017.
- [15] M. F. Abdallah, M. Ameye, S. De Saeger, K. Audenaert, and G. Haesaert, "Biological control of mycotoxigenic fungi and their toxins: an update for the pre-harvest approach," in *Fungi and Mycotoxins—Their Occurrence, Impact on Health and the Economy as Well as Pre- and Postharvest Management Strategies*, P. Berka Njobeh, Ed., Intech Open, London, UK, 2018.
- [16] S. Vichi, A. Romero, J. Tous, and J. Caixach, "The activity of healthy olive microbiota during virgin olive oil extraction influences oil chemical composition," *Journal of Agricultural and Food Chemistry*, vol. 59, no. 9, pp. 4705–4714, 2011.
- [17] S. Cicerale, X. A. Conlan, A. J. Sinclair, and R. S. J. Keast, "Chemistry and health of olive oil phenolics," *Critical Reviews in Food Science and Nutrition*, vol. 49, no. 3, pp. 218–236, 2009.
- [18] A. Salvo, A. Rotondo, G. L. La Torre, N. Cicero, and G. Dugo, "Determination of 1,2/1,3-diglycerides in Sicilian extra-virgin olive oils by ¹H-NMR over a one-year storage period," *Natural Product Research*, vol. 31, no. 7, pp. 822–828, 2017.
- [19] L. Schwingshackl, A. M. Lampousi, M. P. Portillo, D. Romaguera, G. Hoffmann, and H. Boeing, "Olive oil in the

- prevention and management of type 2 diabetes mellitus: a systematic review and meta-analysis of cohort studies and intervention trials," *Nutrition and Diabetes*, vol. 7, no. 4, p. e262, 2017.
- [20] E. Alves, M. R. M. Domingues, and P. Domingues, "Polar lipids from olives and olive oil: a review on their identification, significance and potential biotechnological applications," *Foods*, vol. 7, no. 7, p. 109, 2018.
- [21] E. M. Yubero-Serrano, J. Lopez-Moreno, F. Gomez-Delgado, and J. Lopez-Miranda, "Extra virgin olive oil: more than a healthy fat," *European Journal of Clinical Nutrition*, 2018, In press.
- [22] G. Serreli and M. Deiana, "Biological relevance of extra virgin olive oil polyphenols metabolites," *Antioxidants*, vol. 7, no. 12, p. 170, 2018.
- [23] V. Francisco, C. Ruiz-Fernández, V. Lahera et al., "Natural molecules for healthy lifestyles: oleocanthal from extra virgin olive oil," *Journal of Agricultural and Food Chemistry*, vol. 67, no. 14, pp. 3845–3853, 2019.
- [24] D. L. García-González, R. Aparicio-Ruiz, and R. Aparicio, "Virgin olive oil—chemical implications on quality and health," *European Journal of Lipid Science and Technology*, vol. 110, no. 7, pp. 602–607, 2008.
- [25] M. Aparicio-Soto, M. Sánchez-Hidalgo, M. Á. Rosillo, M. L. Castejón, and C. Alarcón-de-la-Lastra, "Extra virgin olive oil: a key functional food for prevention of immune-inflammatory diseases," *Food & Function*, vol. 7, no. 11, pp. 4492–4505, 2016.
- [26] S. Rigacci and M. Stefani, "Nutraceutical properties of olive oil polyphenols. An itinerary from cultured cells through animal models to humans," *International Journal of Molecular Science*, vol. 17, no. 6, p. 843, 2016.
- [27] M. Piroddi, A. Albini, R. Fabiani et al., "Nutrigenomics of extra-virgin olive oil: a review," *Biofactors*, vol. 43, no. 1, pp. 17–41, 2017.
- [28] B. Saibandith, J. P. E. Spencer, I. R. Rowland, and D. M. Commane, "Olive polyphenols and the metabolic syndrome," *Molecules*, vol. 22, no. 7, p. 1082, 2017.
- [29] A. Alkhatib, C. Tsang, and J. Tuomilehto, "Olive oil nutraceuticals in the prevention and management of diabetes: from molecules to lifestyle," *International Journal of Molecular Science*, vol. 19, no. 7, p. 2024, 2018.
- [30] A. M. Borzi, A. Biondi, F. Basile, S. Luca, E. S. D. Vicari, and M. Vacante, "Olive oil effects on colorectal cancer," *Nutrients*, vol. 11, no. 1, p. 32, 2018.
- [31] M. Crespo, J. Tomé-Carneiro, A. Dávalos, and F. Visioli, "Pharma-nutritional properties of olive oil phenols. Transfer of new findings to human nutrition," *Foods*, vol. 7, no. 6, p. 90, 2018.
- [32] A. Foscolou, E. Critselis, and D. Panagiotakos, "Olive oil consumption and human health: a narrative review," *Maturitas*, vol. 118, pp. 60–66, 2018.
- [33] O. Garcia-Martinez, C. Ruiz, A. Gutierrez-Ibanez, R. Illescas-Montes, and L. Melguizo-Rodriguez, "Benefits of olive oil phenolic compounds in disease prevention," *Endocrine, Metabolic and Immune Disorders Drug Targets*, vol. 18, no. 4, pp. 333–340, 2018.
- [34] A. Santini, E. Novellino, V. Armini, and A. Ritieni, "State of the art of ready-to-use therapeutic food: a tool for nutraceuticals addition to foodstuff," *Food Chemistry*, vol. 140, no. 4, pp. 843–849, 2013.
- [35] R. Andrew and A. A. Izzo, "Principles of pharmacological research of nutraceuticals," *British Journal of Pharmacology*, vol. 174, no. 11, pp. 1177–1194, 2017.
- [36] A. Santini and E. Novellino, "Nutraceuticals—shedding light on the grey area between pharmaceuticals and food," *Expert Review of Clinical Pharmacology*, vol. 11, no. 6, pp. 545–547, 2018.
- [37] A. Santini, S. M. Cammarata, G. Capone et al., "Nutraceuticals: opening the debate for a regulatory framework," *British Journal of Clinical Pharmacology*, vol. 84, no. 4, pp. 659–672, 2018.
- [38] A. Santini, G. C. Tenore, and E. Novellino, "Nutraceuticals: a paradigm of proactive medicine," *European Journal of Pharmaceutical Sciences*, vol. 96, pp. 53–61, 2017.
- [39] P. Daliu, A. Santini, and E. Novellino, "From pharmaceuticals to nutraceuticals: bridging disease prevention and management," *Expert Review of Clinical Pharmacology*, vol. 12, no. 1, pp. 1–7, 2018.
- [40] A. Durazzo, "Extractable and non-extractable polyphenols: an overview," in *Non-Extractable Polyphenols and Carotenoids: Importance in Human Nutrition and Health. Food Chemistry, Function and Analysis*, No. 5, F. Saura-Calixto and J. Pérez-Jiménez, Eds., p. 37, Royal Society of Chemistry, London, UK, 2018.
- [41] A. Durazzo, L. D'Addezio, E. Camilli et al., "From plant compounds to botanicals and back: a current snapshot," *Molecules*, vol. 23, no. 8, p. 1844, 2018.
- [42] A. Durazzo and M. Lucarini, "A Current shot and rethinking of antioxidant research strategy," *Brazilian Journal of Analytical Chemistry*, vol. 5, no. 20, pp. 9–11, 2018.
- [43] F. Aouidi, N. Dupuy, J. Artaud et al., "Rapid quantitative determination of oleuropein in olive leaves (*Olea europaea*) using mid-infrared spectroscopy combined with chemometric analyses," *Industrial Crops and Products*, vol. 37, no. 1, pp. 292–297, 2012.
- [44] M. Jansen and J. Birch, "Composition and stability of olive oil following partial crystallization," *Food Research International*, vol. 42, no. 7, pp. 826–831, 2009.
- [45] E. N. Frankel, "Chemistry of extra virgin olive oil: adulteration, oxidative stability, and antioxidants," *Journal of Agricultural and Food Chemistry*, vol. 58, no. 10, pp. 5991–6006, 2010.
- [46] E. N. Frankel, "Nutritional and biological properties of extra virgin olive oil," *Journal of Agricultural and Food Chemistry*, vol. 59, no. 3, pp. 785–792, 2009.
- [47] M. Celano, V. Maggisano, S. M. Lepore, D. Russo, and S. Bulotta, "Secoiridoids of olive and derivatives as potential adjuvant drugs in cancer: a critical analysis of experimental studies," *Pharmacological Research*, vol. 142, pp. 77–86, 2019.
- [48] J. M. Moran, O. Leal-Hernandez, R. Roncero-Martin, and J. D. Pedrera-Zamorano, "Antitumor perspectives of oleuropein," *Journal of Food Science*, vol. 84, no. 3, p. 384, 2019.
- [49] P. Przychodzen, R. Wyszowska, M. Gorzynik-Debicka, T. Kostrzewa, A. Kuban-Jankowska, and M. Gorska-Ponikowska, "Anticancer potential of oleuropein, the polyphenol of olive oil, with 2-methoxyestradiol, separately or in combination, in human osteosarcoma cells," *Anticancer Research*, vol. 39, no. 3, pp. 1243–1251, 2019.
- [50] M. El Riachy, F. Priego-Capote, L. León, L. Rallo, and M. D. Luque de Castro, "Hydrophilic antioxidants of virgin olive oil. Part 1: hydrophilic phenols: a key factor for virgin olive oil quality," *European Journal of Lipid Science and Technology*, vol. 113, no. 6, pp. 678–691, 2013.
- [51] C. L. Huang and B. E. Sumpio, "Olive oil, the mediterranean diet, and cardiovascular health," *Journal of the American College of Surgeons*, vol. 207, no. 3, pp. 407–416, 2008.

- [52] J. Chandran, N. Nayana, and P. Nisha, "Phenolics in vegetable oils," in *Compounds in Food: Characterization and Analysis Food Analysis & Properties, Chapter 21*, L. M. L. Nollet and J. A. Gutierrez-Urbe, Eds., p. 407, Taylor & Francis Group, Abingdon, UK, 2018.
- [53] A. García, E. Rodríguez-Juan, G. Rodríguez-Gutiérrez, J. J. Rios, and J. Fernández-Bolaños, "Extraction of phenolic compounds from virgin olive oil by deep eutectic solvents (DESs)," *Food Chemistry*, vol. 197, pp. 554–561, 2016.
- [54] B. Bayram, B. Ozcelik, G. Schultheiss, J. Frank, and G. Rimbach, "A validated method for the determination of selected phenolics in olive oil using high-performance liquid chromatography with coulometric electrochemical detection and a fused-core column," *Food Chemistry*, vol. 138, no. 2-3, pp. 1663–1669, 2013.
- [55] G. Cioffi, M. S. Pesca, P. De Caprariis, A. Braca, L. Severino, and N. De Tommasi, "Phenolic compounds in olive oil and olive pomace from Cilento (Campania, Italy) and their antioxidant activity," *Food Chemistry*, vol. 121, no. 1, pp. 105–111, 2010.
- [56] C. Conde, S. Delrot, and H. Gerós, "Physiological, biochemical and molecular changes occurring during olive development and ripening," *Journal of Plant Physiology*, vol. 165, no. 15, pp. 1545–1562, 2008.
- [57] A. Gómez-Rico, M. D. Salvador, and G. Fregapane, "Virgin olive oil and olive fruit minor constituents as affected by irrigation management based on SWP and TDF as compared to ET_c in medium-density young olive orchards (*Olea europaea* L. cv. Cornicabra and Morisca)," *Food Research International*, vol. 42, no. 8, pp. 1067–1076, 2009.
- [58] R. Amarowicz, R. Carle, G. Dongowski et al., "Influence of postharvest processing and storage on the content of phenolic acids and flavonoids in foods," *Molecular Nutrition and Food Research*, vol. 53, no. 2, pp. S151–S183, 2009.
- [59] O. Köseoğlu, D. Sevim, and P. Kadiroğlu, "Quality characteristics and antioxidant properties of Turkish monovarietal olive oils regarding stages of olive ripening," *Food Chemistry*, vol. 212, pp. 628–634, 2016.
- [60] V. Di Stefano and M. G. Melilli, "Effect of storage on quality parameters and phenolic content of Italian extra-virgin olive oils," *Natural Product Research*, vol. 21, pp. 1–9, 2019.
- [61] J. Giacometti, Č. Milin, F. Giacometti, and Z. Ciganj, "Characterisation of monovarietal olive oils obtained from croatian cvs. drobnica and buza during the ripening period," *Foods*, vol. 7, no. 11, p. 188, 2018.
- [62] R. Romano, A. Giordano, L. Le Grottaglie et al., "Volatile compounds in intermittent frying by gas chromatography and nuclear magnetic resonance," *European Journal of Lipid Science and Technology*, vol. 115, no. 7, pp. 764–773, 2013.
- [63] D. Naviglio, R. Romano, F. Pizzolongo et al., "Rapid determination of esterified glycerol and glycerides in triglyceride fats and oils by means of periodate method after transesterification," *Food Chemistry*, vol. 102, no. 1, pp. 399–405, 2007.
- [64] D. Boskou, M. Tsimidou, and G. Blekas, "Olive oil composition," in *Olive Oil: Chemistry and Technology*, D. Boskou, Ed., AOCS Press, Champaign, IL, USA, 2006.
- [65] V. N. Kamvissis, E. G. Barbounis, N. C. Megoulas, and M. A. Koupparis, "A novel photometric method for evaluation of the oxidative stability of virgin olive oils," *Journal of AOAC International*, vol. 91, no. 4, pp. 794–801, 2008.
- [66] R. Ambra, F. Natella, S. Lucchetti, V. Forte, and G. Pastore, " α -Tocopherol, β -carotene, lutein, squalene and secoiridoids in seven monocultivar Italian extra-virgin olive oils," *International Journal of Food Sciences and Nutrition*, vol. 68, no. 5, pp. 538–545, 2017.
- [67] E. Psomiadou and M. Tsimidou, "Pigments in Greek virgin olive oils: occurrence and levels," *Journal of the Science of Food and Agriculture*, vol. 81, no. 7, pp. 640–647, 2001.
- [68] P. Viola and M. Viola, "Virgin olive oil as a fundamental nutritional component and skin protector," *Clinics in Dermatology*, vol. 27, no. 2, pp. 159–165, 2009.
- [69] B. Schrader, *Infrared and Raman Spectroscopy*, VCH Verlagsgesellschaft, Weinheim, Germany, 1995.
- [70] P. R. Griffiths and J. A. De Haseth, *Fourier Transform Infrared Spectrometry*, Wiley, Weinheim, Germany, 2nd edition, 2007.
- [71] H. Haken and H. C. Wolf, *Molecular Physics and Elements of Quantum Chemistry*, Springer, Berlin, Germany, 1995.
- [72] J. Kiefer, N. H. Rasul, P. K. Ghosh, and E. Von Lieres, "Surface and bulk porosity mapping of polymer membranes using infrared spectroscopy," *Journal of Membrane Science*, vol. 452, pp. 152–156, 2014.
- [73] L. A. Averett, P. R. Griffiths, and K. Nishikida, "Effective path length in attenuated total reflection spectroscopy," *Analytical Chemistry*, vol. 80, no. 8, pp. 3045–3049, 2008.
- [74] N. J. Harrick and F. K. du Pré, "Effective thickness of bulk materials and of thin films for internal reflection spectroscopy," *Applied Optics*, vol. 5, no. 11, pp. 1739–1743, 1966.
- [75] C. I. G. Tuberoso, I. Jerković, M. Maldini, and G. Serrelli, "Phenolic compounds, antioxidant activity, and other characteristics of extra virgin olive oils from Italian autochthonous varieties Tonda di Villacidro, Tonda di Cagliari, Semidana, and Bosana," *Journal of Chemistry*, vol. 2016, Article ID 8462741, 7 pages, 2016.
- [76] D. Trombetta, A. Smeriglio, D. Marcoccia et al., "Analytical evaluation and antioxidant properties of some secondary metabolites in northern Italian mono- and multi-varietal extra virgin olive oils (EVOOs) from early and late harvested olives," *International Journal of Molecular Sciences*, vol. 18, no. 4, p. 797, 2017.
- [77] A. Durazzo, "Study approach of antioxidant properties in foods: update and considerations," *Foods*, vol. 6, p. E17, 2017.
- [78] A. Durazzo, J. Kiefer, M. Lucarini et al., "An Innovative and Integrated Food Research Approach: spectroscopy applications to milk and a case study of a milk-based dish," *Brazilian Journal of Analytical Chemistry*, vol. 5, no. 18, pp. 12–27, 2018.
- [79] A. Durazzo, J. Kiefer, M. Lucarini et al., "Qualitative analysis of traditional Italian dishes: FTIR approach," *Sustainability*, vol. 10, no. 11, p. 4112, 2018.
- [80] M. de Luca, W. Terouzi, G. Ioele et al., "Derivative FTIR spectroscopy for cluster analysis and classification of Moroccan olive oils," *Food Chemistry*, vol. 124, no. 3, pp. 1113–1118, 2011.
- [81] A. P. la Mata, A. Dominguez-Vidal, J. M. Bosque-Sendra, A. Ruiz-Medina, L. Cuadros-Rodríguez, and M. J. Ayora-Cañada, "Olive oil assessment in edible oil blends by means of ATR-FTIR and chemometrics," *Food Control*, vol. 23, no. 2, pp. 449–455, 2012.
- [82] A. Rohman and Y. B. Che Man, "Quantification and classification of corn and sunflower oils as adulterants in olive oil using chemometrics and FTIR Spectra," *Scientific World Journal*, vol. 2012, Article ID 250795, 6 pages, 2012.
- [83] O. Jović, T. Smolić, I. Primožič, and T. Hrenar, "Spectroscopic and chemometric analysis of binary and ternary edible oil mixtures: qualitative and quantitative study," *Analytical Chemistry*, vol. 88, no. 8, pp. 4516–4524, 2016.

- [84] M. De Luca, D. Restuccia, M. L. Clodoveo, F. Puoci, and G. Ragno, "Chemometric analysis for discrimination of extra virgin olive oils from whole and stoned olive pastes," *Food Chemistry*, vol. 202, pp. 432–437, 2016.
- [85] A. M. Jiménez-Carvelo, M. T. Osorio, A. Koidis, A. González-Casado, and L. Cuadros-Rodríguez, "Chemometric classification and quantification of olive oil in blends with any edible vegetable oils using FTIR-ATR and Raman spectroscopy," *LWT*, vol. 86, pp. 174–184, 2017.
- [86] K. Georgouli, J. Martínez Del Rincon, and A. Koidis, "Continuous statistical modelling for rapid detection of adulteration of extra virgin olive oil using mid infrared and Raman spectroscopic data," *Food Chemistry*, vol. 217, pp. 735–742, 2017.
- [87] M. H. abadi Sherahi, F. Shahidi, F. Tabatabai Yazdi, and S. M. Bagher Hashemi, "Effect of *Lactobacillus plantarum* on olive and olive oil quality during fermentation process," *LWT—Food Science and Technology*, vol. 82, pp. 572–580, 2018.
- [88] I. Durán Merás, J. Domínguez Manzano, D. Airado Rodríguez, and A. Muñoz de la Peña, "Detection and quantification of extra virgin olive oil adulteration by means of autofluorescence excitation-emission profiles combined with multi-way classification," *Talanta*, vol. 178, pp. 751–762, 2018.
- [89] L. Hadhoum, G. Burnens, K. Loubar, M. Balistrrou, and M. Tazerout, "Bio-oil recovery from olive mill wastewater in sub-/supercritical alcohol-water system," *Fuel*, vol. 252, pp. 360–370, 2019.
- [90] O. Uncu and B. Ozen, "A comparative study of mid-infrared, UV-Visible and fluorescence spectroscopy in combination with chemometrics for the detection of adulteration of fresh olive oils with old olive oils," *Food Control*, vol. 105, pp. 209–218, 2019.
- [91] R. J. Mailer, "Rapid evaluation of olive oil quality by NIR reflectance spectroscopy," *Journal of the American Oil Chemists' Society*, vol. 81, no. 9, pp. 823–827, 2004.
- [92] O. Galtier, N. Dupuy, Y. Le Dréau et al., "Geographic origins and compositions of virgin olive oils determined by chemometric analysis of NIR spectra," *Analytica Chimica Acta*, vol. 595, no. 1-2, pp. 136–144, 2007.
- [93] R. M. Maggio, T. S. Kaufman, M. D. Carlo et al., "Monitoring of fatty acid composition in virgin olive oil by Fourier transformed infrared spectroscopy coupled with partial least squares," *Food Chemistry*, vol. 114, no. 4, pp. 1549–1554, 2009.
- [94] G. Gurdeniz, B. Ozen, and F. Tokatli, "Comparison of fatty acid profiles and mid-infrared spectral data for classification of olive oils," *European Journal of Lipid Science and Technology*, vol. 112, no. 2, pp. 218–226, 2010.
- [95] N. Dupuy, O. Galtier, D. Ollivier, P. Vanlout, and J. Artaud, "Comparison between NIR, MIR, concatenated NIR and MIR analysis and hierarchical PLS model. Application to virgin olive oil analysis," *Analytica Chimica Acta*, vol. 666, no. 1-2, pp. 23–31, 2010.
- [96] M. J. Lerma-García, E. F. Simó-Alfonso, A. Bendini, and L. Cerretani, "Rapid evaluation of oxidised fatty acid concentration in virgin olive oil using Fourier-transform infrared spectroscopy and multiple linear regression," *Food Chemistry*, vol. 124, no. 2, pp. 679–684, 2011.
- [97] O. Uncu and B. Ozen, "Prediction of various chemical parameters of olive oils with Fourier transform infrared spectroscopy," *LWT—Food Science and Technology*, vol. 63, no. 2, pp. 978–984, 2015.
- [98] M. Casale, P. Oliveri, C. Casolino et al., "Characterisation of PDO olive oil Chianti Classico by non-selective (UV-visible, NIR and MIR spectroscopy) and selective (fatty acid composition) analytical techniques," *Analytica Chimica Acta*, vol. 712, pp. 56–63, 2012.
- [99] A. M. Inarejos-García, S. Gómez-Alonso, G. Fregapane, and M. D. Salvador, "Evaluation of minor components, sensory characteristics and quality of virgin olive oil by near infrared (NIR) spectroscopy," *Food Research International*, vol. 50, no. 1, pp. 250–258, 2013.
- [100] E. Valli, A. Bendini, R. M. Maggio et al., "Detection of low-quality extra virgin olive oils by fatty acid alkyl esters evaluation: a preliminary and fast mid-infrared spectroscopy discrimination by a chemometric approach," *International Journal of Food Science & Technology*, vol. 48, no. 3, pp. 548–555, 2013.
- [101] J. A. Cayuela, "Rapid NIR determination of alkyl esters in virgin olive oil," *Grasas Y Aceites*, vol. 68, no. 2, p. 195, 2017.
- [102] V. Lagouri, V. Manti, and T. Gimisis, "Optical non-destructive UV-Vis-NIR-MIR spectroscopic tools and chemometrics in the monitoring of olive oil functional compounds: bioactivity, chemistry and processing," in *Book: Olives and Olive Oil as Functional Foods: Bioactivity, Chemistry and Processing. Chapter 11*, A. Kiritsakis and S. Fereidoon, Eds., , Shahidi Wiley and Sons Ltd., Hoboken, NY, USA, 1st edition, 2017.
- [103] N. Nenadis and M. Z. Tsimidou, "Perspective of vibrational spectroscopy analytical methods in on-field/official control of olives and virgin olive oil," *European Journal of Lipid Science and Technology*, vol. 119, no. 1, article 1600148, 2017.
- [104] I. Gouvinhas, J. M. M. M. de Almeida, T. Carvalho, N. Machado, and A. I. R. N. A. Barros, "Discrimination and characterisation of extra virgin olive oils from three cultivars in different maturation stages using Fourier transform infrared spectroscopy in tandem with chemometrics," *Food Chemistry*, vol. 174, pp. 226–232, 2015.
- [105] M. E. Mora-Ruiz, P. Reboredo-Rodríguez, M. Desamparados Salvador et al., "Assessment of polar phenolic compounds of virgin olive oil by NIR and mid-IR spectroscopy and their impact on quality," *European Journal of Lipid Science and Technology*, vol. 119, no. 1, article 160009, 2017.
- [106] I. Fratoddi, M. Rapa, G. Testa, I. Venditti, F. A. Scaramuzzo, and G. Vinci, "Response surface methodology for the optimization of phenolic compounds extraction from extra virgin olive oil with functionalized gold nanoparticles," *Microchemical Journal*, vol. 138, pp. 430–437, 2018.
- [107] A. Hirri, M. Bassbasi, S. Souhassou, F. Kzaiber, and A. Oussama, "Prediction of polyphenol fraction in virgin olive oil using mid-infrared attenuated total reflectance attenuated total reflectance accessory-mid-infrared coupled with partial least squares regression," *International Journal of Food Properties*, vol. 19, no. 7, pp. 1504–1512, 2016.
- [108] A. Bellincontro, A. Taticchi, M. Servili, S. Esposto, D. Farinelli, and F. Mencarelli, "Feasible application of a portable NIR-AOTF tool for on-field prediction of phenolic compounds during the ripening of olives for oil production," *Journal of Agricultural and Food Chemistry*, vol. 60, no. 10, pp. 2665–2673, 2012.
- [109] S. Trapani, M. Migliorini, L. Cecchi et al., "Feasibility of filter-based NIR spectroscopy for the routine measurement of olive oil fruit ripening indices," *European Journal of Lipid Science and Technology*, vol. 119, no. 6, article 1600239, 2017.
- [110] J. A. Cayuela and J. F. García, "Sorting olive oil based on alpha-tocopherol and total tocopherol content using

- near-infra-red spectroscopy (NIRS) analysis,” *Journal of Food Engineering*, vol. 202, pp. 79–88, 2017.
- [111] C. Lazzerini, M. Cifelli, and V. Domenici, “Pigments in extra-virgin olive oil: authenticity and quality,” in *Products from Olive Tree, Chapter 6*, D. Boskou and M. L. Clodoveo, Eds., pp. 99–114, InTech, Rijeka, Croatia, 1st edition, 2016.
- [112] C. Lazzerini and V. Domenici, “Pigments in extra-virgin olive oils produced in Tuscany (Italy) in different years,” *Foods*, vol. 6, no. 4, p. 25, 2017.
- [113] O. Uncu, B. Ozen, and F. Tokatli, “Use of FTIR and UV-visible spectroscopy in determination of chemical characteristics of olive oils,” *Talanta*, vol. 201, pp. 65–73, 2019.
- [114] E. Borello and V. Domenici, “Determination of pigments in virgin and extra-virgin olive oils: a comparison between two near UV-vis spectroscopic techniques,” *Foods*, vol. 8, no. 1, p. 18, 2019.
- [115] J. A. Cayuela and J. F. García, “Nondestructive measurement of squalene in olive oil by near infrared spectroscopy,” *LWT*, vol. 88, pp. 103–108, 2018.
- [116] X. Lu and B. A. Rasco, “Determination of antioxidant content and antioxidant activity in foods using infrared spectroscopy and chemometrics: a review,” *Critical Review of Food Science and Nutrition*, vol. 52, no. 10, pp. 853–875, 2011.
- [117] D. Cozzolino, “Infrared spectroscopy as a versatile analytical tool for the quantitative determination of antioxidants in agricultural products, foods and plants,” *Antioxidants*, vol. 4, no. 3, pp. 482–497, 2015.
- [118] L. Cerretani, A. Giuliani, R. M. Maggio, A. Bendini, T. Gallina Toschi, and A. Cichelli, “Rapid FTIR determination of water, phenolics and antioxidant activity of olive oil,” *European Journal of Lipid Science and Technology*, vol. 112, no. 10, pp. 1150–1157, 2010.

Research Article

Rapid Recognition of Geoherbalism and Authenticity of a Chinese Herb by Data Fusion of Near-Infrared Spectroscopy (NIR) and Mid-Infrared (MIR) Spectroscopy Combined with Chemometrics

Haiyan Fu,¹ Qiong Shi ,¹ Liuna Wei,¹ Lu Xu ,² Xiaoming Guo,¹ Ou Hu,¹ Wei Lan,¹ Shunping Xie,³ and Tianming Yang ¹

¹The Modernization Engineering Technology Research Center of Ethnic Minority Medicine of Hubei Province, College of Pharmacy, South-Central University for Nationalities, Wuhan 430074, China

²College of Material and Chemical Engineering, Tongren University, Tongren 554300, Guizhou, China

³State Key Laboratory Breeding Base of Green Chemistry-Synthesis Technology, College of Chemical Engineering, Zhejiang University of Technology, Hangzhou 310032, China

Correspondence should be addressed to Lu Xu; lxchemo@163.com and Tianming Yang; tmyang@mail.scuec.edu.cn

Received 30 May 2018; Revised 14 December 2018; Accepted 28 March 2019; Published 30 April 2019

Academic Editor: Massimo Lucarini

Copyright © 2019 Haiyan Fu et al. This is an open access article distributed under the Creative Commons Attribution License, which permits unrestricted use, distribution, and reproduction in any medium, provided the original work is properly cited.

Fourier transform near-infrared (NIR) spectroscopy and mid-infrared (MIR) spectroscopy play important roles in all fingerprint techniques because of their unique characteristics such as reliability, versatility, precision, and ease of measurement. In this paper, a supervised pattern recognition method based on the PLSDA algorithm by NIR and the NIR-MIR fusion spectra has been established to identify geoherbalism of *Angelica dahurica* from different regions and authenticity of *Corydalis yanhusuo* W. T. Wang. Comparing principle component analysis (PCA) cannot successfully identify geographical origins of *Angelica dahurica*. Linear discriminant analysis (LDA) also hardly distinguishes those origins. Furthermore, the PLSDA model based on the data fusion of NIR and IR was more accurate and efficient. But, the identification of authenticity of *Corydalis yanhusuo* W. T. Wang was still inaccurate in the PLSDA model. Consequently, data fusion of NIR-MIR original spectra combined with moving window partial least-squares discriminant analysis was firstly used and showed perfect properties on authenticity and adulteration discrimination of *Corydalis yanhusuo* W. T. Wang. It indicated that data fusion of NIR-MIR spectra combined with MWPLSDA could be considered as the promising tool for rapid discrimination of the geoherbalism and authenticity of more Chinese herbs in the future.

1. Introduction

Herbal medicines are of effective pharmacological functions, low toxicity, and less side effects to human body, so they have been widely used all over the world [1–3]. However, herbal medicines with different geographical origins have different chemical compositions and pharmacological activities [4, 5]. In addition, the processing of herbal medicines often removes morphological properties of species, and some herbal medicines at high cost are often the subject of fraudulent practices by replacing them with ones at low cost [6, 7], which may lead to an unfair competition in the pharmaceutical and harm the interest of consumers. Thus, the quality analysis method of

herbal medicines to distinguish the origins is an important concern for consumers [8–10]. Traditional methods such as high-performance liquid chromatography and mass spectroscopy are time-consuming, expensive, and laborious and have to be performed by highly trained technicians [11, 12]. Therefore, a rapid, more accurate, and sensitive identification method is required to determine herbal medicines.

Most studies focused on specific pharmacological ingredients in herbal medicines; however, the pharmacological activity of herbs is the result of the interaction of all ingredients rather than specific ingredients. Therefore, the specific ingredients could not be used as a proper criterion for characterization of the overall quality of the herbs

[13, 14]. Fourier transform mid-infrared (MIR) [15] and near-infrared (NIR) [16, 17] techniques are efficient tools for studying food and pharmaceutical quality control because of their fast and nondestructive analytical characteristics. For example, Zhu et al. used FT-IR and 2DCOS-IR methods to discriminate the cultivated *Codonopsis lanceolata* in different ages [18], and in the research done by Gayo and Hale, near-infrared spectroscopy was applied to detect and quantify the species authenticity in Crabmeat [19]. By studying the characteristic information of the spectra, different types of samples can be accurately distinguished. Nonetheless, the information obtained from by NIR spectra may be difficult to interpret directly because of the highly overlapped spectra. Although MIR spectra provide some significant differences of spectral peaks, they do not give abundant chemical and structural information of samples like NIR spectra. Therefore, establishing effective and robust chemometric methods has been extensively concerned [20, 21]. For example, Woo's team used Mahalanobis distance and discriminant PLS2 combined with NIR spectroscopy to discriminate herbal medicines according to geographical origins, but there are only two different classes from different geographical origins [22]. Frizon et al. used the PLS in determination of total phenolic compounds in yerba mate and predicted total phenolics with associated errors of 12% [23]. Liu et al. studied on the differentiation of the root of various ginseng by FT-IR and two-dimensional correlation IR spectroscopy, and the cluster analysis demonstrated that the three kinds of ginseng can be distinguished clearly from each other but with an exception [24]. PCA is a multivariate statistical technique that reduces the multidimensionality of data while minimizing information loss [25]. LDA can establish linear transformations to find the best boundary and achieve maximum separation between classes by constructing discriminant functions [26]. From another aspect, as a powerful pattern recognition method, PLSDA has successfully been applied to solve classification problems in many scientific fields [27, 28]. Furthermore, a global model with moving window partial least-squares (MWPLS) [29, 30] like other variable selection methods, MWPLSDA was successfully applied to spectra interval selection for calibration problems, and desirable results were obtained [31]. A subset of the whole wavelengths to develop the calibration model, the wavelengths carrying serious heteroscedastic noises, and especially the spectral ranges contaminated by external factors are excluded from the model, and wavelength ranges sensitive only to the chemical compositions of the samples are selected to develop a simplified yet stable calibration model.

Sometimes, it is difficult to discriminate the origins of herbal medicines only through the pattern recognition method by single NIR or MIR spectra [32] combined with chemometrics, and it is necessary to extract from the data fusion of NIR and MIR spectroscopy [33]. There is abundant information related to combinatory MIR and NIR spectroscopy coupled with chemometrics for quality control of herbal medicines.

In this study, different supervised pattern recognition algorithms including principal component analysis

(PCA), linear discriminant analysis (LDA), and partial least squares discriminant analysis (PLSDA) with raw NIR spectra were used to discriminate five different geographical origins of *Angelica dahurica*. Moreover, moving window partial least-squares discriminant analysis (MWPLSDA) and the fusion spectra variables evaluate authenticity and adulteration of *Corydalis yanhusuo* W. T. Wang. The result shows that PLSDA model is of great performance than PCA and LDA in identifying geographical origins of herbal medicines. In addition, the full spectra information fused by NIR and MIR combined with MWPLSDA showed the best ability in determination of authenticity of herbal medicines. This method provides pattern recognition models that can be applied in geographical origin discrimination or authenticity and adulteration recognition at the same time and can further be widely used in various herbal medicines.

2. Material and Methods

2.1. Collection of Raw Materials. A total of 50 *Angelica dahurica* samples from five geographical origins (Hebei, Anhui, Yunnan, Zhejiang, and Sichuan) were purchased from the Derentang pharmacy, and each region included 10 batches. Besides, two kinds of authentic *Corydalis yanhusuo* W. T. Wang (Zhejiang) were purchased from the Derentang pharmacy and the Kangderuiqi flagship store, while three kinds of adulterations *Corydalis decumbens* (Thunb.) Pers., *Typhonium flagelliforme* (Lodd.) Blume, and *Dioscorea opposita* (Thunb.) were, respectively, collected from Anhui, Jiangsu, and Fujian, and the aforementioned five samples for identification of adulteration were collected in 10 batches.

2.2. Apparatus. The following apparatuses were used: Nicolet 6700 FT-IR, OMNIC 8.2 spectral collecting software (Thermo Fisher Scientific Inc., USA); Antaris II FT-NIR spectrometer, RESULT 3.0 spectral collecting software (Thermo Electron Co., USA); DZF-6021 vacuum oven (Shanghai YIHENG Technical Co., Ltd); and FW135 herbal grinder (Tianjin Taisite Instrument Co., LTD).

2.3. Methods of Sample Measurement and Data Preprocessing by NIR and MIR. All samples used in NIR were crushed with the grinder, sieved into fine powders by a 200 mesh sieve, then vacuum-dried at 60°C for 24 hours, and stored in a dryer spare. The sample powder was placed directly into the quartz cup, and the air background was subtracted. Spectra were collected by integrating sphere diffuse reflectance with the collecting region at 4000–10000 cm^{-1} and a resolution of 8 cm^{-1} . Data processing was performed using the average of the five measured spectra for each sample. In total, 250 spectra from different geographic origins (5 samples \times 10 batched \times 5 measurements) were obtained. And 250 spectra were discriminated for the authenticity and adulteration of *Corydalis yanhusuo* W. T. Wang.

2.4. Method of Chemometrics. PCA, LDA, PLSDA, and MWPLSDA methods were written and performed through a Matlab 2010a (MathWorks, Natick, MA, USA). All pre-processing in those chemometrics only used the original spectra. PLSDA is based on the simultaneous decomposition response matrix and the class matrix extraction factor. By arranging the extraction factors in order of their correlation, the virtual vectors are encoded to represent different classes, wherein the virtual vector f_j encoded for the j th element is 1. The other elements are 0 for the j th class, and then each column of the response matrix is associated with the class matrix. The principle of moving window partial least-squares discriminant analysis (MWPLSDA) is that a suitable window moves along the full spectral interval according to our past study [34, 35]. In MWPLSDA, a suitable window of width H is constructed and moved along the entire spectrum to select useful wavelength intervals, and then the selected spectral spacing is used to construct the PLSDA model. The principle of MWPLSDA is based on the virtual setting of a window, which contains the number of variables from the first wavelength to the end of $(i+H-1)$ wavelength. A series of submatrices are obtained continuously by moving the window. According to the variables in the moving window, a series of PLS submodels are constructed. Then, according to the principle of least residual square (SSR), the interval of measurement matrix with smaller classification error and latent variable is selected as the final MWPLSDA model.

3. Results and Discussion

3.1. Geographical Origin Discrimination of *Angelica dahurica* by NIR. In order to analyze the five different samples more effectively, the classical quick data analysis, and non-destructive analytical technique, NIR was used in the measurement. The average NIR spectra of each group are displayed to reflect the overlay in Figure 1. The peaks located at 8319 cm^{-1} might be associated with the second overtone of C-H, O-H, and N-H stretching modes and those around 6780 cm^{-1} were caused by the C-H deformation vibration of CH_3 . Due to the second overtone of the C=O stretching vibration, bands at 5164 cm^{-1} emerge and the C-H combination and second overtone can be seen at $4200\text{--}4300\text{ cm}^{-1}$. However, owing to the overlaps and the systematic noise in NIR spectra, chemometric methods were required to extract useful information for the recognition of *Angelica dahurica* samples. Herein, three classical chemical pattern recognition methods using principal component analysis (PCA), linear discriminant analysis (LDA), and partial least squares discriminant analysis (PLSDA) models were associated with virtual coding of original NIR spectral variables of different sample sets. The 250 sample spectra of five different *Angelica dahurica* samples were randomly divided into a training set and a prediction set (Table 1). The model was built using the training set, the number of latent variables (LVs) was determined to be 5 by eightfold cross-validation using the prediction set, and the discrimination results were analyzed for comparison.

Firstly, as a common method in the chemical pattern recognition which is mainly used for classification in the analytical processes of Chinese herbal identification, principal component analysis (PCA) is one of the most classic high-dimensional methods, which reduces the high-dimensional data of FTNIR and converts 1557 raw variables into fewer new principal components. PCA used fewer principal component features to represent the original features of the sample by decomposing the sample matrix in the training set and prediction. Based on the PCA technology, the vector scores of the training and prediction sets of the aforementioned samples are reflected in Figure 1(b), and all samples from five different geographic origins in the training and prediction sets could not be clearly distinguished, but these samples were with same shape. This phenomenon could be attributed to small differences in the chemical properties reflected in its geographical origin. The results demonstrated that the PCA method can effectively reduce and extract fewer new variables from the original high-dimensional data, but the restoration process also leads to loss some information useful for sample differentiation.

Other than looking for the vector space that can best describe the original data like PCA, linear discriminant analysis (LDA) is a linear discriminant function based on input response variables for searching linear transformations and dimensionality reduction. The axes of interest for LDA can maximize the distinction between classes, projecting feature spaces (multidimensional samples in the dataset) into smaller dimensional k -dimensional subspaces while maintaining information that distinguishes categories. Figure 1(c) shows the vector scores of the first two latent variables based on the LDA model for the training and prediction sets of samples. It clearly distinguished samples from different geographical origins in the training set, while those in the prediction set were not clearly distinguished. The result may be due to some special requirements of the LDA model, of which at least one of the needs to be nonsingular. In addition, when the so-called outlier class dominates in estimating the scattering matrix, the LDA model cannot guarantee that the optimal subspace is found [36]. Furthermore, PLSDA can reduce the effects of multicollinearity between variables, and it can simultaneously decompose the extraction factors of the prediction measurement matrix and the class matrix and arrange them according to the correlation between them. Five different geographical sources of *Angelica dahurica* are identified based on the maximum virtual coding position of the NIR spectral data. In order to optimize the predictive power of the PLSDA model and simplify the complexity of the PLSDA model, we selected the number of latent variables (LV) as 5 by 8-fold cross-validation. Figure 1(d) shows the plots of dummy codes of the training and prediction sets for five group samples of different geographic origins. Table 1 shows the virtual code attribution maps for the training and prediction sets of the original spectra in the PLSDA model. We encode five sets of samples into f_1 (1, 0, 0, 0, 0), f_2 (0, 1, 0, 0, 0), f_3 (0, 0, 1, 0, 0), f_4 (0, 0, 0, 1, 0), and f_5 (0, 0, 0, 0, 1), respectively, according to the position of the largest virtual code. As shown in Figure 1(d), all training and prediction samples belonging to

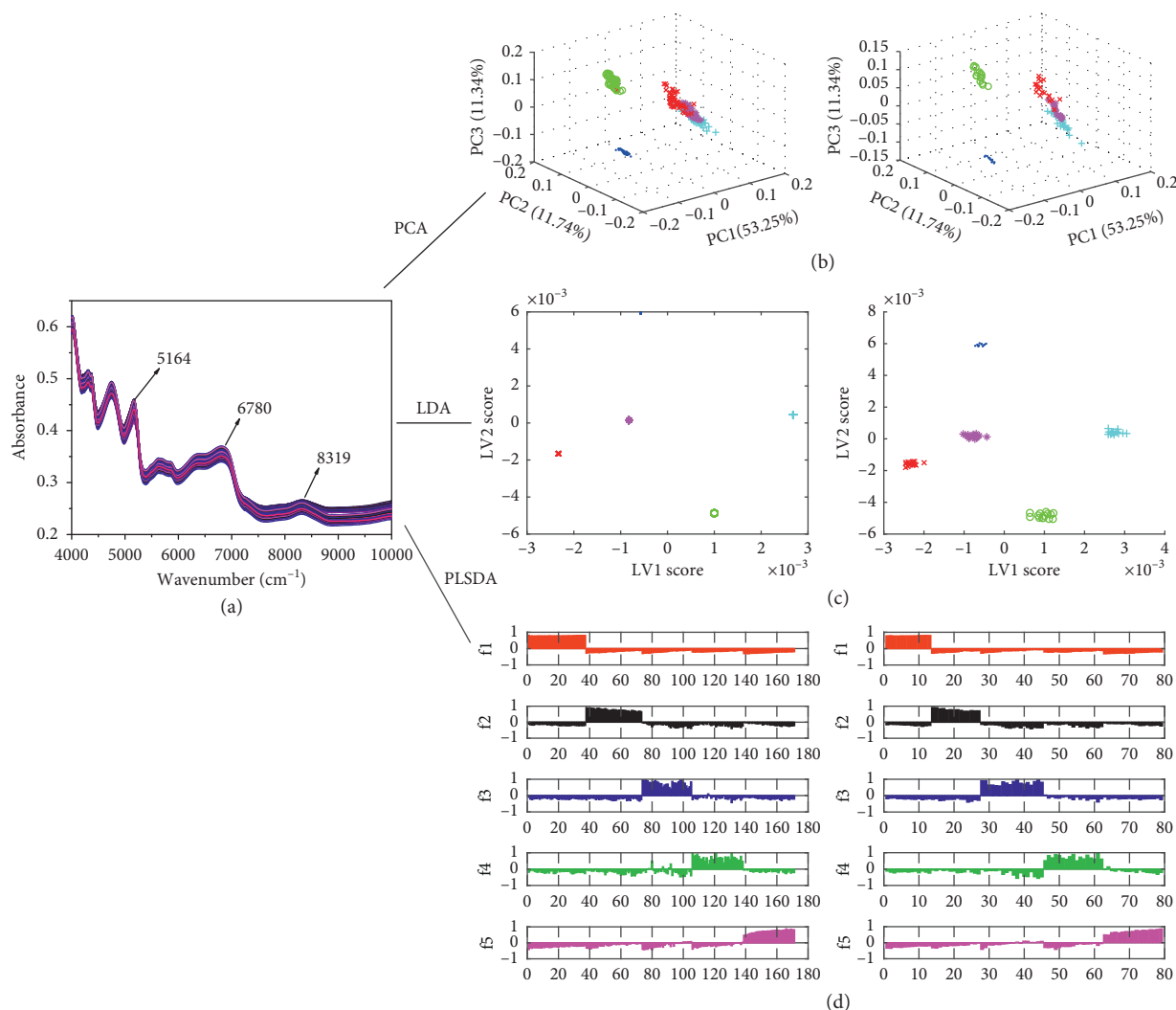


FIGURE 1: The raw NIR spectra of five different origins of *Angelica dahurica* (a) and the results by PCA (b), LDA (c), and PLSDA (d).

TABLE 1: A detailed list for the training set and the prediction set of five different kinds of *Angelica dahurica* samples.

Groups code	f1	f2	f3	f4	f5
Sample group	1	2	3	4	5
Symbol	.	○	×	+	*
PCA, LDA, or PLSDA training set	1st–37th	38th–73rd	74th–105th	106th–138th	139th–171st
PCA, LDA, or PLSDA prediction set	1st–13th	14th–27th	28th–45th	46th–62nd	63rd–79th

all groups of *Angelica dahurica* by original NIR spectra combined with PLSDA were identified accurately with a perfect recognition rate of 100%. This demonstrated that the PLSDA model successfully discriminates *Angelica dahurica* samples of different geographic origins. This further revealed that NIR spectroscopy combined with PLSDA method can be used to identify herbal medicines more rapidly, effectively, and reliably than the traditional ones.

3.2. Authenticity and Adulteration Discrimination of *Corydalis yanhusuo* W. T. Wang by NIR and Combinatory of NIR. Herbal medicine processing often removes morphological properties of species, which leads to failure of distinguishing

one type from another. For this reason, NIR spectra were used to discriminate the authenticity and adulteration of *Corydalis yanhusuo* W. T. Wang. As is shown Figure 2(a), the peaks around 6826 cm^{-1} were due to the C-H deformation vibration of CH_3 . Due to the C-H first overtone of $-\text{CH}_2-$ groups, bands at 5800 and 5600 cm^{-1} were observed and bands at 5172 cm^{-1} were the second overtone of the C=O stretching vibration. Furthermore, the C-H combination and second overtone can be seen at $4200\text{--}4300\text{ cm}^{-1}$. The seriously overlapped raw spectra hardly reflect the differences between samples. Thus, PCA technology and LDA and PLSDA models were used to relate the dummy code for the full original and preprocessing spectral variables. 250 sample spectra of two kinds of authenticity,

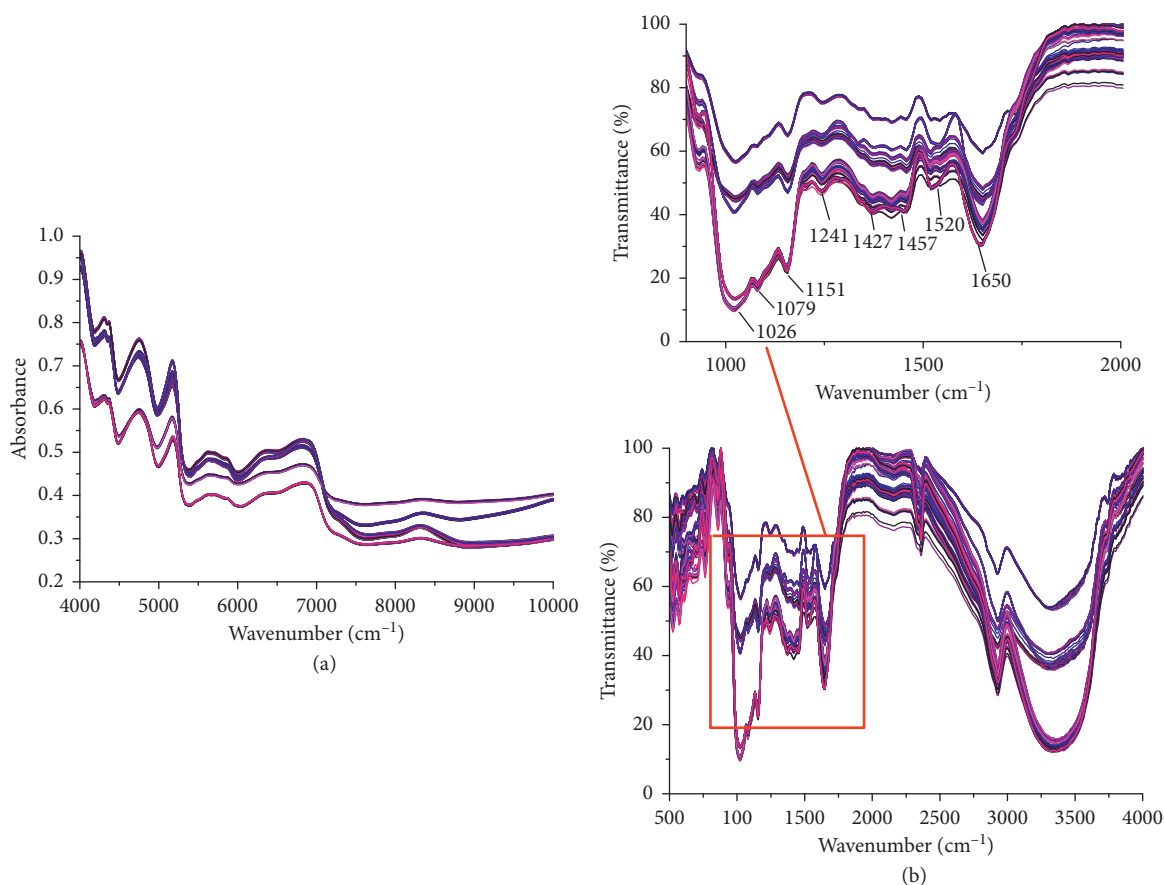


FIGURE 2: Raw NIR (a) and MIR (b) spectra of two kinds of *Corydalis yanhusuo* W. T. Wang, *Corydalis decumbens* (Thunb.) Pers, *Typhonium flagelliforme* (Lodd.) Blume, and *Dioscorea opposita* (Thunb.).

Corydalis yanhusuo W. T. Wang 1 and 2, and three kinds of adulteration, *Corydalis decumbens* (Thunb.) Pers. (3), *Typhonium flagelliforme* (Lodd.) Blume (4), and *Dioscorea opposita* (Thunb.) (5) were randomly divided into the training set and the prediction set (Table 2). However, both PCA technology and LDA model failed to show the correct results in prediction sets for five different groups by NIR (not shown here). Thus, PLSDA was adopted for the identification of authentic *Corydalis yanhusuo* W. T. Wang.

In our work, all training and prediction samples were correctly identified except for the two samples in the training set (34th and 88th) and the two samples in the prediction set (35th and 82nd). The 34th sample in the training set of f2 is incorrectly discriminated as f1, and the 84th sample of f5 is erroneously classified as f2. Furthermore, the 35th sample in the prediction set of f2 is incorrectly assigned as f3, and the 82nd sample in the prediction set belonging to f5 is incorrectly classified as f2. It may account for the useless information of some spectral variables. The total correction rate was 97.94% on the test set in PLSDA models. On the other hand, MIR spectroscopy provides more specific and distinct absorption bands than NIR spectroscopy. As is shown in Figure 2(b), the band centered at 2931 cm⁻¹ is due to a stretching vibration of aliphatic C-H in terminal CH₃ groups. The strong single peak of the C=O stretching vibration of ketone groups is observed at about 1635 cm⁻¹,

whereas the band centered at 1250 cm⁻¹ is due to the antisymmetric stretching vibrations of =C-O-C.

In order to better identify the origin of Chinese herbal medicines, we combined the mid-infrared spectrum with the near-infrared spectrum to obtain fusion spectra with more abundant sample information (Figure 3). The PLSDA was also applied to relate the dummy code for the full fused spectral variables.

As is shown in Figure 3(a), only the 17th sample in the prediction set of f1 was misclassified as f2 in fusion spectra (Table 3). It suggested that fusion spectra of NIR and MIR spectroscopy combined with PLSDA has better use in authenticity and adulteration discrimination of *Corydalis yanhusuo* W. T. Wang. But, it also failed to get 100% predictive accuracy.

In MWPLSDA, the appropriate window with H width is constructed, and the useful wavelength range is selected by moving the whole spectrum. Then, all the selected windows are constructed into the PLSDA model. Finally, according to the minimum SSR principle of the MWPLSDA algorithm, the feature differences among the five samples are extracted. As shown in Figure 3(b), when the window size is 20, the optimum number of potential variables in the MWPLSDA model is 12. Figure 3(b) shows that when the number of variables in the fusion spectrum of NIR and MIR is 140-200, 750-930, and 1250-1380, the SSR is the smallest. At this time, MWPLS-DA

TABLE 2: A detailed list of two kinds of *Corydalis yanhusuo* W. T. Wang, *Corydalis decumbens* (Thunb.) Pers., *Typhonium flagelliforme* (Lodd.) Blume, and *Dioscorea opposita* (Thunb.)

Groups code	f1	f2	f3	f4	f5
Sample group	1	2	3	4	5
NIR training set	1st–33rd	34th–66th	67th–89th	90th–121st	122nd–154th
NIR prediction set	1st–17th	18th–34th	35th–61st	62nd–79th	80th–96th
Fusion training set	1st–33rd	34th–66th	67th–89th	90th–121st	122nd–154th
Fusion prediction set	1st–17th	18th–34th	35th–61st	62nd–79th	80th–96th

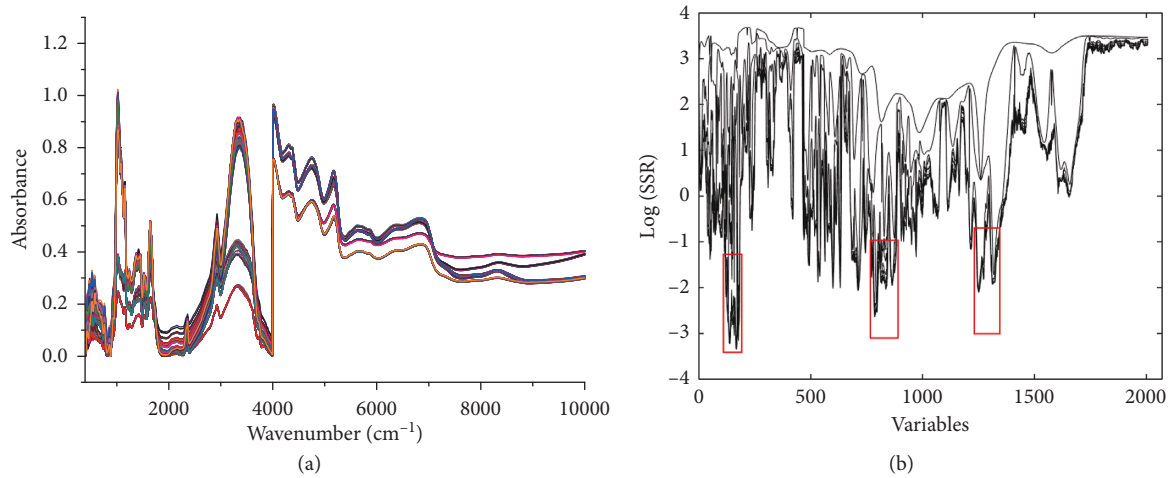


FIGURE 3: Data fusion of NIR and MIR spectroscopy for authenticity or adulteration discrimination of *Corydalis yanhusuo* W. T. Wang (a) and the residue line obtained by MWPLSDA for the training sets (b).

TABLE 3: Forecasted results of NIR-MIR fusion spectra of two kinds of *Corydalis yanhusuo* W. T. Wang, *Corydalis decumbens* (Thunb.) Pers., *Typhonium flagelliforme* (Lodd.) Blume, and *Dioscorea opposita* (Thunb.) by PLSDA and MWPLSDA.

Sample sets	Discrimination	Combinatory spectra	
		PLSDA	MWPLSDA
Training	Accuracy (%)	100	100
	Error number	0	0
Prediction	Accuracy (%)	98.97	100
	Error number	1	0

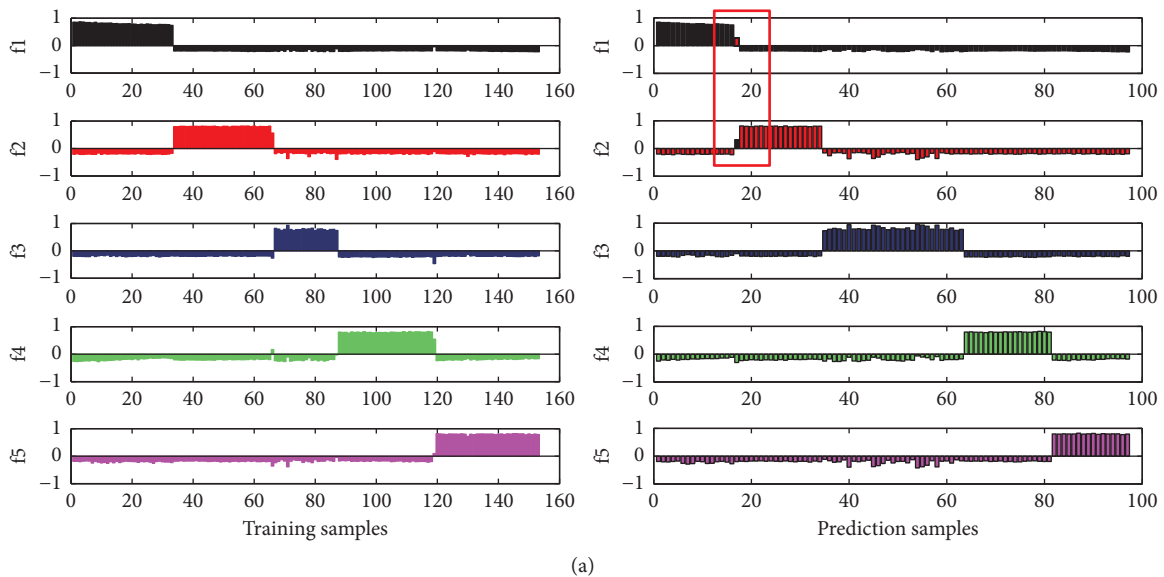


FIGURE 4: Continued.

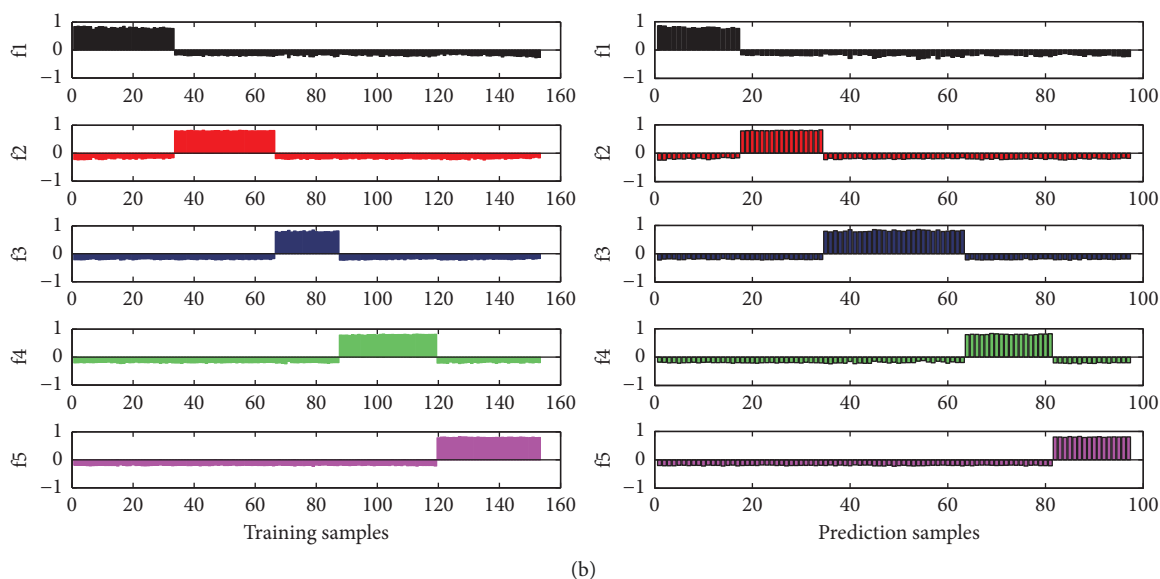


FIGURE 4: Assigned plots of dummy codes of the training set and prediction set for the raw fusion MIR-NIR spectra in the PLSDA model (a) and the MWPLSDA (b) model.

was benefited in the selection of combined informative fusion spectral regions of $660\text{--}950\text{ cm}^{-1}$, $3550\text{--}4400\text{ cm}^{-1}$, and $5900\text{--}6600\text{ cm}^{-1}$ for classification modeling of all samples and yielded the results better than that obtained from a partial least squares-discrimination analysis (PLS-DA) model built by using the whole NIR spectral region. As shown in Figure 4(b) and Table 3, all training and prediction set samples were correctly predicted by 100%. MWPLSDA can improve sample classification accuracy by eliminating useless information variables and noncomponent-related factors.

4. Conclusions

Supervised pattern recognition methods based on PLSDA and MWPLSDA algorithms by NIR and the data fusion of both NIR and MIR has been established to study *Angelica dahurica* and to identify the authenticity of *Corydalis yanhusuo* W. T. Wang. In addition, it was clarified from the results that other than PCA and LDA that can merely have well learning performance and do well in the training sets, the PLSDA model shows good performance in the area of identification of *Angelica dahurica* or *Corydalis yanhusuo* W. T. Wang and can be employed in the analysis of the geographical origins of *Angelica dahurica* and the authenticity or adulteration of *Corydalis yanhusuo* W. T. Wang. Furthermore, the full spectrum information of NIR and MIR spectroscopy combined with MWPLSDA performed much better than the single NIR spectra or PLSDA model and demonstrated an unparalleled ability of herbal medicine discrimination. This new recognition method provided a promising approach for the identification of herbal medicines widely.

Data Availability

The data used to support the findings of this study are available from the corresponding author upon request.

Conflicts of Interest

The authors declare that they have no conflicts of interest.

Acknowledgments

This work was financially supported by the National Natural Science Foundation of China (21576297, 21776321, and 21665022), the Talented Youth Cultivation Program from the “Fundamental Research Funds for the Central University,” South-Central University for Nationalities (No. CRZ18002), and the Key Research Program (Nos. 2015ZD001 and 2015ZD002) from the Modernization Engineering Technology Research Center of Ethnic Minority Medicine of Hubei Province. Lu Xu is financially supported by Guizhou Provincial Department of Science and Technology (Nos. QKHJC[2017]1186 and QKHZC[2019]2816) and the Talented Researcher Program from Guizhou Provincial Department of Education (QJHKYZ[2018]073). We also gratefully acknowledge the help of Yao Fan, Ji Yang, Li Liu, Hanyue Lan, Chuang Ni, and Yuan-Bin She.

Supplementary Materials

A figure depicting rapid recognition of geotherbalism and authenticity of herbal medicines using near-infrared, mid-infrared, and data fusion spectroscopy combined with chemometric methods. (*Supplementary Materials*)

References

- [1] F.-T. Chau, H.-Y. Chan, C.-Y. Cheung, C.-J. Xu, Y. Liang, and O. M. Kvalheim, “Recipe for uncovering the bioactive components in herbal medicine,” *Analytical Chemistry*, vol. 81, no. 17, pp. 7217–7225, 2009.
- [2] M.-Y. Lee, C.-S. Seo, J.-A. Lee et al., “Anti-asthmatic effects of *Angelica dahurica* against ovalbumin-induced airway

- inflammation via upregulation of heme oxygenase-1," *Food and Chemical Toxicology*, vol. 49, no. 4, pp. 829–837, 2011.
- [3] K.-M. Ng, Z. Liang, W. Lu et al., "In vivo analysis and spatial profiling of phytochemicals in herbal tissue by matrix-assisted laser desorption/ionization mass spectrometry," *Analytical Chemistry*, vol. 79, no. 7, pp. 2745–2755, 2007.
- [4] X. R. Liang, M. L. Ma, and W. K. Su, "Fingerprint analysis of *Hibiscus mutabilis* L. leaves based on ultra performance liquid chromatography with photodiode array detector combined with similarity analysis and hierarchical clustering analysis methods," *Pharmacognosy Magazine*, vol. 9, no. 35, pp. 238–243, 2013.
- [5] H. Zhu, Y. Wang, H. Liang, Q. Chen, P. Zhao, and J. Tao, "Identification of *Portulaca oleracea* L. from different sources using GC-MS and FT-IR spectroscopy," *Talanta*, vol. 81, no. 1-2, pp. 129–135, 2010.
- [6] Q. Jiang, W. Gao, X. Li, and J. Zhang, "Characteristics of native and enzymatically hydrolyzed *Zea mays* L., *Fritillaria ussuriensis* Maxim. and *Dioscorea opposita* Thunb. Starches," *Food Hydrocolloids*, vol. 25, no. 3, pp. 521–528, 2011.
- [7] M. S. M. Preto, M. I. B. Tavares, P. J. O. Sebastião, and R. B. V. Azeredo, "Determination of herb authenticity by low-field NMR," *Food Chemistry*, vol. 136, no. 3-4, pp. 1272–1276, 2013.
- [8] S. Y. K. Fong, M. Liu, H. Wei et al., "Establishing the pharmaceutical quality of Chinese herbal medicine: a provisional BCS classification," *Molecular Pharmaceutics*, vol. 10, no. 5, pp. 1623–1643, 2013.
- [9] S. Anubala, R. Sekar, and K. Nagaiah, "Development and validation of an analytical method for the separation and determination of major bioactive curcuminoids in *Curcuma longa* rhizomes and herbal products using non-aqueous capillary electrophoresis," *Talanta*, vol. 123, pp. 10–17, 2014.
- [10] J. Kang, L. Zhou, J. Sun, J. Han, and D.-A. Guo, "Chromatographic fingerprint analysis and characterization of furocoumarins in the roots of *Angelica dahurica* by HPLC/DAD/ESI-MSn technique," *Journal of Pharmaceutical and Biomedical Analysis*, vol. 47, no. 4-5, pp. 778–785, 2008.
- [11] M. Z. Končić, D. Kremer, W. Schühly, A. Brantner, K. Karlović, and Z. Kaloder, "Chemical differentiation of *Berberis croatica* and *B. Vulgaris* using HPLC fingerprinting," *Croatica Chemica Acta*, vol. 83, pp. 451–456, 2010.
- [12] S. Su, W. Cui, W. Zhou, J.-A. Duan, E. Shang, and Y. Tang, "Chemical fingerprinting and quantitative constituent analysis of Siwu decoction categorized formulae by UPLC-QTOF/MS/MS and HPLC-DAD," *Chinese Medicine*, vol. 8, no. 1, pp. 5–20, 2013.
- [13] D. Kumar, H. Kumar, J. R. Vedasiromoni, and B. C. Pal, "Bioassay guided isolation of α -glucosidase inhibitory constituents from *Hibiscus mutabilis* leaves," *Phytochemical Analysis*, vol. 23, no. 5, pp. 421–425, 2012.
- [14] C. Wang, S. Wang, G. Fan, and H. Zou, "Screening of antinociceptive components in *Corydalis yanhusuo* W. T. Wang by comprehensive two-dimensional liquid chromatography/tandem mass spectrometry," *Analytical and Bioanalytical Chemistry*, vol. 396, no. 5, pp. 1731–1740, 2010.
- [15] Y. Wang, P. Wang, C. Xu et al., "Macro-fingerprint analysis-through-separation of licorice based on FT-IR and 2DCOS-IR," *Journal of Molecular Structure*, vol. 1070, pp. 1–9, 2014.
- [16] J. Lu, B. Xiang, H. Liu, S. Xiang, S. Xie, and H. Deng, "Application of two-dimensional near-infrared correlation spectroscopy to the discrimination of Chinese herbal medicine of different geographic regions," *Spectrochimica Acta Part A: Molecular and Biomolecular Spectroscopy*, vol. 69, no. 2, pp. 580–586, 2008.
- [17] A. P. Craig, A. S. Franca, L. S. Oliveira, J. Irudayaraj, and K. Ilejli, "Application of elastic net and infrared spectroscopy in the discrimination between defective and non-defective roasted coffees," *Talanta*, vol. 128, pp. 393–400, 2014.
- [18] Y. Zhu, C.-H. Xu, J. Huang et al., "Rapid discrimination of cultivated *Codonopsis lanceolata* in different ages by FT-IR and 2DCOS-IR," *Journal of Molecular Structure*, vol. 1069, pp. 272–279, 2014.
- [19] J. Gayo and S. A. Hale, "Detection and quantification of species authenticity and adulteration in crabmeat using visible and near-infrared spectroscopy," *Journal of Agricultural and Food Chemistry*, vol. 55, no. 3, pp. 585–592, 2007.
- [20] L. M. Dale, A. Thewis, C. Boudry et al., "Discrimination of grassland species and their classification in botanical families by laboratory scale NIR hyperspectral imaging: preliminary results," *Talanta*, vol. 116, pp. 149–154, 2013.
- [21] H. Yang, J. Irudayaraj, and M. Paradkar, "Discriminant analysis of edible oils and fats by FTIR, FT-NIR and FT-Raman spectroscopy," *Food Chemistry*, vol. 93, no. 1, pp. 25–32, 2005.
- [22] Y.-A. Woo, H.-J. Kim, J. Cho, and H. Chung, "Discrimination of herbal medicines according to geographical origin with near infrared reflectance spectroscopy and pattern recognition techniques," *Journal of Pharmaceutical and Biomedical Analysis*, vol. 21, no. 2, pp. 407–413, 1999.
- [23] C. N. T. Frizon, G. A. Oliveira, C. A. Perussello et al., "Determination of total phenolic compounds in yerba mate (*Ilex paraguariensis*) combining near infrared spectroscopy (NIR) and multivariate analysis," *LWT—Food Science and Technology*, vol. 60, no. 2, pp. 795–801, 2015.
- [24] D. Liu, Y.-G. Li, H. Xu, S.-Q. Sun, and Z.-T. Wang, "Differentiation of the root of cultivated ginseng, mountain cultivated ginseng and mountain wild ginseng using FT-IR and two-dimensional correlation IR spectroscopy," *Journal of Molecular Structure*, vol. 883–884, pp. 228–235, 2008.
- [25] E. K. Kemsley, "Discriminant analysis of high-dimensional data: a comparison of principal components analysis and partial least squares data reduction methods," *Chemometrics and intelligent laboratory systems*, vol. 33, no. 1, pp. 47–61, 1996.
- [26] R. A. Fisher, "The use of multiple measurements in taxonomic problems," *Annals of Eugenics*, vol. 7, no. 2, pp. 179–188, 1936.
- [27] J. Peerapattana, H. Shinzawa, K. Otsuka, Y. Hattori, M. Otsuka, and J. Peerapattana, "Partial least square discriminant analysis of mangosteen pericarp powder by near infrared spectroscopy," *Journal of Near Infrared Spectroscopy*, vol. 21, no. 3, pp. 195–202, 2013.
- [28] H.-Y. Fu, D.-C. Huang, T.-M. Yang, Y.-B. She, and H. Zhang, "Rapid recognition of Chinese herbal pieces of *Areca catechu* by different concocted processes using Fourier transform mid-infrared and near-infrared spectroscopy combined with partial least-squares discriminant analysis," *Chinese Chemical Letters*, vol. 24, no. 7, pp. 639–642, 2013.
- [29] Y. P. Du, Y. Z. Liang, J. H. Jiang, R. J. Berry, and Y. Ozaki, "Spectral regions selection to improve prediction ability of PLS models by changeable size moving window partial least squares and searching combination moving window partial least squares," *Analytica Chimica Acta*, vol. 501, no. 2, pp. 183–191, 2004.
- [30] S. Fang, M. Q. Zhu, and C. H. He, "Moving window as a variable selection method in potentiometric titration multivariate calibration and its application to the simultaneous determination of ions in Raschig synthesis mixtures," *Journal of Chemometrics*, vol. 23, no. 3, pp. 117–123, 2010.

- [31] L. Xu, H. Y. Fu, C. B. Cai, and Y. B. She, "Quality degradation of Chinese white lotus seeds caused by dampening during processing and storage: rapid and nondestructive discrimination using near-infrared spectroscopy," *Journal of Analytical Methods in Chemistry*, vol. 2015, no. 12, p. 345352, 2015.
- [32] M. Casale, P. Oliveri, C. Casolino et al., "Characterisation of PDO olive oil chianti classico by non-selective (UV-visible, NIR and MIR spectroscopy) and selective (fatty acid composition) analytical techniques," *Analytica Chimica Acta*, vol. 712, pp. 56–63, 2012.
- [33] Y. Wang, M. Mei, Y. Ni, and S. Kokot, "Combined NIR/MIR analysis: a novel method for the classification of complex substances such as *Illicium verum* Hook. F. and its adulterants," *Spectrochimica Acta Part A: Molecular and Biomolecular Spectroscopy*, vol. 130, pp. 539–545, 2014.
- [34] W. Luo, S. Huan, H. Fu et al., "Preliminary study on the application of near infrared spectroscopy and pattern recognition methods to classify different types of apple samples," *Food Chemistry*, vol. 128, no. 2, pp. 555–561, 2011.
- [35] H.-Y. Fu, S.-Y. Huan, L. Xu et al., "Construction of an efficacious model for a nondestructive identification of traditional Chinese medicines liuwei dihuang pills from different manufacturers using near-infrared spectroscopy and moving window partial least-squares discriminant analysis," *Analytical Sciences*, vol. 25, no. 9, pp. 1143–1148, 2009.
- [36] H. Zhao, B. Guo, Y. Wei, and B. Zhang, "Near infrared reflectance spectroscopy for determination of the geographical origin of wheat," *Food Chemistry*, vol. 138, no. 2-3, pp. 1902–1907, 2013.

Research Article

Real-Time Release Testing of Herbal Extract Powder by Near-Infrared Spectroscopy considering the Uncertainty around Specification Limits

Guolin Shi ¹, Bing Xu ^{1,2}, Xin Wang,³ Zhong Xue,⁴ Xinyuan Shi,^{1,2} and Yanjiang Qiao ^{1,2}

¹Research Center of TCM Information Engineering, Beijing University of Chinese Medicine, Beijing 100029, China

²Beijing Key Laboratory for Production Process Control and Quality Evaluation of Traditional Chinese Medicine, Beijing 100029, China

³Tianjin Children's Hospital, Tianjin 300204, China

⁴School of Pharmacy, Hebei Medical University, Shijiazhuang 050017, China

Correspondence should be addressed to Bing Xu; xubing@bucm.edu.cn and Yanjiang Qiao; yjqiao@263.net

Received 5 October 2018; Revised 15 January 2019; Accepted 23 January 2019; Published 3 March 2019

Academic Editor: Alessandra Durazzo

Copyright © 2019 Guolin Shi et al. This is an open access article distributed under the Creative Commons Attribution License, which permits unrestricted use, distribution, and reproduction in any medium, provided the original work is properly cited.

The concept of real-time release testing (RTRT) has recently been adopted by the production of pharmaceuticals in order to provide high-level guarantee of product quality. Process analytical technology (PAT) is an attractive and efficient way for realizing RTRT. In this paper, near-infrared (NIR) determination of *cryptotanshinone* and *tanshinoneII_A* content in *tanshinone* extract powders was taken as the research object. The aim of NIR analysis is to reliably declare the extract product as compliant with its specification limits or not. First, the NIR quantification method was developed and the parameters of the multivariate calibration model were optimized. The reliable concentration ranges covering the specification limits of two APIs were successfully verified by the accuracy profile (AP) methodology. Then, with the designed validation data from AP, the unreliability graph as the decision tool was built. Innovatively, the β -content, γ -confidence tolerance intervals (β -CTIs) around the specification limits were estimated. During routine use, the boundary of β -CTIs could help decide whether the NIR prediction results are acceptable. The proposed method quantified the analysis risk near the specification limits and confirmed that the unreliable region was useful to release the product quality in a real-time way. Such release strategy could be extended for other PAT applications to improve the reliability of results.

1. Introduction

Radix *Salvia Miltiorrhizae* is the dried root of *Salvia miltiorrhiza* Bge [1]. It is widely used in several therapy systems for the treatment of angina pectoris, coronary heart disease and myocardial infarction, atherosclerosis, chronic renal failure, and liver fibrosis [2]. *Tanshinone* extract, the important components in Radix *Salvia Miltiorrhizae*, is listed in the Chinese Pharmacopoeia (ChP, 2015 edition). The *tanshinone* extract powders were generally manufactured using a series of batch operations, including extracting, filtering, concentrate, washing, drying, and milling.

Traditionally, the quality of *tanshinone* extract powder was assured by laboratory testing after the manufacturing

was completed. And two active pharmaceutical ingredients (APIs), i.e., the *cryptotanshinone* and the *tanshinoneII_A*, were assayed by the HPLC method. However, the HPLC analysis is time-consuming and requires labor-intensive protocols including sample collection, sample pre-treatment, sample analysis, and data processing procedures. Besides, this conventional approach was conducted on limited samples and had been at risk in providing qualified products to the public.

Since the promulgation of the process analytical technology (PAT) guidance in September 2004 [3], the American Food and Drug Administration (FDA) has encouraged the pharmaceutical manufacturers to adopt new technologies in pharmaceutical process, mainly for designing, analyzing,

and controlling manufacturing through timely measurements of critical quality and performance attributes of raw and in-process materials and processes with goal of ensuring final product quality. Real-time release testing (RTRT) [4], which is advocated to substitute the end-point testing, is the ability to evaluate and ensure the quality of in-process and/or final product based on process data, which typically include a valid combination of measured material attributes and process controls. Advances in quality by design (QbD) have shown that the application of RTRT in any stage of the manufacturing process and any type of finished product may provide greater assurance of product quality than finished product testing alone [5].

The rapid spectroscopy techniques are important part of RTRT plans. Near-infrared (NIR) spectroscopy has proven to be effective for both qualitative [6–8] and quantitative analysis [9–12] in the pharmaceutical industry due to its high efficiency, nondestructive nature, and capacity to measure both physical and chemical properties with minimal or no sample preparation [13]. It is more and more considered as an attractive and promising analytical tool for PAT. Recently, the NIR spectroscopy has been introduced into the Chinese herbal medicine production processes, such as the extraction process of *Epimedium brevicornum* Maxim [14] and *Qizhiweitong* granules [15], the alcohol precipitation process of *Reduning* injection [16], the purification process of *Aesculi semen* extracts [17], the enrichment process of *Danhong* injection [18], the fluidizing drying process of *Poria cocos* formula granules [19], and the mixing process [20]. By summarizing the NIR analysis results of Chinese medicine materials from the reported literatures, it was found that the relative standard errors of prediction (RSEP) were in the range of 1.51% to 10.41% [13–19] and the prediction error of some herbal samples exceeded the general target acceptance criteria for bulk drug (2%) or dosage form (10%) [21]. Therefore, the operable region and unreliability region of these analytical methods should be judged to confirm their scope of application.

Conventionally, the performance of the NIR analytical method was evaluated by chemometric indicators [22–25], such as the root-mean-square error (RMSE) [26], the correlation coefficient (r), the ratio of performance to deviation (RPD) [27], which only gave the average level of information about errors and bias of NIR method and did not provide the uncertainty of each individual prediction over the range of measurement [28]. Therefore, more and more researchers adopted the accuracy profile (AP) approach to evaluate the risk or confidence of the NIR method [29–32]. The core of the AP methodology, in agreement with the ICH Q2A guidance, is to use the β -expectation tolerance interval (β -ETI) to integrate the trueness, the intermediate precision coefficient variation, as well as the β chance for future results [33]. Based on the validation results from the AP approach, Rozet et al. [34] further identified the unreliable region around the specification limit by intersection of the upper and lower β -ETIs with the specification limit. Such methods were successfully applied for HPLC-UV quantification of (R)-timolol impurity in (S)-timolol drug substance and for NIRS quantification of acetaminophen in the uniformity of dosage units (UDU) test [34, 35].

As reported by Saffaj et al., the β -content, γ -confidence tolerance interval (β -CTI) could provide a better estimate of measurement risk than β -expectation tolerance interval and gave the best guarantee concerning the decision of declaring a method as valid and reliable [36–38]. Our previous work also revealed that the overall uncertainty estimated by the β -CTI from the total error (bias and standard deviation) was similar to the overall uncertainty assessed from validation data according to the trueness, precision, and robustness experiments [39]. In this work, NIR was used as a rapid detective tool to assay the APIs content of *tanshinone* extract powder. The traditional figures of merit were used to optimize the multivariate calibration model. A full factorial design generating the validation data was used to calculate statistical intervals. The β -content, γ -confidence tolerance interval was for the first time used to develop the unreliable region around the specification limit of *tanshinone* extract powder, in order to increase the confidence when releasing the multicomponents natural product in a real-time way.

2. Experimental

2.1. Reagents and Materials. The *tanshinone* extract powders were purchased from Xi'an Changyue Phytochemistry Co., Ltd (Xi'an, China, lot: 140420), Xi'an Honson Biotechnology Co., Ltd. (Xi'an, China, Lot: 141029.) and Shanxi Undersun Bimedtech Co., Ltd (Shanxi, China, Lot: Udst130507). The *cryptotanshinone* reference standard (lot number: 110852–200806) and *tanshinoneII_A* reference standard (lot number: 110776–200619) were purchased from the National Institutes for Food and Drug Control (Beijing, China). The acetonitrile and phosphoric acid of HPLC grade were purchased from the Thermo Fisher Scientific Inc. (Massachusetts, USA), and pure water was purchased from Wahaha Co., Ltd. (Hangzhou, China).

2.2. Acquisition of Spectroscopic Data. The sample was held in a circular sample cuvette with a solid cap, and the NIR spectra were collected in the integrating sphere diffuse reflectance mode with the Antaris Nicolet FT-NIR system (Thermo Fisher Scientific Inc., USA) at ambient temperature. Each spectrum was the average of 64 scans with 8 cm^{-1} resolution. The range of spectra was from 10000 to 4000 cm^{-1} . The background spectrum was taken daily in air.

2.3. Reference Method. The reference method used for *cryptotanshinone* and *tanshinoneII_A* determination was HPLC assay recommended by the Chinese Pharmacopoeia (2015 Edition) for the extract of *Salvia miltiorrhiza* Bge. Firstly, samples were dissolved by methanol properly after NIR scanning. Then, the solution was filtered through a Millipore membrane filter with an average pore diameter of $0.45\text{ }\mu\text{m}$. Finally, $10\text{ }\mu\text{L}$ of filtrate was injected into the HPLC system for analysis.

An Agilent 1100 series HPLC apparatus, equipped with a quaternary solvent delivery system, an auto sampler, a DAD detector, and HP workstation for data processing were used. The concentration of *cryptotanshinone* and *tanshinoneII_A*

were analyzed by reverse-phase chromatography on an Agilent XDB C18 column (4.6 × 250 mm, 5 μm) with gradient. The mobile phase A is acetonitrile, and the mobile phase B is phosphoric acid water (0.026%). The elution procedures are as follows: 0~25 min, 60%~90% A; 25~30 min, maintaining 90% A; 30~31 min, 90%~60% A; 31~40 min, 60%~60% A. The column temperature was 25°C, the flow rate was 1.2 mL·min⁻¹, and the detection wavelength at 270 nm was set.

2.4. Calibration and Validation Protocols. The experimental protocols were created for both calibration and validation sets in order to obtain a robust model. A total of 103 samples were collected in the calibration set. Four grams of *tanshinone* extract powder sample was weighed and then directly measured by NIR under the conditions specified in Section 2.2.

The external validation set was built with the same method as the calibration set. The validation protocol used the “8 × 5 × 3” full factorial experimental design. Eight different concentration levels of *cryptotanshinone*, i.e., 0.20%, 0.31%, 0.50%, 1.18%, 2.05%, 2.26%, 5.29%, and 9.68%, were investigated. Eight different concentration levels of *tanshinoneII_A*, i.e., 0.10%, 0.15%, 0.36%, 0.54%, 2.04%, 6.03%, 18.76%, and 27.64%, were investigated. Each concentration level was performed in 5 replicates on 3 different days, resulting in 120 samples in the validation set for both two components. Moreover, all validation samples were from different batches of *tanshinone* extract powders to test the robustness of the NIR model.

2.5. NIR Method Development. To perform the quantitative determination of *cryptotanshinone* and *tanshinoneII_A* content in *tanshinone* extract powders, the partial least squares (PLS) regression was applied for the sake of linking the NIR spectra with the reference values analyzed by the HPLC method [39]. In order to improve the performance of the PLS model, a variety of spectroscopic data pretreatment methods were investigated to extract the useful information. For example, the first-order derivatives (1std) [40], the second-order derivatives (2ndd) [41] could be used to remove the baseline drift and decrease the overlapping. The multiplicative scatter correction (MSC) [42, 43] and the standard normal variate transformation (SNV) [44] could reduce the light scattering effects. The wavelet denosing of spectra (WDS) [45] and the Savitzky–Golay (SG) smoothing [46] can effectively eliminate the noise.

During the NIR method development process, correlation coefficients r for both the calibration and validation sets, the root-mean-square error of calibration (RMSEC), the root-mean-square error of cross-validation (RMSECV), the root-mean-square error of prediction (RMSEP), and RPD were used to evaluate and select the best NIR calibration model. The optimal latent variables (LVs) used to build PLS model were selected according to comprehensive consideration of RMSEC, RMSECV, RMSEP, and cumulative prediction error sum of square (PRESS) values.

2.6. The Unreliability Graph. The unreliability graph as a decision making tool is a 2D-graphical representation of tolerance intervals aiming at helping the analyst to decide whether an analytical result is reliable or not. For details about the theory, the authors are recommended to refer to the published literatures [36, 47].

2.6.1. Estimation of the β -Content, γ -Confidence Tolerance Interval. The “ $I \times J \times K$ ” full factorial validation protocol was designed to obtain the validation dataset, where the effect of three aspects, i.e., conditions ($I, i = 1, 2, \dots, m$), the number of repetitions ($J, j = 1, 2, \dots, n$), and the level of concentrations ($K, k = 1, 2, \dots, a$), were taken into account [48]. The β -content, γ -confidence tolerance interval can be expressed by the following formula:

$$P_{\bar{Y}, \hat{\sigma}_b^2, \hat{\sigma}_c^2} (P_Y [\bar{Y} - k\hat{\sigma}_M < Y < \bar{Y} + k\hat{\sigma}_M \mid \bar{Y}, \hat{\sigma}_M] \geq \beta) = \gamma. \quad (1)$$

In equation (1), \bar{Y} is the average value of the results at each concentration level K ; $\hat{\sigma}_M$, $\hat{\sigma}_b^2$, and $\hat{\sigma}_c^2$, respectively means the intermediate precision, the interseries, and the intraseries variances; k denotes the coverage factor and is related to β and γ .

Mee’s approach is used for estimating the β -content, γ -confidence tolerance interval as follows [36, 49]:

$$[L, U] = [\bar{Y} - k_C \hat{\sigma}_M; \bar{Y} + k_C \hat{\sigma}_M], \quad (2)$$

$$\text{with } k_C = \sqrt{\frac{v' \chi_{1;\beta}^2(\tau)}{\chi_{v';1-\gamma}^2}}, \quad (3)$$

$$v' = \frac{(R' + 1)^2}{((R' + (1/n))^2 / (m - 1)) + ((1 - (1/n)) / mn)}, \quad (4)$$

$$\tau = \frac{1}{mnB'}, \quad (5)$$

$$B' = \frac{R' + 1}{nR' + 1}, \quad (6)$$

$$R' = \max \left[0, \frac{1}{n} \left(\frac{F}{F_\eta} - 1 \right) \right], \quad (7)$$

where the lower (L) and upper (U) limits denote a specified proportion β of measured results that will fall within the interval $[L, U]$ at specified confidence level. k_C is an approximation to k . $\chi_{1;\beta}^2(\tau)$ denotes the β quantile of a noncentral chi-square distribution under the freedom degree of 1. τ means the noncentral parameter. $\chi_{v';1-\gamma}^2$ with degrees of freedom v' denotes the $1 - \gamma$ quantile of a noncentral chi-square distribution. And, F denotes the mean square ratio MS_B/MS_E . MS_B and MS_E , respectively, denote the mean square of the interseries and the intraseries variances. Under degree freedom $v_1 = m(n - 1)$ and $v_2 = m - 1$, F_η is the 100 η percentile of an F distribution. The recommended values of

η are 0.85, 0.905, and 0.975, which are corresponding to 0.90, 0.95, and 0.99 for γ , respectively [47].

The β -content, γ -confidence tolerance interval could also be written in a relative form:

$$[L(\%), U(\%)] = [\text{bias}(\%) - k_C \text{RSD}(\%), \text{bias}(\%) + k_C \text{RSD}(\%)],$$

$$\text{RSD}(\%) = \frac{\hat{\sigma}_M}{X_r} \times 100, \quad (8)$$

where X_r is the theoretical value.

2.6.2. Establishment of the Accuracy Profile. In order to globally validate accuracy and robustness of the NIR quantitative method, the accuracy profile is developed as follows [50]:

- (1) Set acceptance limits $\pm 20\%$ for natural product in this paper
- (2) Calculate the β -content, γ -confidence relative tolerance intervals $[L(\%), U(\%)]$ for each concentration level based on equation (8) at a desired confidence level γ
- (3) Construct a 2D-accuracy graph with the horizontal axis for the validation standards concentration and vertical axis for the relative tolerance interval limits $[L(\%), U(\%)]$ and accuracy
- (4) If $[L(\%), U(\%)]$ at given concentration levels are within acceptance limits ($\pm 20\%$), it demonstrates that the developed method is accuracy and robustness; otherwise, the method cannot be accepted

2.6.3. Establishment of the Unreliability Graph. The unreliability graph was used as a decision making tool to increase the confidence of real-time release testing at the specification limit. The procedures for developing the unreliability graph are as follows [35, 39]:

- (1) Set the specification limit (λ) according to the requirement.
- (2) Calculate the $[L, U]$ for each concentration level based on equation (2) at the desired confidence level γ .
- (3) Develop a 2D graph with the horizontal axis for the validation standards concentrations and vertical axis for the observed concentrations.
- (4) Locate the tolerance limits L and U for each validation concentration on the 2D graph. The tolerance limit L at each concentration level was connected into a broken line in turn. The same procedures were also performed on tolerance limits U .
- (5) Make a straight line perpendicular to the horizontal axis at the specification limit (λ). The intersections of the lower and upper tolerance interval with the specification limit line are defined as L_{API} and U_{API} , respectively.
- (6) Make two straight lines parallel to horizontal axis through the intersections. The area between the two parallel straight lines is the unreliability region around the specification limits.

- (7) If the analytical results exceed the U_{API} , the target product can be immediately released; otherwise, it cannot be directly released.

2.7. Software. The SIMCA-P 11.5 (Umetrics, US) and Unscrambler 7.0 (CAMO, Norway) software were used to perform spectral pretreatments. The Matlab 7.0 (Mathwork, USA) with PLS Toolbox 2.1 (Eigenvector Research Inc., USA) was used to carry out the PLS regression. For calculation of the β -content, γ -confidence tolerance intervals, the Matlab codes were referred to [47].

3. Results and Discussion

3.1. NIR Method Development. In this study, raw spectra of 103 samples were obtained by NIR scanning of the extract powders, as shown in Figure 1. It was difficult to observe the differences from the original spectra because the wave bands were seriously overlapped. Partial least square, one of the most commonly used chemometric methods, was applied to handle the overdetermined problem in the calibration process. And, the PLS1 algorithm was used predict the concentrations of each API in *tanshinone* extract. Before ascertaining the structure and finetuning the coefficients of PLS model, the Kennard–Stone (K-S) algorithm [51] was used to split the original data set into a calibration set (75 samples) and a test set (28 samples).

Then, various data preprocessing methods in Section 2.5 were used to extract useful information from the noisy spectral data. Tables 1 and 2 show the PLS modeling results in both calibration and prediction of *cryptotanshinone* and *tanshinoneII_A* content, respectively. The PLS model based on the second-order derivative NIR absorption spectrum has the optimal results, where the RMSECV and RMSEP values were smallest and the RPD values were highest. This revealed that the robustness of the quantitative models with 2ndd pretreatment was satisfactory and the models had excellent predictive ability. Figure 2 shows the full spectra of all samples through 2ndd preprocessing method. It can be seen that this method can obviously eliminate the baseline drift, remove the background interference, and distinguish the absorption peaks. The characteristic absorption waveband was from 6400 cm^{-1} to 4000 cm^{-1} . Thereby, 2ndd was chosen as the preprocessing method.

The number of latent variables (LVs) was an important parameter and could directly affect the accuracy of the model. LVs listed in Tables 1 and 2 are optimized by the leave-one-out cross-validation. As can be seen from Figure 3, the RMSE and cumulative PRESS values gradually decreased and eventually did not change as the number of latent variables increased. Consequently, 10 LVs and 8 LVs were, respectively, used to establish the PLS models for *cryptotanshinone* and *tanshinoneII_A*, respectively. The RPD value in prediction of *tanshinoneII_A* was 15.6, which was larger than that in prediction of *cryptotanshinone* (RPD = 5.3). The reason may be that the standard deviation of *tanshinoneII_A* content in the test set was higher than that of *cryptotanshinone*.

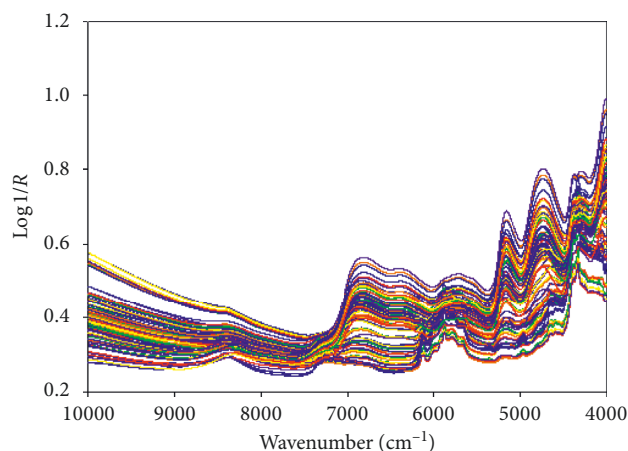


FIGURE 1: Raw NIR spectra of 103 samples.

TABLE 1: PLS model characteristics for *cryptotanshinone*.

Pretreatment	LVs	Calibration set				Validation set			
		r_{cal}	RMSEC	RMSECV	$BIAS_{cal}$	r_{val}	RMSEP	RPD	$BIAS_{val}$
Origin	11	0.9821	0.470	0.640	0.380	0.9712	0.5835	4.3	0.440
1std	10	0.990	0.344	0.557	0.261	0.9737	0.528	4.7	0.376
2ndd	10	0.9992	0.102	0.422	0.084	0.9818	0.466	5.3	0.341
S-G	11	0.9819	0.472	0.642	0.381	0.9709	0.587	4.2	0.441
MSC	12	0.9872	0.397	0.708	0.305	0.9761	0.536	4.6	0.399
SNV	12	0.9860	0.386	0.664	0.325	0.9713	0.583	4.3	0.420
WDS	11	0.9960	0.644	0.912	0.535	0.9516	0.755	3.3	0.623

TABLE 2: PLS model characteristics for *tanshinoneII_A*.

Pretreatment	LVs	Calibration set				Validation set			
		r_{cal}	RMSEC	RMSECV	$BIAS_{cal}$	r_{val}	RMSEP	RPD	$BIAS_{val}$
Origin	12	0.9840	1.322	2.012	0.999	0.9966	1.288	11.4	1.035
1std	10	0.9969	0.947	1.849	0.696	0.9970	1.141	12.8	0.807
2ndd	8	0.9991	0.512	1.775	0.376	0.9981	0.934	15.6	0.744
S-G	12	0.9938	1.338	2.040	1.012	0.9965	1.312	11.2	1.052
MSC	12	0.9970	0.938	2.023	0.739	0.9974	1.087	13.5	0.849
SNV	11	0.9973	0.891	1.674	0.622	0.9979	1.009	14.5	0.553
WDS	12	0.9896	1.736	2.478	1.292	0.9925	1.947	7.5	1.494

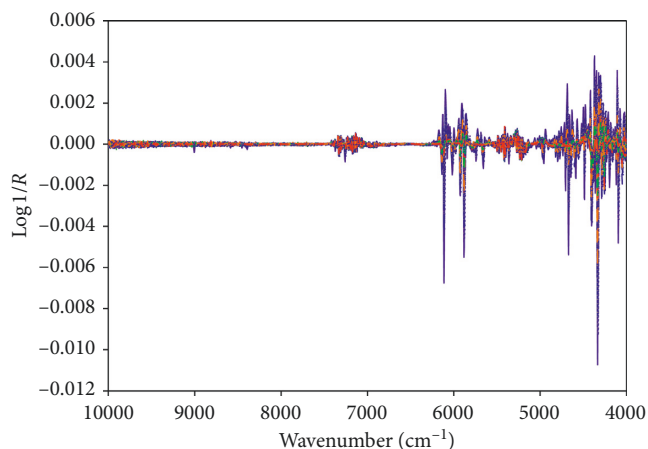


FIGURE 2: NIR spectra with the 2ndd preprocessing method.

3.2. NIR Method Validation. According to the ICH Points to consider (R2) document [52], the PLS quantitative model could be classified into high impact model, since the APIs content of *tanshinone* extract powder predicted by the multivariate calibration models were key indicators for quality control. Consequently, it is necessary to implement method validation to ensure the accuracy and robustness of the quantitative model. After 120 validation samples were prepared according to validation protocols illustrated in Section 2.4, the concentrations of *cryptotanshinone* and *tanshinoneII_A* were predicted by the developed NIR calibration model and are listed in appendix Tables S1 and S2, respectively.

The validation statistics for NIR quantitative method are shown in Tables 3 and 4 for *cryptotanshinone* and *tanshinoneII_A*, respectively. Taking the validation results of *cryptotanshinone* for example, the range of concentration

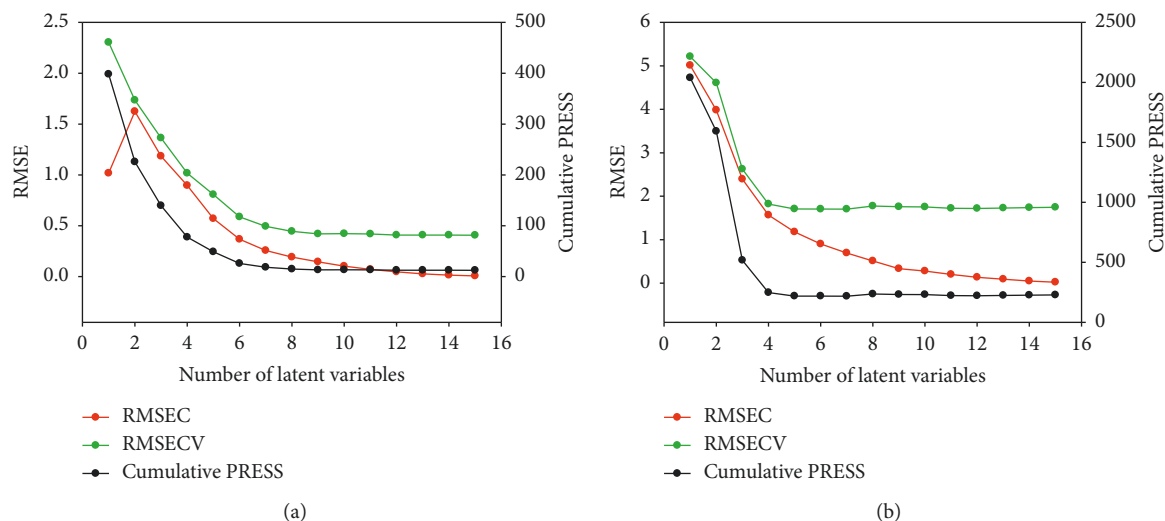


FIGURE 3: Calibration characteristics vs. number of latent factors. (a) The *cryptotanshinone* model; (b) the *tanshinoneII_A* model.

TABLE 3: The validation results for NIR determination of *cryptotanshinone*.

Theoretical concentration (%)	Mean calculated content (%)	Trueness			Precision	
		Relative bias (%)	Recovery (%)	Repeatability (%)	Intermediate precision (%)	
0.20	0.40	100.00	200.00	73.58	92.85	
0.31	0.46	46.88	146.88	46.34	52.73	
0.50	0.69	38.93	138.93	29.16	35.68	
1.18	0.86	-26.89	73.11	26.98	26.98	
2.05	2.06	0.33	100.33	7.67	7.97	
2.26	2.48	9.72	109.72	9.24	9.97	
5.29	4.92	-6.99	93.01	3.48	4.28	
9.68	9.51	-1.72	98.28	2.99	3.06	

TABLE 4: The validation results of NIR determination of *tanshinoneII_A*.

Theoretical concentration (%)	Mean calculated content (%)	Trueness			Precision	
		Relative bias (%)	Recovery (%)	Repeatability (%)	Intermediate precision (%)	
0.10	-0.20	-294.70	-194.70	390.80	390.80	
0.15	-0.13	-184.44	-84.44	250.76	250.76	
0.36	0.24	-32.96	67.04	87.85	93.70	
0.54	0.85	58.02	158.02	47.40	47.40	
2.04	1.60	-21.67	78.33	16.04	17.95	
6.03	5.95	-1.34	98.66	6.37	6.37	
18.76	18.34	-2.26	97.74	3.31	3.36	
27.64	26.45	-4.30	95.70	1.63	1.91	

studied in Table 3 can be divided into two parts. Part 1 and part 2 were the concentration range of [0.20–1.18]% and [2.05–9.68]%, respectively. In the first part, variances of trueness and precision were exceptionally severe, indicating that the precision and the accuracy of analytical method were anomalous. In part 2, it can be seen that the recovery was closed to 100% and the relative bias was small, indicating that the precision and accuracy of the quantitative model were acceptable within this range. With the same analysis procedures for *tanshinoneII_A*, it was easy to draw a conclusion that the contents of *tanshinoneII_A* within [0.10–2.04]% cannot be accurately detected since the precision and accuracy were anomalous. By contrast, the analytical method

can accurately determine the *tanshinoneII_A* in the range [6.03–27.64]%. In conclusion, the NIR method can be used for the determination of *cryptotanshinone* and *tanshinoneII_A* both in the second parts of the concentration range.

According to Section 2.6.2, the accuracy profile (AP) was used to globally assess the NIR quantitative analysis method, as shown in Figure 4. The $\beta = 66.7\%$ and $\gamma = 90\%$ suggested by Saffaj's were applied to estimate the β -content, γ -confidence tolerance interval [36], and the results were listed in Tables 5 and 6. It was clearly seen from Figure 4(a) that the relative tolerance intervals for the first 4 concentrations visibly came out of the two acceptance limits, revealing that the contents within [0.20–1.18]% cannot be accurately

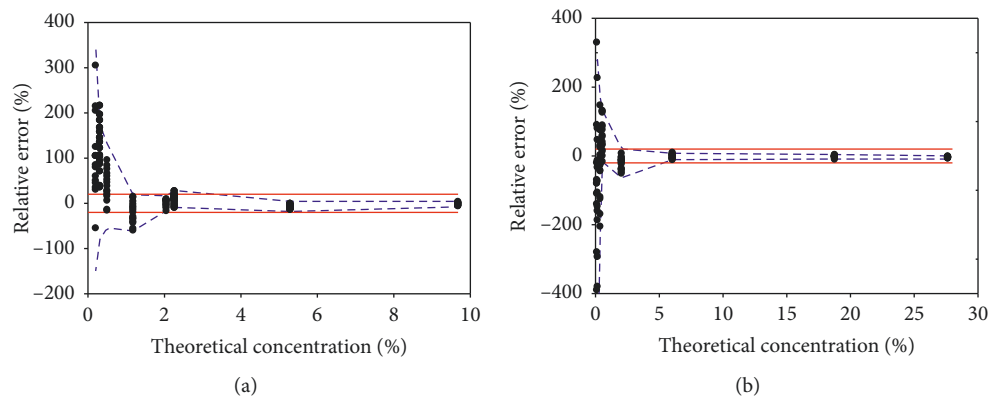


FIGURE 4: Accuracy profile for NIR quantitative methods. (a) Quantification of *cryptotanshinone* content; (b) quantification of *tanshinoneII_A* content. The medium blue dashed lines are the 66.7% β -content, 90% γ -confidence tolerance intervals and the red lines are the acceptance limits ($\pm 20\%$); the black point at each concentration level represents the relative bias for each predictive value.

measured. Although at content of 2.26% the relative tolerance intervals slightly exceeded upper acceptance limit, the most contents measured by calibration model were acceptable and the recovery in this concentration was no more than 110%. It indicated that the PLS model could determine the contents of *cryptotanshinone* in this concentration level. However, the tolerance intervals of the last 4 concentration levels fell within the acceptance limits. Consequently, the method was considered to be valid in the concentration range within [2.05–9.68]%. By using the same analysis method, a conclusion can be clearly drawn that the NIR method was valid only for the last 3 concentration levels in detecting the *tanshinoneII_A*, as shown in Figure 4(b). These findings are consistent with the validation results above.

3.3. Real-Time Release Testing for Tanshinone Extract Powders

3.3.1. The Specification Limit. According to the ChP (2015 Edition) [1], the minimum mass content of *cryptotanshinone* and *tanshinoneII_A* in *tanshinone* extract powders are 2.1% and 9.8%, respectively. The specification limits were well located within the reliable concentration regions in Section 3.2, indicating that the developed NIR analysis method can be used to release the *tanshinone* extract powders in real time.

3.3.2. Unreliability Graph Development. By, respectively, connecting the tolerance limits L and U listed in Tables 5 and 6 at each concentration level, the unreliability graph could be drawn. Figures 5(a) and 6(a) show the unreliability graphs for *cryptotanshinone* and *tanshinoneII_A* at full concentration ranges, respectively. The β -content, γ -confidence tolerance interval at the specification limit was then estimated. Taking *cryptotanshinone* for instance, a line passing through two points, i.e., the upper tolerance limits at 2.39% and 2.98%, was dropped, and the linear function was regressed as $y = 2.810 \times x - 3.370$ (x and y mean validation and observed concentration, respectively). The specification limit of *cryptotanshinone* was substituted into this function, and U_{API} of *cryptotanshinone* were calculated to be 2.53%. Then,

TABLE 5: The β -content, γ -confidence tolerance intervals estimated for different concentration levels of *cryptotanshinone*.

Concentration level (%)	L	U	L (%)	U (%)
0.20	-0.097	0.895	-149.64	348.98
0.31	0.062	0.847	-79.99	173.75
0.50	0.23	1.15	-54.29	132.15
1.18	0.45	1.40	-61.29	18.81
2.05	1.72	2.39	-16.10	16.75
2.26	1.98	2.98	-12.33	31.68
5.29	4.33	5.51	-18.21	4.23
9.68	8.93	10.10	-7.80	4.35

TABLE 6: The β -content, γ -confidence tolerance intervals estimated for different concentration levels of *tanshinoneII_A*.

Concentration level (%)	L	U	L (%)	U (%)
0.10	-0.76	0.38	-864.48	275.14
0.15	-1.15	0.79	-864.79	423.90
0.36	-0.49	0.98	-236.06	170.13
0.54	0.45	1.26	-16.77	132.82
2.04	0.74	2.46	-63.86	20.52
6.03	5.39	6.50	-10.51	7.84
18.76	17.11	19.56	-8.80	4.27
27.64	25.14	27.77	-9.06	0.46

another line passing through the lower tolerance limits at 1.72% and 1.98% was regressed as $y = 1.238 \times x - 0.818$. 2.1% was substituted into this function, and L_{API} of *cryptotanshinone* were calculated to be 1.78%. Similarly, as for *tanshinoneII_A*, the tolerance interval around 9.8% was estimated to be from 8.86% to 10.37%. Figures 5(b) and 6(b) show the unreliable regions for *cryptotanshinone* and *tanshinoneII_A* around the specification limits, respectively.

3.3.3. Real-Time Release Testing. The unreliable region around the specification limit can be seen as risk region or

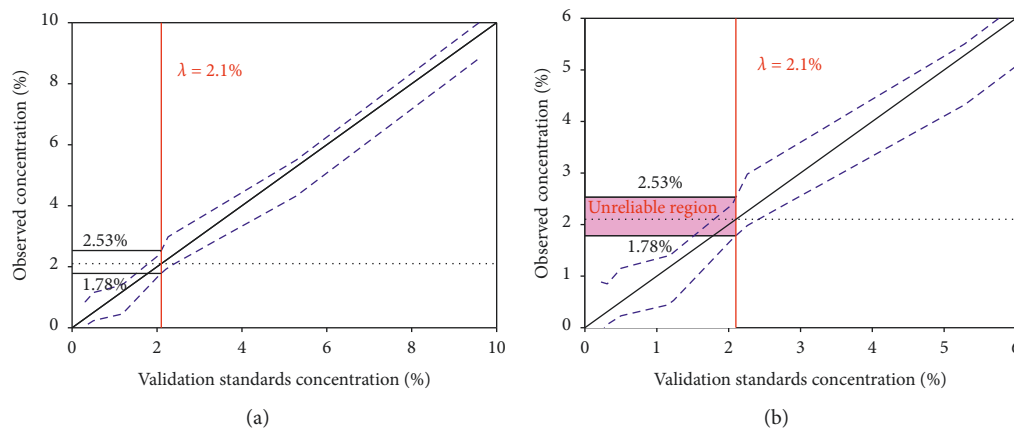


FIGURE 5: (a) The unreliability graph of *cryptotanshinone*. (b) The unreliable region estimated around the specification limit of *cryptotanshinone* in *tanshinone* extract. Blue dashed lines are the 66.7% β -content, 90% γ -confidence tolerance intervals; the diagonal continuous line is the identity line $y = x$; the red vertical straight line and the black horizontal dashed line are the API specification limits; the shaded region corresponds to the unreliable region.

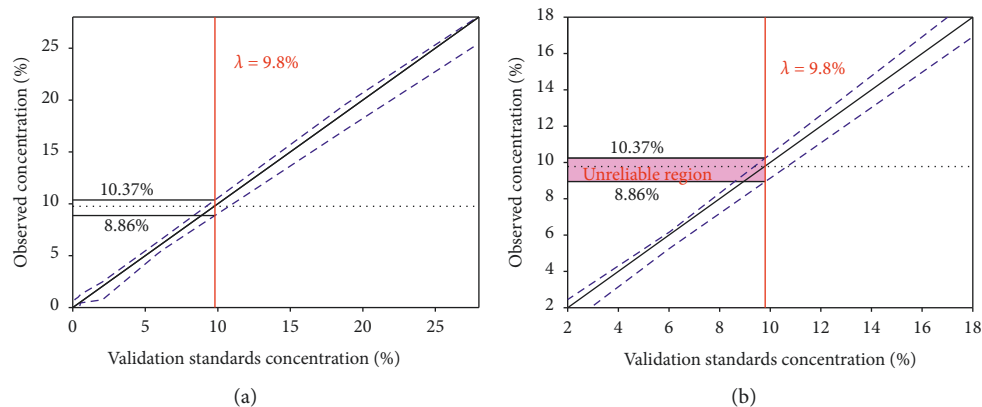


FIGURE 6: (a) The unreliability graph of *tanshinoneII_A*. (b) The unreliable region estimated around the specification limit of *tanshinoneII_A* in *tanshinone* extract. Blue dashed lines are the 66.7% β -content, 90% γ -confidence tolerance intervals; the diagonal continuous line is the identity line $y = x$; the red vertical straight line and the black horizontal dashed line are the API specification limits; the shaded region corresponds to the unreliable region.

guard-banding, since there was a certain risk in the results of NIR quantitative analysis. During routine use, if the NIR analysis result is larger than the upper limit of the built unreliable region, it is assured that the content would satisfy the specification. And, for the analysis result within the unreliable region, it cannot accurately determine whether the content meets the specification or not. If the NIR analysis result is located under the lower limit of the unreliable region, it absolutely does not meet the target requirements.

For real-time release testing of *tanshinone* extract powders by NIR analytical method, the release standard was that the contents of *cryptotanshinone* and *tanshinoneII_A* must be no less than 2.53% and 10.37%, respectively. Only in this way, the *tanshinone* extract powder can be directly released to the next pharmaceutical manufacture units or to markets. Otherwise, the *tanshinone* extract powders cannot be released. The NIR spectroscopy combined with the unreliability graph significantly increases the confidence about the compliance of the product in a real-time way.

4. Conclusions

In this paper, a new release strategy based on the unreliability graph methodology which incorporated the β -content, γ -confidence tolerance intervals, has successfully been achieved. Firstly, the *cryptotanshinone* and *tanshinoneII_A* content in *tanshinone* extract powders were rapidly detected by NIR using the PLS quantitative model. And secondly, this quantitative model was validated by the accuracy profile. The NIR methods can accurately determine the *cryptotanshinone* in the range [2.05–9.68]% and the *tanshinoneII_A* in the range [6.03–27.64]%. Finally, the release strategy with NIR quantitative model based on the unreliability graph was applied to real-time release test of *tanshinone* extract powders. The proposed approach offered a formal statistical framework to show when the analytical methods will provide daily results that can be used efficiently to make adequate decisions. Besides, the release strategy proposed can be applied to any quantitative analytical

method and provide greater assurance for the quality of the final products, to achieve the purpose of real-time release.

Data Availability

The data used to support the findings of this study are available from the corresponding author upon request.

Additional Points

(1) A release strategy was proposed to determine whether the analytical results were reliable in real-time release testing (RTRT). (2) The β -content, γ -confidence tolerance intervals were applied to establish the unreliability graph as the decision tool. (3) The new release strategy can be used for quality control of the complex system of Chinese medicine product.

Conflicts of Interest

There are no conflicts of interests regarding the publication of this manuscript.

Acknowledgments

The authors are thankful to the research funding supports from the National Science and Technology Major Projects (No. 2018ZX09201011-006, China) and Scientific Research Project of Beijing University of Chinese Medicine (No. 2019-JYB-JS-015).

Supplementary Materials

Table S1: predicted concentrations of *cryptotanshinone* validation samples expressed as mass content (%). Table S2: predicted concentrations of *tanshinone*IIA validation samples expressed as mass content (%). (*Supplementary Materials*)

References

- [1] Chinese Pharmacopoeia Commission, *Chinese Pharmacopoeia 2015 Edition*, Beijing Chemical industry press, Beijing Shi, China, 2015.
- [2] J. Luo, W. Song, G. Yang, H. Xu, and K. Chen, "Compound Danshen (*Salvia miltiorrhiza*) dripping pill for coronary heart disease: an overview of systematic reviews," *American journal of Chinese medicine*, vol. 43, pp. 25–43, 2015.
- [3] Food and Drug Administration, *Guidance for Industry Guidance for Industry PAT—a Framework for Innovative Pharmaceutical Development, Manufacturing and Quality Assurance*, US Department of Health and Human Services, Food and Drug Administration, Center for Biologics Evaluation and Research, Rockville Google Scholar, Washington, DC, USA, 2004.
- [4] European Commission, *EU Guidelines to Good Manufacturing Practice Medicinal Products for Human and Veterinary Use*, European Commission, Brussels, Belgium, 2009.
- [5] H. F. Xu, X. Zhang, and Y. L. Ma, *Real time release testing extends to the overall manufacturing process*, FDA, Silver Spring, MD, USA, 2004.
- [6] M. Blanco and I. Villarroya, "NIR spectroscopy: a rapid-response analytical tool," *TrAC Trends in Analytical Chemistry*, vol. 21, no. 4, pp. 240–250, 2002.
- [7] H. Yang, J. Irudayaraj, and M. Paradkar, "Discriminant analysis of edible oils and fats by FTIR, FT-NIR and FT-Raman spectroscopy," *Food Chemistry*, vol. 93, no. 1, pp. 25–32, 2005.
- [8] Y. Roggo, L. Duponchel, and J.-P. Huvenne, "Comparison of supervised pattern recognition methods with McNemar's statistical test," *Analytica Chimica Acta*, vol. 477, no. 2, pp. 187–200, 2003.
- [9] M. Blanco and M. Alcalá, "Content uniformity and tablet hardness testing of intact pharmaceutical tablets by near infrared spectroscopy," *Analytica Chimica Acta*, vol. 557, no. 1-2, pp. 353–359, 2006.
- [10] P. R. Wahl, G. Fruhmann, S. Sacher, G. Straka, S. Sowinski, and J. G. Khinast, "PAT for tableting: inline monitoring of API and excipients via NIR spectroscopy," *European Journal of Pharmaceutics and Biopharmaceutics*, vol. 87, no. 2, pp. 271–278, 2014.
- [11] M. Blanco, M. Alcalá, J. M. González, and E. Torras, "A process analytical technology approach based on near infrared spectroscopy: tablet hardness, content uniformity, and dissolution test measurements of intact tablets," *Journal of Pharmaceutical Sciences*, vol. 95, no. 10, pp. 2137–2144, 2006.
- [12] M. Otsuka and I. Yamane, "Prediction of tablet properties based on near infrared spectra of raw mixed powders by chemometrics: scale-up factor of blending and tableting processes," *Journal of Pharmaceutical Sciences*, vol. 98, no. 11, pp. 4296–4305, 2009.
- [13] M. Jamrógiewicz, "Application of the near-infrared spectroscopy in the pharmaceutical technology," *Journal of Pharmaceutical and Biomedical Analysis*, vol. 66, pp. 1–10, 2012.
- [14] X. U. Ding-Zhou, L. I. Jing, C. H. Liu, L. Yang, L. I. Yu, and M. Zhong, "Application of near-infrared spectroscopy technology in online detection of *Epimedium brevicornum* Maxim extraction process," *China Modern Medicine*, vol. 23, pp. 4–6, 2014.
- [15] X. S. Meng, Y. Tan, Y. F. Zhang et al., *Method and Application for Rapid Detection of the Water Extraction Process of Qizhi weitong Granules by Near Infrared Spectroscopy*, CN106383096A, 2017.
- [16] Y. X. Wang, H. J. Mi, C. L. Zhang et al., "Near infrared spectroscopy on-line and real-time monitoring of alcohol precipitation process of reduning injection," *China Journal of Chinese Materia Medica*, vol. 39, pp. 4608–4614, 2014.
- [17] Y. L. Xue, A. X. Zuo, X. S. Liu et al., *An Automatic Judgment and Control Method in the Process of Extracting Liquid Receiving Eluent Aesculi*, CN103203123B, 2013.
- [18] Y. Jin, Y. J. Wu, and X. S. Liu, *Online Detection Method for Double Effect Concentration Process of Danhong Injection*, CN103913433A, 2014.
- [19] J. W. Zhang, Y. Y. Zhang, Y. Liu, M. Jia, and G. L. Zhao, *NIR On-Line Detection Method for Paeoniflorin Content in Extract of Paeonia Lactiflora Pall*, CN102058682A, 2011.
- [20] H. Y. Chen, L. I. Qiong-Ya, J. L. Chen, L. J. Luan, and Y. X. Dai, "End point judgment of blending process of zhengtian pills by near infrared spectroscopy," *Chinese Journal of Experimental Traditional Medical Formulae*, vol. 22, pp. 13–16, 2016.
- [21] V. P. Shah, K. K. Midha, S. Dighe et al., "Analytical methods validation: bioavailability, bioequivalence, and pharmacokinetic

- studies," *Journal of Pharmaceutical Sciences*, vol. 81, no. 3, pp. 309–312, 1992.
- [22] M. Blanco and A. Peguero, "Analysis of pharmaceuticals by NIR spectroscopy without a reference method," *TrAC Trends in Analytical Chemistry*, vol. 29, no. 10, pp. 1127–1136, 2010.
- [23] C. V. Liew, A. D. Karande, and P. W. S. Heng, "In-line quantification of drug and excipients in cohesive powder blends by near infrared spectroscopy," *International Journal of Pharmaceutics*, vol. 386, no. 1-2, pp. 138–148, 2010.
- [24] H. Grohganz, D. Gildemyn, E. Skibsted, J. M. Flink, and J. Rantanen, "Towards a robust water content determination of freeze-dried samples by near-infrared spectroscopy," *Analytica Chimica Acta*, vol. 676, no. 1-2, pp. 34–40, 2010.
- [25] C. C. Corredor, D. Bu, and D. Both, "Comparison of near infrared and microwave resonance sensors for at-line moisture determination in powders and tablets," *Analytica Chimica Acta*, vol. 696, no. 1-2, pp. 84–93, 2011.
- [26] L. Norgaard, A. Saudland, J. Wagner, J. P. Nielsen, L. Munck, and S. B. Engelsen, "Interval partial least-squares regression (iPLS): a comparative chemometric study with an example from near-infrared spectroscopy," *Applied Spectroscopy*, vol. 54, no. 3, pp. 413–419, 2000.
- [27] R. Leardi and L. Nørgaard, "Sequential application of backward interval partial least squares and genetic algorithms for the selection of relevant spectral regions," *Journal of Chemometrics*, vol. 18, no. 11, pp. 486–497, 2005.
- [28] A. C. Olivieri, N. M. Faber, J. Ferré, R. Boqué, J. H. Kalivas, and H. Mark, "Uncertainty estimation and figures of merit for multivariate calibration (IUPAC Technical Report)," *Pure and Applied Chemistry*, vol. 78, no. 3, pp. 633–661, 2006.
- [29] P. Hubert, J.-J. Nguyen-Huu, B. Boulanger et al., "Harmonization of strategies for the validation of quantitative analytical procedures," *Journal of Pharmaceutical and Biomedical Analysis*, vol. 36, no. 3, pp. 579–586, 2004.
- [30] Z. Wu, B. Xu, M. Du, C. Sui, X. Shi, and Y. Qiao, "Validation of a NIR quantification method for the determination of chlorogenic acid in *Lonicera japonica* solution in ethanol precipitation process," *Journal of Pharmaceutical and Biomedical Analysis*, vol. 62, pp. 1–6, 2012.
- [31] Y.-C. Feng and C.-Q. Hu, "Construction of universal quantitative models for determination of roxithromycin and erythromycin ethylsuccinate in tablets from different manufacturers using near infrared reflectance spectroscopy," *Journal of Pharmaceutical and Biomedical Analysis*, vol. 41, no. 2, pp. 373–384, 2006.
- [32] J. Mantanus, E. Rozet, K. Van Butsele et al., "Near infrared and Raman spectroscopy as Process Analytical Technology tools for the manufacturing of silicone-based drug reservoirs," *Analytica Chimica Acta*, vol. 699, no. 1, pp. 96–106, 2011.
- [33] P. Hubert, J.-J. Nguyen-Huu, B. Boulanger et al., "Harmonization of strategies for the validation of quantitative analytical procedures," *Journal of Pharmaceutical and Biomedical Analysis*, vol. 45, no. 1, pp. 82–96, 2007.
- [34] E. Rozet, E. Ziemons, R. D. Marini, B. Boulanger, and P. Hubert, "Quality by design compliant analytical method validation," *Analytical Chemistry*, vol. 84, no. 1, pp. 106–112, 2011.
- [35] E. Rozet, E. Ziemons, R. D. Marini, B. Boulanger, and P. Hubert, "Methodology for the validation of analytical methods involved in uniformity of dosage units tests," *Analytica Chimica Acta*, vol. 760, pp. 46–52, 2013.
- [36] T. Saffaj and B. Ihssane, "Uncertainty profiles for the validation of analytical methods," *Talanta*, vol. 85, no. 3, pp. 1535–1542, 2011.
- [37] T. Saffaj and B. Ihssane, "Response to comments on "Uncertainty profiles for the validation of analytical methods"," *Talanta*, vol. 94, pp. 361–362, 2012.
- [38] T. Saffaj and B. Ihssane, "Remarks on "Reply to the responses to the comments on "uncertainty profiles for the validation of analytical methods" by Saffaj and Ihssane"," *Talanta*, vol. 106, pp. 155–157, 2013.
- [39] Z. Xue, B. Xu, X. Shi et al., "Overall uncertainty measurement for near infrared analysis of cryptotanshinone in tanshinone extract," *Spectrochimica Acta Part A: Molecular and Biomolecular Spectroscopy*, vol. 170, pp. 39–47, 2017.
- [40] V. J. Barclay, R. F. Bonner, and I. P. Hamilton, "Application of wavelet transforms to experimental spectra: smoothing, denoising, and data set compression," *Analytical Chemistry*, vol. 69, no. 1, pp. 78–90, 1997.
- [41] M. C. Sarragaça and J. A. Lopes, "Quality control of pharmaceuticals with NIR: from lab to process line," *Vibrational Spectroscopy*, vol. 49, no. 2, pp. 204–210, 2009.
- [42] T. Isaksson and T. Næs, "The effect of multiplicative scatter correction (MSC) and linearity improvement in NIR spectroscopy," *Applied Spectroscopy*, vol. 42, no. 7, pp. 1273–1284, 2016.
- [43] I. Helland, T. Næs, and T. Isaksson, "Related versions of the multiplicative scatter correction method for preprocessing spectroscopic data," *Chemometrics and Intelligent Laboratory Systems*, vol. 29, no. 2, pp. 233–241, 1995.
- [44] R. J. Barnes, M. S. Dhanoa, and S. J. Lister, "Standard normal variate transformation and de-trending of near-infrared diffuse reflectance spectra," *Applied Spectroscopy*, vol. 43, no. 5, pp. 772–777, 2016.
- [45] D. Cozzolino, M. Kwiatkowski, M. Parker et al., "Prediction of phenolic compounds in red wine fermentations by visible and near infrared spectroscopy," *Analytica Chimica Acta*, vol. 513, no. 1, pp. 73–80, 2004.
- [46] Y. de Micalizzi, N. Pappano, and N. Debattista, "First and second order derivative spectrophotometric determination of benzyl alcohol and diclofenac in pharmaceutical forms," *Talanta*, vol. 47, no. 3, pp. 525–530, 1998.
- [47] T. Saffaj, B. Ihssane, F. Jhail, H. Bouchafra, S. Laslami, and S. A. Sosse, "An overall uncertainty approach for the validation of analytical separation methods," *The Analyst*, vol. 138, no. 16, pp. 4677–4691, 2013.
- [48] B. Govaerts, W. Dewé, M. Maumy, and B. Boulanger, "Pre-study analytical method validation: comparison of four alternative approaches based on quality-level estimation and tolerance intervals," *Quality and Reliability Engineering International*, vol. 24, no. 6, pp. 667–680, 2008.
- [49] R. W. Mee, " β -Expectation and β -content tolerance limits for balanced one-way ANOVA random model," *Technometrics*, vol. 26, no. 3, pp. 251–254, 1984.
- [50] Z. Xue, B. Xu, C. Yang et al., "Method validation for the analysis of licorice acid in the blending process by near infrared diffuse reflectance spectroscopy," *Analytical Methods*, vol. 7, no. 14, pp. 5830–5837, 2015.
- [51] R. Galvao, M. Araujo, G. Jose, M. Pontes, E. Silva, and T. Saldanha, "A method for calibration and validation subset partitioning," *Talanta*, vol. 67, no. 4, pp. 736–740, 2005.
- [52] ICH 2011, *ICH Points to Consider (R2), ICH-Endorsed Guide for ICH Q8/Q9/Q10 Implementation*, 2011, http://www.ich.org/fileadmin/Public_Web_Site/ICH_Products/Guidelines/Quality/Q8_9_10_QAs/PtC/Quality_IWG_PtCR2_6dec2011.pdf.

Research Article

FT-IR Spectroscopy Applied for Identification of a Mineral Drug Substance in Drug Products: Application to Bentonite

H. Ouhaddouch ¹, A. Cheikh ², M. O. B. Idrissi,¹ M. Draoui,¹ and M. Bouatia ¹

¹Laboratory of Analytical Chemistry, Team of Formulation and Quality Control of Health Products, Faculty of Medicine and Pharmacy, Mohammed V University, Rabat, Morocco

²Faculty of Pharmacy, Abulcasis University, Rabat, Morocco

Correspondence should be addressed to H. Ouhaddouch; hind.ouhaddouch@yahoo.fr

Received 4 December 2018; Revised 28 January 2019; Accepted 5 February 2019; Published 3 March 2019

Academic Editor: Alessandra Durazzo

Copyright © 2019 H. Ouhaddouch et al. This is an open access article distributed under the Creative Commons Attribution License, which permits unrestricted use, distribution, and reproduction in any medium, provided the original work is properly cited.

The aim of this study is to prove the effectiveness of IR spectroscopy as an identification test able to discriminate between mineral compounds in mixtures. This work is concerned with the physical characterisation of purified bentonite, bentonite in organic mixtures and organic excipients, and mineralized organic mixture containing bentonite using FT-IR spectroscopy. The different spectra were compared with each other in order to determine fingerprints of bentonite represented by bands located at 3632 cm^{-1} and 3437 cm^{-1} . The analysis of the spectra of the nonmineralized mixture demonstrates the presence of two bands at 1454 cm^{-1} and 2928 cm^{-1} , superimposed on those of the excipients and which disappear after 2 hours of mineralization at 500°C . Finally, we notice a displacement of the stretching band of H_2O to the right with increasing the proportion of the excipients.

1. Introduction

Over the last decade, infrared (IR) spectroscopy had proved to be a powerful analytical method widely applied in quality control in the field of agricultural, environment, food, and especially pharmaceutical. It is the best technique used in the investigation and identification of clays and clay minerals, especially bentonite, by a combination of spectroscopic and spatial information [1, 2]. Using this method, selected sample areas can be analyzed with reference to the identification and localization of chemical species by Fourier-transform infrared spectroscopy (FT-IR) in the transmission or attenuated total reflection (ATR) mode [3].

On the other hand, FT-IR is an excellent technique for pharmaceutical analysis which offers many advantages since it is easy to use, sensitive, selective, green, and fast (the total analysis time including making the pellets, measurement, identification, and report generation is lower than 10 minutes) and helps ensure regulatory compliance through validation protocols. Contrary to high-performance liquid chromatography (HPLC) which is less fast, requires the preliminary preparation of the mobile phase, and is not

applied in the field of mineral chemistry, this spectroscopic method is the reference for identification of organic substances in pharmacopeia. The IR spectroscopy is mainly complementary to X-ray diffraction (XRD) and other methods used to study clays.

The interpretation of the different IR spectra remains empirical and consists most often in comparing the results obtained with previously recorded reference spectra or to put in evidence important structural parts of the molecules with intense vibration bands [4–6], even if the substance is in mixtures or complexes [7]. It is based mainly on the analysis of IR spectra of isolated molecules. However, since these spectra can serve as fingerprints for identification, we are interested in proving the effectiveness of this spectral method in the identification of a mineral product that cannot be detected by HPLC in a mixture.

The aim of this study is to develop a new method for identification of the drug substance as purified bentonite in a drug product, using FT-IR spectroscopy in order to apply it in several fields such as industrial pharmacy to analyze mineral intestinal adsorbents [8].

2. Materials and Methods

2.1. Preparation of Mixture. The starting material is bentonite clay, which belongs to the family of crystalloids. Five mixtures of drug products were prepared of each proportion of bentonite (Sigma-Aldrich, analytical grade), pure glucose monohydrate (Riedel-de Haën, analytical grade), and menthol (BASF, pharmaceutical grade) (Table 1). The mixtures thus formed are triturated in a porcelain mortar to reduce the average particle size to 1-2 μm in order to promote the homogeneity of the samples [9]. In effect, the size of the particles influences the amount of absorption of the sample and the intensity of the absorption peaks of its spectrum. The difference in particle size between the different constituents of the mixture then complicates the analysis of the mixture spectra in which the coarsest compound becomes predominant [10].

The aim is to have mixtures sufficiently simple to acquire a knowledge of the interaction spectra related to the superposition of the absorption spectra of the different species, knowing that the additivity of the absorbances is an ideal case. The mixtures thus prepared will be read after by IR spectroscopy.

2.2. Mineralization of the Mixture. The determination of the time required for the complete mineralization of glucose and menthol (excipients) led us to prepare six samples of mixture 80% (M80) and one sample of purified bentonite (B). Each 100 mg sample was placed in a porcelain crucible at a temperature of 500°C in a temperature-controlled oven of the Conacom Italia type. The crucibles of the mixture were recovered one after the other every 30 minutes for 3 hours, in order to be analyzed by FT-IR spectroscopy using the transmission mode.

2.3. Measurement by Fourier-Transform Infrared Spectroscopy (FT-IR). The FT-IR spectroscopy using the transmission mode is an intuitive method which does not require sophisticated sampling accessories. The sample can be placed directly into the path of the infrared beam (with the help of a sample holder), and 128 scans were collected with a resolution of 4 cm^{-1} for each measurement over the spectral range of 500–4000 cm^{-1} .

FT-IR spectroscopy using KBr-pressed disk technique was conducted on a JASCO FT-IR 460 PLUS spectrometer (Pike Technologies, Madison, USA) equipped with a pyroelectric DLATGS detector. 2.5 mg of each mineralized sample and 100 mg of potassium bromide (Honeywell Fluka, infrared grade) were weighted, ground in an agate mortar, and pressed for 2 minutes at 10 tonnes/cm^2 to form a semitransparent pellet which lets light to be transmitted to the detector [11, 12]. The pellet was placed in the IR beam using the sample transmission holder. The samples analyzed were nonmineralized glucose (G), purified bentonite (B), mineralized bentonite (MB), nonmineralized mixture 80% (M80), mineralized mixture 80% (MM80), nonmineralized mixture 60% (M60), and nonmineralized mixture 40% (M40). Three measurements were carried out in the transmission mode for each

TABLE 1: Composition of the studied mixtures.

Code	Mixtures	Bentonite (mg)	Glucose (mg)	Menthol (mg)
M80	Mixture 80%	80	19	1
M60	Mixture 60%	60	39	1
M40	Mixture 40%	40	59	1
B	Bentonite	100	—	—
G	Glucose	—	100	—

sample. Spectra Manager II spectroscopy software developed by JASCO ensures spectral acquisition and processing.

The first part of this work was reserved to record the spectra of mineralized mixture MM80 for different durations in the aim to determine the time required for the complete mineralization of glucose and menthol (excipients). The second part of this work is to identify functional groups of nonmineralized mixture by measuring the absorption at specific wavelengths of bonds that vibrate independently of one another in order to confirm that the FT-IR spectroscopy is the most efficient method able to discriminate between different compounds of drug product.

3. Results and Discussion

3.1. Mineralization of the Mixture. Disappearance of functional groups during the process of mineralization can be successfully monitored by transmission FT-IR spectrometry. The focus was on the band located at 2928 cm^{-1} corresponding to C-H stretching which is specific to organic compounds: glucose and menthol. The IR spectra of the mixture M80 mineralized at 500°C for 30, 60, 90, and 120 min (Figures 1 and 2) show a gradual decrease in the intensity of this band, until disappearance from the second hour (crucibles 4, 5, and 6). The disappearance of this peak testifies to a complete mineralization of the organic matter used in the preparation of the mixture (glucose and menthol). Consequently, the MM80 mixture used in our study represents a M80 mixture mineralized at 500°C for 2 hours.

3.2. Data Processing of the Infrared Spectrometry. IR spectroscopy analysis of the different mixtures studied requires an understanding of the absorption bands attributable to the different physical and chemical properties of the material and which are used to assist in the identification of the various compounds that make up the mixture.

It is well known that molecule analyzed by IR spectroscopy absorbs only the frequencies of IR light that match vibrations that cause a change in the dipole moment of the molecule. Every molecule, with the exception of enantiomers, has a unique infrared spectrum. This is due to the fact symmetrical structures and identical groups at each end of one bond will not absorb in the IR range [13]. The spectrum has two regions. The fingerprint region is unique for a molecule, and the functional group region is identical for molecules with the same functional groups [13].

The FT-IR spectral examination of purified bentonite revealed different bands (Table 2) comparable to those

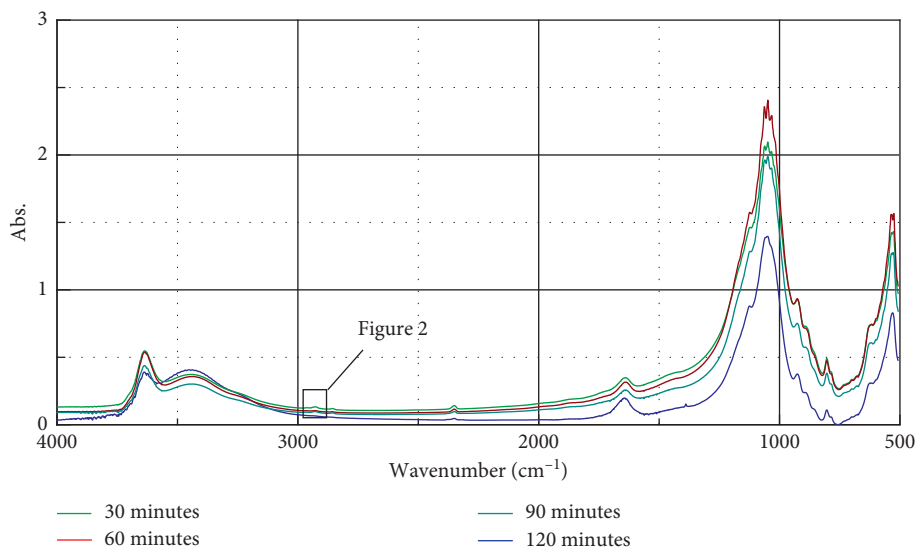


FIGURE 1: FT-IR spectra of nonmineralized mixture 80% (M80) mineralized at 500°C for different durations.

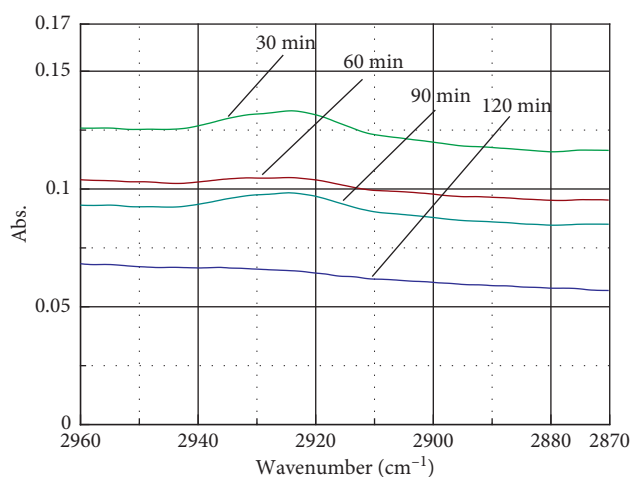


FIGURE 2: Spectral band characteristic of nonmineralized mixture 80% (M80) after mineralization at 500°C for 30, 60, 90, and 120 minutes.

TABLE 2: IR bands characteristic of the purified bentonite spectrum.

Transmission vibrational frequency (cm^{-1})	Strength	Functional groups
3632	Medium	OH stretching
3437	Medium	H_2O stretching
1638	Weak	H_2O bending
1042	Broad	Si-O stretching
915	Broad	Al-OH-Al bending
884	Medium	Al-OH-Fe bending
842	Medium	Al-OH-Mg bending
795	Weak	Si-O stretching of quartz and silica
622	Weak	Al-O + Si-O out-of-plane vibration
522	Broad	Al-O-Si bending

defined by the literature [14–18]. Two bands of different intensities, located at 3632 cm^{-1} and 3437 cm^{-1} , also defined by Jeddi et al. [19], constitute the spectral signature specific to bentonite which allows its identification in a mixture of species. These bands correspond, respectively, to the vibrational modes of hydroxyl groups and water molecules absorbed in the interstitial spaces of the bentonite.

According to the spectra of the mineralized bentonite and purified bentonite obtained (Figure 3), the general appearance is similar, but we can see a significant decrease in the intensity of the band at 3437 and 1638 cm^{-1} related to H_2O absorbed on the samples, and a well-resolved band at 3632 cm^{-1} assigned to OH- stretching vibrations of structural hydroxyls remained [20]. This change of intensity means that the hydrophilicity of the bentonite decreased.

Figure 4 shows FT-IR spectra of the mineralized bentonite and the excipients as well as those of the mixtures M80 and MM80. The different spectra were compared with each other in order to obtain information on the differences between the mineralized bentonite and the mixtures M80 and MM80. The spectra of the mixture MM80 are completely confused with those of the mineralized bentonite. However, those of the mixture M80, unlike the mixture MM80, have in the field ranging from 1300 to 4000 cm^{-1} and in addition to the bands characteristic of the hydroxyl group (3632 cm^{-1}) and water (3437 , 1638 cm^{-1}), a small band at 1454 cm^{-1} and a sharper band at 2928 cm^{-1} . This supports the additivity of absorbances of the excipients and the bentonite.

The FT-IR spectroscopy of the mixtures M80, M60, M40, and excipients shown in Figure 5 was carried out for a comparative purpose in order to obtain information about the modification of the mixture spectra while increasing the proportion of the excipients. The position, the shape, and the intensity of the stretching band of H_2O at 3437 cm^{-1}

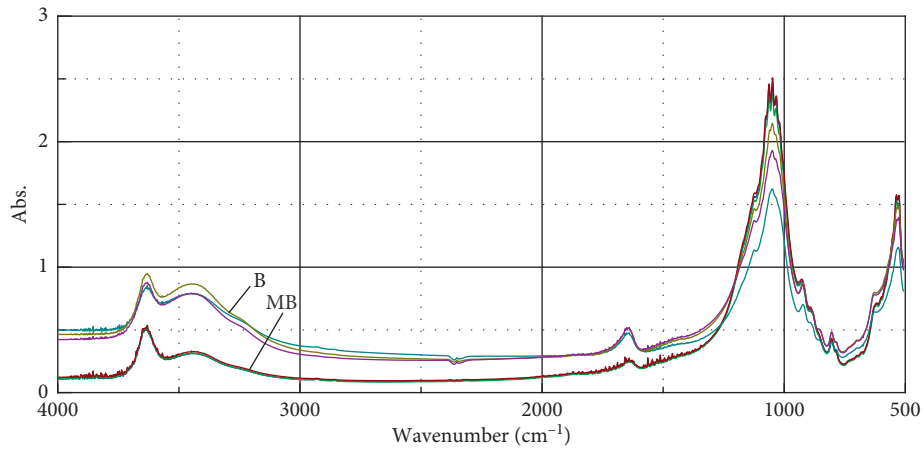


FIGURE 3: FT-IR spectra of purified bentonite (B) and mineralized bentonite (MB).

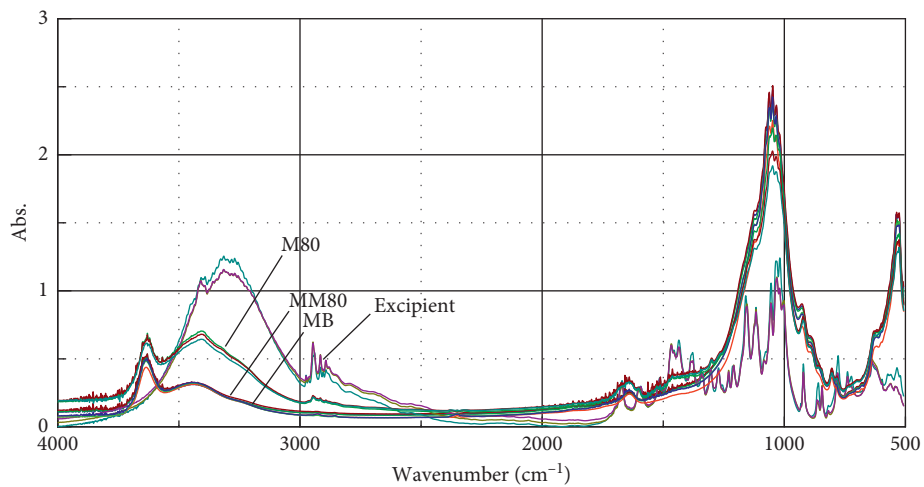


FIGURE 4: FT-IR spectra of mineralized bentonite (MB) and mineralized mixture 80% (MM80) versus those of nonmineralized mixture 80% (M80) and excipients.

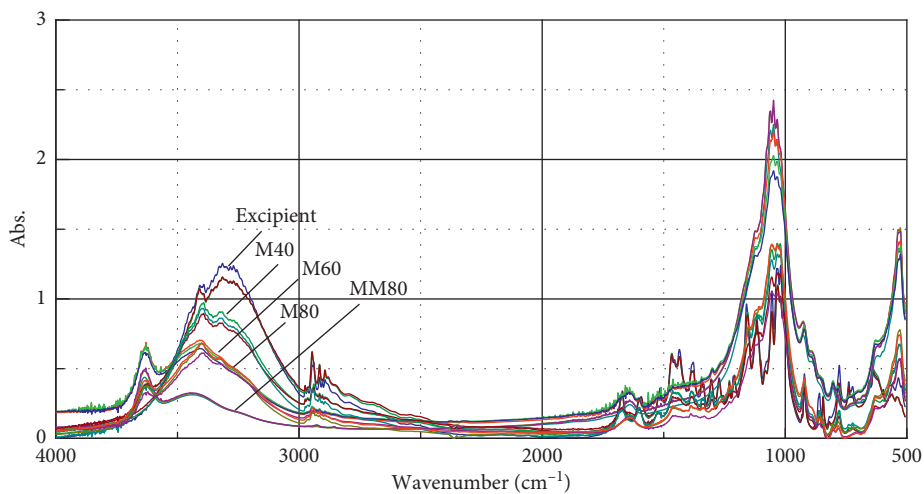


FIGURE 5: FT-IR spectra of mineralized mixture 80% (MM80), nonmineralized mixture 80% (M80), nonmineralized mixture 60% (M60), nonmineralized mixture 40% (M40), and excipients.

were influenced by the addition of the excipients. Indeed, we notice a displacement of this band to the right with increase in its intensity while going from the mixture M80 to the mixture M40. The absorption bands observed at 1454 and 2928 cm^{-1} in the FT-IR spectra of the M80 mixture increase their intensity with increasing concentration of the excipients.

Unlike to FT-IR spectroscopy which is a simple, fast, cheaper, and extremely useful for the characterisation of both organic products and inorganic products, the HPLC is a method which represents some limitations rarely discussed that promotes the utilisation of FT-IR spectroscopy.

The HPLC requires a sophisticated instrumentation with bewildering number of modules, columns, and mobile phases, operating parameters render HPLC difficult for the novice, and it is relatively expensive [21]. It can also be time-consuming, tedious, arduous, involve extensive chemical use, need regular maintenance requirements, and sometime, require pretreatment of samples [21, 22]. But, the main drawbacks of HPLC are the lack of a high-sensitivity universal detector and the insufficient chromatographic efficiency to separate many complexes like the inorganic products [22–24].

Therefore, we can confirm that the FT-IR spectroscopy, applied to study drug product, is a very sensitive technique that provides a relatively easy and fast way to determine an unknown mineral drug substance, by giving detailed qualitative information on chemical composition of the analyzed material along with a unique fingerprint that often enables confirmation of its identity [25]. This identification and recognition of its presence in mixtures are more certain when its absorption bands are numerous and sharply defined and if there appears a distinctive region of the spectrum.

4. Conclusions

The present study clearly demonstrates that FT-IR spectroscopy is an efficient method for the characterisation of the purified bentonite in an organic mixture. This technique remains economical, rapid, and specific. The spectrum can be obtained in a few minutes using the inexpensive instruments, which can be available in many analytical laboratories and can be served as a fingerprint for new drugs of mineral origin as an alternative to chromatographic retention time in HPLC.

Indeed, the FT-IR spectroscopy can be combined with other spectral methods such as X-ray diffraction in order to increase the specificity of the technique.

Data Availability

The data used to support the findings of this study are included within the article.

Conflicts of Interest

The authors declare that they have no conflicts of interest regarding the publication of this article.

References

- [1] M. L. McKelvy, T. R. Britt, B. L. Davis et al., "Infrared spectroscopy," *Analytical Chemistry*, vol. 68, pp. 93–160, 1996.
- [2] B. Stuart, *Modern Infrared Spectroscopy*, p. 180, John Wiley & Sons, New York and Chichester, UK, 1996.
- [3] O. Kolomiets, U. Hoffmann, P. Geladi, and H. W. Siesler, "Quantitative determination of pharmaceutical drug formulations by near-infrared spectroscopic imaging," *Applied Spectroscopy*, vol. 62, no. 11, pp. 1200–1208, 2008.
- [4] A. A. Bunaciu, H. Y. Aboul-Enein, and S. Fleschin, "Application of Fourier transform infrared spectrophotometry in pharmaceutical drugs analysis," *Applied Spectroscopy Reviews*, vol. 45, no. 3, pp. 206–219, 2010.
- [5] J. M. Chalmers and P. R. Griffiths, *Handbook of Vibrational Spectroscopy*, John Wiley & Sons, London, UK, 2002.
- [6] B. Özlem, *Determination of Narcotic and Psychotropic Substances Using Infrared Spectroscopy*, M.S. Thesis, Middle East Technical University Ankara, 2005.
- [7] E. A. Budura, D. Lupuleasa, C. Aramă, G. M. Nitulescu, and T. Balaci, "Preparation and characterization of inclusion complexes formed between simvastatin and hydroxypropyl- β -cyclodextrin," *Farmacia*, vol. 59, p. 512, 2011.
- [8] GUIDELINE, "ICH Harmonized Tripartite, "Specifications: test procedures and acceptance criteria for new drug substances and new drug products: chemical substances Q6A", " Current Step 4 version, Dated October 6, 1999, 2015.
- [9] G. Krishna, M. Muthukumaran, B. Krshnamoorthy, and A. Nishat, "A critical review on fundamental and pharmaceutical analysis of FTIR spectroscopy," *International Journal of Pharmacy*, vol. 3, p. 396, 2013.
- [10] J. K. Crowley and N. Vergo, "Near-infrared reflectance spectra of mixtures of kaolin-group minerals: use in clay mineral studies," *Clays and Clay Minerals*, vol. 36, no. 4, pp. 310–316, 1988.
- [11] J. Madejová, "FTIR techniques in clay mineral studies," *Vibrational Spectroscopy*, vol. 31, no. 1, pp. 1–10, 2003.
- [12] L. Ohannesian and A. J. Streeterhandbook, *Handbook of Pharmaceutical Analysis*, Marcel Dekker, New York, NY, USA, 2002.
- [13] A. E. Segneanu, I. Gozescu, A. Dabici, P. Sfirloaga, and Z. Szabadai, "Organic compounds FT-IR spectroscopy," in *Macro To Nano Spectroscopy*, InTech, Romania, 2012.
- [14] J. Madejová and P. Komadel, "Baseline studies of the clay minerals society source clays: infrared methods," *Clays and Clay Minerals*, vol. 49, no. 5, pp. 410–432, 2001.
- [15] A. Eisazadeh, K. A. Kassim, and H. Nur, "Solid-state NMR and FTIR studies of lime stabilized montmorillonitic and lateritic clays," *Applied Clay Science*, vol. 67–68, no. 5, pp. 5–10, 2012.
- [16] Z. Hubicki, E. Zieba, G. Wojcik, and J. Ryczkowski, "FT-IR/PAS and SEM EDX studies on aluminosilicates modified by Cs(I), Th(IV) and U(VI)," *Acta Physica Polonica A*, vol. 116, no. 3, pp. 312–314, 2009.
- [17] S. İşçi, C. H. Ünlü, O. Atici, and N. Güngör, "Rheology and structure of aqueous bentonite polyvinyl alcohol dispersions," *Bulletin of Materials Science*, vol. 29, no. 5, pp. 449–456, 2006.
- [18] A. Eisazadeh, A. K. Kassim, and H. Nur, "Physicochemical characteristics of phosphoric acid stabilized bentonite engineering," *EJGE*, vol. 15, p. 327, 2010.
- [19] S. Jeddi, A. Ouassini, M. El Ouahhaby, and H. Mghafri, "Valorisation of natural mineral substances (NMS) at adsorption techniques: case of olive oil mill waste waters,"

- Journal of Materials and Environmental Science*, vol. 7, p. 488, 2016.
- [20] P. Djomgoue and D. Njopwouo, "FT-IR spectroscopy applied for surface clays characterization," *Journal of Surface Engineered Materials and Advanced Technology*, vol. 03, pp. 275–282, 2013.
- [21] M. W. Dong, "The essence of modern HPLC: advantages, limitations, fundamentals, and opportunities," *LCGC North America*, vol. 31, p. 472, 2013.
- [22] J. C. J. Bart, *Additives in Polymers: Industrial Analysis and Applications*, John Wiley & Sons, Geleen, Netherlands, 2005.
- [23] M. W. Dong, *Modern HPLC for Practicing Scientists*, Wiley, Hoboken, NJ, USA, 2006.
- [24] M. Swartz, M. Emmanuel, A. Awad, and D. Hartley, "Advances in HPLC systems technology," *Supplement to LCGC North America*, vol. 27, p. 40, 2009.
- [25] R. I. Iliescu, E. Andronescu, G. Voicu, A. Fikai, and C. I. Covaliu, "Hybrid materials based on montmorillonite and citostatic drugs: preparation and characterization," *Applied Clay Science*, vol. 52, no. 1-2, pp. 62–68, 2011.

Review Article

Photoacoustic Spectroscopy in the Optical Characterization of Foodstuff: A Review

Claudia Hernández-Aguilar ¹, **Arturo Domínguez-Pacheco**,¹ **Alfredo Cruz-Orea** ²,
and Rumen Ivanov³

¹Programa en Ingeniería de Sistemas-SBAAM, SEPI-ESIME, Instituto Politecnico Nacional-ESIME Zacatenco, Col. Lindavista. 07738, Ciudad de México, Mexico

²Departamento de Física, CINVESTAV-IPN, A. P. 14-740. 07360, Ciudad de México, Mexico

³Unidad Académica de Física, Universidad Autónoma de Zacatecas, A.P. 580, Zacatecas, Mexico

Correspondence should be addressed to Claudia Hernández-Aguilar; clauhaj@yahoo.com

Received 24 June 2018; Revised 25 October 2018; Accepted 18 November 2018; Published 13 January 2019

Academic Editor: Johannes Kiefer

Copyright © 2019 Claudia Hernández-Aguilar et al. This is an open access article distributed under the Creative Commons Attribution License, which permits unrestricted use, distribution, and reproduction in any medium, provided the original work is properly cited.

In this review, the application of the photoacoustic spectroscopy (PAS) is presented as an option to evaluate the quality of food. This technique is a type of spectroscopy based on photothermal phenomena, which allow spectroscopic studies. According to the literature review, it was found that its application is increasing in several countries. Spectroscopic studies carried out by employing PAS in the food industry include, among others, fruit, vegetables, condiments, grains, legumes, flours, “tortillas,” milk, water, eggs, etc. Additionally, this technique has been used to evaluate adulterated, irradiated, and contaminated food and so on. The literature review has shown the applicability of PAS to one of the problems of the real world, i.e., food quality assessment. Therefore, PAS can contribute in the future with a wide potential for new applications in the food agroindustry.

1. Introduction

One of the problems worldwide is the quality and quantity of food. In developing countries, this is even more evident, causing several chronic diseases such as cancer and malnutrition, according to Hernández et al. [1]. Therefore, the development of technologies to improve global food production is necessary since one of the main challenges of our time is to feed a growing worldwide population [2–6]. In this order of ideas, it is also mandatory to develop technologies that evaluate food quality, before the direct impact that they have on population’s health and consequently on their quality of life. Several authors and public health professionals indicate a relationship between dietary behaviour and the food quality associated with the risk of some cancers and other existing chronic diseases [7, 8]. In this sense, the quality of the food is very important; in the case of cancer diseases, a close relationship between the diet and the

different types of cancers has been reported [9–11]. Cancer, among other factors, could be due to the intake of compounds in food that initiate or promote it. The food and its substances which are consumed provide the nutritional support for an organism and help for the disease prevention. However, sometimes they increase chemical substances, and instead of helping, they damage the organism [8]. This highlights the need for a greater level of food control: equal in quantity and quality (i.e., sometimes foodstuff contains both substances that harm and benefit human health. That is to say, to evaluate food in order to avoid consuming contaminated or degraded food (chemically or biologically) and to promote the consumption of food rich in phytonutrients (increasing the proposals for food integrated with superfood and/or fibre), etc. This, among other aspects, is relevant to the prevention of diseases [12]. In food production chain, it is known that contamination and/or degradation can occur at any stage due to contaminants: environmental,

agricultural, or incorporated during some agroindustrial process or storage [13]. On the one hand, it is essential to be aware of not consuming food that exceeds allowed limits of mycotoxins, nitrates, and nitrites, harmful fats, addition of preservatives, dyes, or sugar solutions. On the other hand, it is essential to consume food that provides health benefits, such as super-food, cholesterol free, rich source of proteins, minerals, iron, etc. Food rich in phytochemical may play an important role in the reduction of mortality. For the aforementioned facts, the need of a rapid and reliable quantification of compounds in food that contains disease-preventing constituents or food constituents that cause them is urgent, as it is recognized by the food processing industry [14].

Then, the development of technologies that support the evaluation of food quality every day becomes more relevant, due to the increase of diseases. Among the technologies for food analysis and determination of compounds, the photothermal techniques stand out. In particular, photoacoustic spectroscopy (PAS) is considered by some authors as a “green” technology for the food analysis [15], i.e., a method with less chemical waste and a minimal sample amount and a nondestructive technique [16]. PAS has some additional characteristics such as the fact that it does not require extraction or sample preparation and it does not use solvents, among others [17]. The reduction or elimination of the use of solvents is very important. For example, in the process of manufacturing, the use and disposal of chemical products and many toxic materials that are dangerous to humans and to the environment are frequent. In fact, these techniques are promising because they can be carried out by nondestructive analysis and without the use of solvents [15].

Currently, PAS technique, thanks to the technological advances, could be a convenient option to be incorporated in the agrofood industry, for example, in food quality assessment systems, with diverse specific applications (according to production systems and specific food of each case). PAS technique allows to obtain optical qualities of food, depending on its colour, which is the most useful parameter in the agrofood industry since quality and food flavours are closely associated with its colour [18]. Therefore, our objective is to perform a literature review of PAS applications in the food characterization from its origin to recent advances. In this way, it will be possible to know the current state, what has been done and what still needs to be done to reach the application of it in the real world. The PAS experimental setup continues to be optimized and focused on the specific problems of the real world where it could serve as a supportive technique, in order to improve and have attainable techniques for the evaluation of food quality and their respective control in the production process. It is one of the great worries of humanity, both to increase the food production and to take care of its quality, being this a key element in the development and life quality of societies.

1.1. Era before Photoacoustic Spectroscopy in Agriculture and Food. Isaac Newton in 1666, using a prism, observed and

recorded the dispersion of white (visible) light into its constituent colours [19] to describe the colours of the rainbow. He used the word “spectrum” for the first time in history. More than 100 years later, in 1802, Hyde Wollaston expanded Newton’s earlier observation by showing that sunlight possesses discrete bands of light, rather than a continuous spectrum. Wollaston became one of the most famous scientists for his observations of dark lines in the solar spectrum, which eventually led to the discovery of the Sun elements. In 1814, Fraunhofer discovered over 500 bands of sunlight, afterward called “Fraunhofer lines.” In 1859, Kirchoff and Bunsen invented the spectroscope [20], and they were the ones who developed the chemical analysis by using spectral lines [21, 22].

1.2. Photoacoustic Spectroscopy History. The photoacoustic (PA) effect was discovered, according to Rosencwaig [23, 24], by Tyndall, Röntgen, and Alexander Graham Bell, in 1881. Bell was working together with Charles Summer Tainter in the photophone. Bell discovered that selenium (and other solid materials) emits a sound when illuminated by a modulated light, which was achieved by passing it through a rotating disk with holes. Bell, using the spectrophotometer, discovered that the emitted sound intensity depends on the wavelength or colour of the incident light and that therefore the effect should be attributed to an optical absorption process [25].

Fifty years after its discovery, the PA effect was used in gas studies. It has ever since become a well-established technique for gas analysis and was well understood [26] with some applications also in environmental and food areas. However, the PA’s effect in solids was apparently ignored for 90 years until 1973, when Rosencwaig began his study of the PA effect in solids. Probably, this delay was due to the lack of sensitive sound detectors and high-power light sources [27].

The first photoacoustic spectra obtained by Rosencwaig were specifically of carbon-black, powder of Cr_2O_3 (normalized), a Cr_2O_3 crystal, rhodamine-B in a glycerol solution, and rhodamine-B powder [24]. Photoacoustic spectroscopy as a new tool for solid research was presented by Rosencwaig [27]. Since that time, he pointed out the main advantages of photoacoustic spectroscopy, paraphrasing him: “The principal advantage of photoacoustic spectroscopy is that it enables to obtain similar spectra on any type of solid or semisolid material, whether it be crystalline, powder, amorphous, smear, gel, etc. Furthermore, since only the absorbed light is converted to sound, light scattering (a very serious problem when dealing with many solid materials by conventional spectroscopic techniques) presents no difficulties in PAS.” In this sense, the PAS applications were divided under three main headings: bulk, surface, and de-excitation studies.

Also, pioneer applications of PAS in biology were made by Rosencwaig [27]. He obtained the photoacoustic spectra of smears of whole blood, of red blood cells freed from plasma, and of haemoglobin extracted from red blood cells, using the spectral region from 200 to 800 nm. Also, PAS

spectra of guinea pig epidermis (250–650 nm) in different conditions were obtained. He also reported a block diagram of single-beam photoacoustic spectrometer with digital data acquisition, integrated by: Xe Lamp, monochromator, chopper, photoacoustic cell, lock-in amplifier, voltage frequency converter, and multichannel analyzer. The first commercial spectrometer (Model 6001) was manufactured in 1980 by Princeton Applied Research Corporation [26, 28].

Other results were obtained with dried solids containing several other hemoproteins, including both soluble ones, such as cytochrome c and insoluble or membrane-bound ones such as cytochrome P-450. Further experiments showed that it is possible to identify absorbing substances (including some drugs) in dried urine samples (e.g., drops of urine over the filter paper)[28].

Regarding the area of the agrofood industry, the first photoacoustic spectra in plants were obtained in flowers by Harshbarger and Robin [29] among others.

1.3. Applications of PAS. Spectroscopy is the study of the interaction of electromagnetic radiation with atoms and molecules to provide qualitative and quantitative chemical and physical (structural) information, that is contained within the wavelength or frequency spectrum of energy that is either absorbed or emitted [30]. According to Sunandana [31]; Photoacoustic spectroscopy (PAS), the oldest form of photothermal techniques, is a type of spectroscopy and its name “photoacoustic” (PA) generally implies a particular technique or mechanism of detecting and measuring the optical absorption of opaque and diffuse materials, among others. The basic principle of photothermal spectroscopy is the detection of heat produced in a sample due to non-radiative de-excitation processes resulting from the absorption of intensity-modulated light (wave of pulsed light) by the sample. Thus, according to its basic principle, the PAS has been applied in Biology, Biophysics, Physics, Medicine, and in the Agrofood areas [32], rescuing an old technology for today’s needs.

Bicanic [14] mentioned that PAS is a sort of spectroscopy, nondestructive based on photothermal phenomena, which allows spectroscopic studies. The basic configuration uses Xe lamps, mainly in the UV-VIS range. This conventional configuration has been applied to the foodstuff analysis (obtaining PA spectra, as a function of wavelength) including plants, seeds, etc. Among the foodstuff that have been investigated by using PAS are grains and legumes (*Zea mays* L., *Triticum*, *Hordeum vulgare*, *Phaseolus vulgaris* L., and coffee), vegetables (spinach, lettuce, *Raphanus sativus* L., *Solanum lycopersicum* L., and *Capsicum annuum*), marine vegetables (algae and phytoplankton), fruit (açai, cupuaçu, Brazil nut, persimmon, mango, and strawberries), other liquids or semiliquid food (e.g., milk, water, juice, mustard, and ketchup), flours (maize, wheat, soybeans, peas, white bread flour, and rye), “tortillas” (maize (white and blue), wheat flour (integral or not integral), maize and “nopal,” linseed and “nopal,” etc.), condiments (turmeric and “chile pasilla”), powder (gelatins, curry, and cacao), food with coloring additives, etc. Furthermore,

adulterated food and fortified food, among others, have been analysed by using PAS technique.

The first PA spectra (in plants or food) were obtained in black-eyed susan petals, red rose petals, green leaf, and chloroplast of lettuce, marine algae, and spinach [27, 28, 29, 33, 34], among others. Harshbarger and Robin [30] reported photoacoustic spectra (PA or optoacoustic) of flower petals. With regard to susan blackeyed petals, the authors obtained an optical absorbance spectral band corresponding to carotenoids and another band in the ultraviolet region, related to the content of flavonol glucosides. The photoacoustic spectrum of a rose petal had two maximums, at 530 and 340 nm; the first maxima is due to cyanine absorbance in the flower, and the second one must be due to some other ultraviolet-absorbing compound in the petal.

Meanwhile, Rosencwaig showed photoacoustic spectrum of an intact green leaf with all the optical characteristics of leaf chloroplasts, including Soret’s peak (420 nm), carotenoids (450–550 nm), and chlorophylls (600–700 nm) bands. He points out that PAS can be used to observe secondary metabolites. Species of air-dried marine algae were also evaluated by Rosencwaig and Hall [32]. The authors showed that PAS can be used to estimate the amount of certain metabolites, and they also suggested that PAS could reduce the amount of material required for the screening of such substances (since extraction procedures generally require more material) and that it can greatly reduce the time required for the identification of plant components. Adams et al. [34] studied spinach leaf, where he demonstrated that the major absorbing components in the spinach were the chlorophylls. The chlorophylls are similar to the hemoproteins; they contain a porphyrin ring, this being chelated to magnesium at the ring centre. Then, the technique allowed it to be useful to determine quickly and easily the spinach components, directly and only using a small piece of spinach (10 mm), in the spectral region from 250 to 700 nm, finding spectral peaks at 450 and 650 nm. Other photoacoustic spectra were also obtained, in the initial era of photoacoustic applications for this purpose, in cotyledons, *Raphanus* pigments, *Tradescantia* leaves, etc. [35–37].

Since the initial PAS applications in agriculture and food until now, different spectral regions have been used, from ultraviolet to far infrared, including UV (200–400 nm), visible light (400–700 nm), and near infrared radiation (750–1100 nm). Also, it is important to take into account the lamp power, and there are several studies that indicate that the optimal Xe lamp power ranges from 300 to 1600 W.

According to the present review on PAS applications in food and plants, from the PA spectrum obtained by PAS, it is possible to determine concentrations or presence of compounds: rutin, red beet (in case of adulterated food), flavonoids and flavonols, carotenoids (lycopene, capsanthin, capsorubin, carotene, zeaxanthin, cryptoxanthin, lutein, etc.), basic amino acids (tryptophan, lysine, leucine, phenylalanine, etc.), anthocyanins, peroxide, and lead tetraoxide, among others. Also, by using PAS, it is possible to

detect changes in seeds due to induced radiation effects, use of dyes, differences in sanitary qualities, adulterated food, etc. In this sense, for some researchers, PAS is considered as an analytical method.

1.4. PAS Applications in Food and Agrofood Industry.

One of the industries which could be benefited by the use of PAS technology would be the milk industry. Martel et al. [30] carried out measurements by PAS of milk products. They analysed whole milk, 3.25% fat, skim milk, part skim, milk 2% fat, mild cheddar cheese, aged cheddar cheese, plain yogurt, and strawberry-flavoured yogurt drink. Their obtained spectra were in the ultraviolet region. They found a strong absorption peak at 280 nm for all products. For cheese samples, they observed in the spectra a tail, corresponding to fat presence, from 250 to 260 nm. Photoacoustic signal increases when protein concentration increases; the authors relate the UV absorbance band with aromatic amino acids (tryptophan, tyrosine, and phenylalanine), as a measure of protein content. They demonstrated the applicability of PAS to study different milk products, highlighting their utility for the milk industry.

PA spectra of tablets, made out of lyophilized raw milk, showed an absorption peak at 280 nm, corresponding to the absorption of proteins and a smaller absorbance band in the visible (400–500 nm) that might be assigned to milk carotenoids. When the tablets were heated, they gradually turn brown, which contributed to the changes in the PA spectra, appearing to a new band around 335 nm as a consequence of the Maillard reactions. The spectra became broader, to the red side of the spectrum. This could be the sign of many other reactions occurring in the sample according to Nsoukpog-Kossi et al. [38], demonstrating another possible utility of the photoacoustic technique.

Another use of PAS in the milk industry has been the possibility to measure different powdered milk protein concentrates, enriched with Fe in the form of ferrogluconate at different concentrations. Dóka et al. [39] obtained PA spectra, in these powdered samples, as a function of ferrogluconate concentration, obtaining an increase in the photoacoustic signal in the UV spectral region. The peaks, at 348, 380, and 552 nm, varied depending on the Fe concentration, resulting in a nonlinear relationship between the ferrogluconate content and the PA signal. In this way, the authors demonstrated that PAS measurements (in the UV-visible range) on milk protein concentrates are capable of determining the Fe content in ferrogluconate form. This demonstrates another possible application of PAS. As with the other applications to detect adulterated milk, it has been proven useful, for example, to detect skimmed milk adulterated with whey powder, when analyzing PA spectra at 370 nm wavelength [40].

PAS application in milk analysis was also reported in other studies, for example, milk (fresh and oxidized) was evaluated by using PAS. In these investigations, Dóka et al. [41] used fresh whole milk exposed to UV-C radiation and heat. The PA spectra, obtained by PAS, encompassed the spectral region from 200 to 500 nm. It was reported,

absorption peaks at 290 nm (for all evaluated cases), which is associated with the presence of aromatic amino acids in the milk powders. Spectral changes, induced by the accelerated oxidative treatment, were detectable in the 320–360 nm absorbance band (absorbance changes in this range are due to the reaction of aldehydes with a variety of amino compounds). The oxidation of whole milk powder and browning processes were mutually interrelated (i.e., if the oxidation took place, then the color of the powder would turn brown). The authors recommended PAS as a method for routine and rapid assessment of peroxide values in oxidized whole milk powder.

Another PAS application, useful in foodstuff area, is in the assessing of induced radiation effects. For example, irradiated egg powders were evaluated by PAS, finding two peaks, corresponding to the absorbance maxima, in the optical spectrum. One centered at 275 nm, which is related with the aromatic amino acids content in the sample. While the other peak, centered at 480 nm, is related to the presence of carotenoids. It is interesting that PA signal at 480 nm suggests a carotenoid decomposition due to the irradiation [42]. In summary, the foodstuff irradiation processes is another potential area for PAS applications.

On the other hand, the usefulness of PAS has been demonstrated to identify adulterated samples with lead tetraoxide (also called minium or red lead). Dóka et al. [43] obtained the PA spectra of pure paprika, red lead, and all adulterated samples, in the wavelength range from 320 to 700 nm. The normalised PA signal in a wavelength range from 600 to 700 nm was generally lower; a weak signal was observed at 670 nm. The PA signal from pure red lead was substantially larger than those obtained from adulterated samples. The PA spectra of the four adulterated samples show a peak at 545 nm. In this case, the potential of PAS, as a candidate method for rapid detection of gross amounts of red lead (Pb_3O_4) adulterant, in a ground sweet red paprika, was demonstrated. Although the authors recognize that the performance of this method was undoubtedly inferior to that of advanced methods, the PAS method is very practical and rapid in routine situations.

Other food sample types studied by PAS have been reported by Bicanic et al. [44], who mentioned that PAS technique could be used to detect red beet, added as a colorant to tomato ketchup. The associated changes of colour, resulting in changes of optical absorbance, were monitored in the 500 nm region, corresponding to the absorbance maxima of lycopene. Also, Bicanic [14] indicates that the argon laser line at 514 nm has been used for lycopene measurements because there is a high absorbance of lycopene and low interference of betacarotene. It is noteworthy that Bicanic (1943–2018) made a notable contribution to photoacoustic and photothermal science with numerous applications in agriculture, environmental science, and food quality, among other issues [45].

1.5. *Grains and Legumes.* PA spectra, as a function of wavelength, allow to obtain information about the sample. Also, it is possible to characterize samples regarding its

atomic or molecular composition according to De Oliveira et al. [17]. In the case of corn grains, Dominguez et al. [46] obtained the PA spectrum of maize, in the 300–800 nm wavelength range. They found absorbance bands associated with different natural pigments. This group used white, yellow, and blue maize; in the case of white maize seed, a broad absorbance band was observed in the UV region, from 300 to 400 nm, with a signal peak around 360 nm. While for the yellow and blue maize seeds, the band of PA signal decays around 435 nm. This band could be due to the presence of flavonoids and flavonols. In the case of yellow and blue maize seeds, they have an absorbance band ranging from 470 to 540 nm, being this band associated with the presence of carotenoids. Specifically, for blue maize seed, an absorbance spectrum ranging from 500–690 nm was observed, which is due to the presence of anthocyanins.

Another characteristic of corn seed is its structure type, crystalline or floury. From the photoacoustic signal, Hernández-Aguilar et al. [47] found the optical absorption coefficient (β) and optical penetration length (l_p), as a function of wavelength. The floury seed variety had a higher β value at 650 nm. In this sense, the authors showed that by means of the optical absorption coefficient, differences between maize varieties of different structures are observed. The PA signal amplitude is higher for floury seeds. Similarly, significant statistical differences were found in the optical absorption coefficient spectra of white maize seeds (of different white), with an absorbance band ranging from 325 to 425 nm wavelength. Also, other authors found differences between the spectra of the first derivative obtained from the β values [48]. Other researches, such as De Oliveira et al. [17], have indicated that the PA signal amplitude is directly proportional to the concentration of absorbing analytes, where analyte is a component (element, compound, or ion) of analytical interest on a sample. According to Dóka et al. [49], PAS could be an analytic technique and also a fast and relatively cheap technique.

Other authors have used mathematical analysis on the PA signals, such as the first and second derivatives or mobile standard deviation. This has allowed to distinguish better the maximum peaks of maize grains with different pigmentations, identifying differences of the corn seeds [50]. The use of derivatives in spectra enhances the identification of differences among spectra, resolves overlapping bands, and especially improves the detectability of weaker spectral shoulders. In this sense, PAS could be used in quantitative analyses of compounds [16]. Also, photoacoustic spectroscopy is useful to study dyed samples, not only with natural pigments.

Other studies have pointed out the role of PAS: by using different light modulation frequencies, it is possible to explore different seed depths, e.g., Hernández-Aguilar et al. [47] obtained the PA spectra of maize seeds (*Zea mays* L.) at different frequencies (17, 30, and 50 Hz). They compared these spectra with the ones obtained from the phase-resolved method, used to separate the spectra of the seed pericarp and endosperm. Also, photoacoustic spectra, of separate structural components of the seed, were obtained (pericarp, aleuronal layer, and endosperm) and compared with those

obtained by the phase-resolved method. The authors indicated that the absorbance band from 550 to 750 nm is due to the anthocyanins in the aleurone layer. So, the PAS technique has a potential for depth profile analysis on complex specimens with different structural components and also, through the absorbance bands, to determine the associated components.

Moreover, PAS has been applied to study wheat, barley, and beans among other grains and legumes, where from PA spectra, it is possible to analyse the differences of the characteristic spectra obtained among the evaluated materials. For example, Dóka et al. [49] by using PAS in buckwheat found PA spectra, as a function of wavelength and observed two absorbance peaks, at 275 and 378 nm, related to the protein content and rutin, respectively. PA signal appears to be proportional to the rutin content of the samples across the entire wavelength range. Thus, the authors reported that UV-PAS could be an analytical tool for rapid and simple quantification of rutin in buckwheat, and they found a decrease of the time required for the analysis of buckwheat samples when a calibrated curve, of known rutin content, is used.

Photoacoustic spectrum decreases as a function of the frequency, and differences are obtained in the spectra of the deteriorated and nondeteriorated grains. The authors reported lower PA signal in the young seeds when compared with the older ones, due to deterioration in the older seeds because of the presence of fungi or bacteria during storage. This fact produces dark regions and, as a consequence, a higher signal, pointing out another possibility of PAS use, to evaluate sanitary quality of grains [51].

1.6. Flours and “Tortilla”. Other potential applications that some authors have proposed for PAS are for quality control in the food processing industry. For example, Favier et al. [52] determined the PA spectra (350–700 nm) of white bread flours, dried pea flour, rye flour, and bread flour. PAS technique appears to be capable of producing reproducible spectra of powdered food samples. The PA spectra of white bread flours have absorbance bands around 370, 385, and 410 nm. For wavelengths above 410 nm, the PA signal decreases rapidly and drops to a nearly zero amplitude at 700 nm. Unlike this, the dried pea flour is the only sort that has a maximum signal at 410 nm. Soya flour exhibits a broader spectrum, whereas rye flour resembles that of the bread flour and also produced the highest signal of all the samples. On this basis, the researchers propose PAS as a viable method for the determination of basic amino acids present in biological samples.

Dóka et al. [53] obtained PA spectra, in the range from 250 to 550 nm, of sorghum (*Sorghum bicolor* L.) grain flour. They related the PA spectrum with the presence of aromatic amino acids, flavonoids, and phenolic compounds due to the absorbance peaks located at 285 and 335 nm; they also found that the PA signal decreases when the wavelength is increased. The authors indicated that the main advantage of PAS technique, with respect to a conventional analysis method, is that it is possible to study directly powdered

samples, i.e., as they are, without sample preparation. This fact greatly reduces the time needed for its analysis. On the other hand, determination of water contents in the wheat flour (soft and hard), corn starch, and potato starch by PAS also have been evaluated [54].

Different types of “tortillas” elaborately corn (white and blue) and wheat flour (integral and not integral)—manually processed or not, fortified, and/or supplemented with “nopal,” linseed, “epazote,” and spinach—among others, were analysed by PAS. From the photoacoustic signal, it was possible to obtain the optical absorption coefficient, which was decreasing with the increase in wavelength [55]. In general, photoacoustic spectroscopy is a sensitive technique to characterize inhomogeneous materials.

1.7. Fruit, Vegetables, and Condiments. In Brazilian tropical fruit and vegetables, carotenoids and flavonoids were identified by PAS. Biomolecules of β -carotenes and flavonoids were identified in acerola, pumpkin, broccoli, cabbage, cauliflower, spinach, purple-cabbage, orange tangerine, mango, rucula, and cuité. In addition to the biomolecules of beta-carotene and flavonoids, chlorophyll was also found in watercress and lettuce. Regarding β -carotene, lycopene, lutein, lutein 5, and 6 epoxide were identified in carrots. β -carotene and lycopene were determined at tomato; β -carotene, chlorophyll, and zeaxanthin were found in maize leaves; and β -carotene, lycopene, and possible capsanthin were found in red pepper [56]. Finally, PAS technique can contribute to select and classify fruit, leaves, and other vegetables according to their phytotherapeutic and nutritive properties. Lima and Filho [57] reported that PAS is a rapid, direct, and efficient analytical method in biomaterials, particularly in the promising field of photochemistry and photobiology.

Other authors have shown the potential of photoacoustic spectroscopy in the assessment of stages of maturity of strawberries using the spectral ratio of anthocyanin and protein bands. Characteristic bands were found: a major one at 278 nm, related to proteins, and a second band around 510 nm attributed to anthocyanin pigments. The authors highlight that PAS is a non-destructive technique that might be extended to other horticultural crops [57].

In this way, PAS is a type of absorption spectroscopy, which allows to obtain optical absorbance spectra, as a function of wavelength, which provides information about the optical absorbance processes that occur in the sample. It is also possible to characterize samples regarding its atomic or molecular composition according to De Oliveira et al. [17]. Over the years, different methods have been used for the analysis of signals by PAS (Table 1): methods of subtraction, statistical analysis, correlation, variance analysis, derivatives (1 and 2), Gaussian deconvolutions, regression model, multivariable analysis, etc. Using these methods, the extraction of information of the PA signal has been improved. Some researchers have validated this by the use of other conventional techniques such as the UV-Vis spectrophotometer with an integrating sphere.

In general, according to Dóka et al. [53], PAS offers several advantages over other analytical techniques: it is nondestructive, requires no pre-preparation of the sample, and is applicable to specimens such as powders as well as optically opaque and gelatinous samples.

Table 1 summarizes the reached progress regarding the applications of PAS, according to the literature review carried out, from its origin to the last years, as a result of several scientific activities around the world in this area. It is possible to observe different food types and agricultural material, which have been evaluated by PAS, using conventional instrumentation, to obtain its optical spectra. The meaning of the different columns is as follows: (0) type of sample, (1) some characteristics of the experimental condition and/or sample preparation, (2) the spectral region used for the sample investigation, (3) the applied lamp power and/or light modulation frequency, (4) wavelengths of the absorbance peaks or spectral region, (5) applied mathematical methods, and finally (6) significant results reported in the literature.

Photoacoustic spectroscopy can be said to have been applied successfully in foodstuff analysis. Figure 1 shows the regions or absorbance peaks related to compounds (e.g., Figure 1) by photoacoustic spectroscopy, which have served to relate the absorbance spectra with these compounds. Even for some compounds, through calibration curves and mathematical analysis, the concentration of the compound has been obtained.

PAS using the conventional configuration, xenon lamp, lock-in, photoacoustic cell, chopper, etc. It has been used, since its first applications and up to date, among other purposes, to obtain photoacoustic spectra of plants and then of foodstuff. There is evidence of a potential application in the future, since its use has increased as can be seen in Figure 2. It is possible to observe that, at the beginning of the application of PAS in foodstuff and plants, there were fewer scientific reports than those that exist now. According to the present literature review, it was found that, in the decade of the 70's, there were only four articles (in this area and in order to obtain only absorption spectra, the motive of the present review), in comparison of the recent included period (2010–2018), where there were 24 articles (considering only those analyzed in the summary of applications of photoacoustic spectroscopy in foodstuff and plants in this review).

It is possible to observe a positive tendency of PAS applications in the foodstuff area, in this particular case, to characterize foodstuff through optical absorbance spectra, making calibrations and mathematical analysis of data. It is known that different photoacoustic configurations have diverse applications in several areas of the knowledge and with the possibility of being used for the obtaining of spectra not only as a function of wavelength, but as well as a function of light modulation frequency. It is worth mentioning that not only amplitude spectra but also phase ones and signals depending on the frequency can be obtained, which would lead to the application of other methods and mathematical analysis to obtain nonradiative relaxation times and sample depth analysis [95–100], among other optical and thermal parameters.

TABLE 1: Summary of applications of photoacoustic spectroscopy in foodstuff and plants.

Specimen	Experimental criterion	Spectral region λ (nm)	Source (power (W)) and modulation frequency (Hz)	Region or centers absorbing (CA) λ (nm)	Mathematical analysis	Significant findings/results	Country
Red lettuce and chard seeds	Pieces of fresh fruit were used.	250–750	Xenon lamp $P = 700$ W (chopper, 17 Hz)	600, 300	None	By using PAS, aged seeds in vegetable were evaluated. Nonaged seeds had higher β values than aged seeds (Pardo et al.) [58]. By using PAS, band peaks were found corresponding to phenolic acids: p-hydroxybenzoic, gallic, protocatechuic, vanillic, cinnamic, p-coumaric, caffeic, and ferulic (Neto et al.) [59]. The level of photoacoustic signal is diminished depending on the quality of lemon evaluated. The lower quality corresponds lower photoacoustic signal level. The band of greatest absorption for lemon juice was found at 300–400 nm, related to the flavonoid region (Corzo-Ruiz et al.) [60]. Photoacoustic signal increases as a function of the dehydration time; the authors relate the flavonoid region between 265 and 400 nm (Zendejas-Leal et al.) [61].	Mexico
Acai, cupuaçu, Brazil nut, and persimmon	Pieces of fresh fruit were used.	200–400	Xe arc lamp $P = 1000$ W (chopper, 30 Hz)	218.4, 224.6, 227.2, 207.1, 218.4, etc.	Spectral deconvolution		Brazil
Persian lime juice (<i>Citrus latifolia</i>)	Persian limes were divided into four categories: the highest quality, the second-class, the third-class, and waste-class.	300–800	Xe lamp $P = 1000$ W (chopper, 17 Hz)	314, 359, 445, 496, 684	Second derivative		Mexico
Chili pasilla peppers (<i>Capsicum annuum</i> L.)	Chile pasilla was used dehydrated.	250–700	Xe lamp $P = 1000$ W (chopper, 17 Hz)	265–400	None		Mexico

TABLE I: Continued.

Specimen	Experimental criterion	Spectral region λ (nm)	Source (power (W)) and modulation frequency (Hz)	Region or centers absorbing (CA) λ (nm)	Mathematical analysis	Significant findings/results	Country
Maize (<i>Zea mays</i> L.): White, yellow, and blue	Sample adapted to the cell size (6 mm).	300–800	Xe lamp $P = 700$ W	300–350 300–450 300–460	Variance analysis and least significant difference (LSD) test	Indicated a ratio of the absorbance bands of each maize evaluated (white, yellow, and blue colors), with components such as flavonoids, flavonols, carotenoids, and anthocyanins (Dominguez-Pacheco et al.) [46]. Using PAS, it was possible to observe two absorbent peaks at 280 and 378 nm related to protein content and rutin, respectively (Dóka et al.) [49]. Flavonoids show at least two absorbance bands: one ranging from 240 to 280 nm and another from 300 to 400 nm. The correlation between the PA absorption spectra of the samples and their total phenolic content was found. The phenolic content of the samples was linearly associated with its normalized PA signal at 475 nm (De Oliveira et al.) [17].	Mexico
Buckwheat grain meal	Whole meal was prepared from the grain.	250–600	Xe lamp 1000 W (chopper, 17 Hz)	280, 378	Standard deviations, correlation		Hungary Netherlands Italy
Mushrooms <i>Agaricus brasiliensis</i>	A volume of 80 mm ³ of each sample was used.	270–1000	Xe arc lamp $P = 1000$ W (chopper, 16 Hz)	300–400 475	Multivariate analysis, linear correlation		Brazil

TABLE 1: Continued.

Specimen	Experimental criterion	Spectral region λ (nm)	Source (power (W)) and modulation frequency (Hz)	Region or centers absorbing (CA) λ (nm)	Mathematical analysis	Significant findings/results	Country
Maize (<i>Zea mays</i> L.)	The seeds used were three: crystalline white maize, crystalline yellow corn, and floury blue maize.	300–800	Xe lamp $P = 700$ W (chopper, 17 Hz)	350	Statistical analysis	It was indicated, the main absorption center was found at 350 nm of wavelength, and it was associated to the presence of flavonoids and flavonols. At 470 nm, the absorption centers could be due to the presence of carotenoids, and at 650 nm, the absorption centers are associated mainly with the presence of anthocyanins (Dominguez-Pacheco et al.) [46]. The optical absorption coefficient of two growing regions in Mexico was found to have a similar behavior in all grains (Rodríguez-Páez et al.) [62]. From the photoacoustic signal, the optical absorption coefficient (β) and optical penetration length (l_β), both as a function of the wavelength, were measured, identifying differences between the floury and crystalline seeds β value at 650 nm (Hernández-Aguilar et al.) [63].	Mexico
Maize (<i>Zea mays</i> L.)	Prior to the study, the seed lot was standardized in size and color.	270–500	Xe lamp $P = 700$ W (chopper, 17 Hz)	350	Statistical analysis		Mexico
Maize (<i>Zea mays</i> L.)	The seed varieties used were crystalline and floury.	325–700	Xe lamp $P = 700$ W (chopper, 17 Hz)	350 650	Variance analysis		Mexico

TABLE 1: Continued.

Specimen	Experimental criterion	Spectral region λ (nm)	Source (power (W)) and modulation frequency (Hz)	Region or centers absorbing (CA) λ (nm)	Mathematical analysis	Significant findings/results	Country
Maize seed (<i>Zea mays</i> L.)	The seed genotypes had bluish pigmentation.	330–800	Xe lamp $P = 1000$ W (chopper, 17 Hz)	450	Phase resolved	PA signal phase can be used to characterize layers at different depths. The authors reported the optical absorbance spectra at different light modulation frequencies and compared these spectra with the ones obtained from the phase-resolved method in order to separate the optical absorption spectra of seed pericarp and endosperm. Absorption band in the range of 550–750 nm is attributed to anthocyanins in the aleurone layer (Hernández-Aguilar et al.) [47]. The curcuma and “curry” have a higher optical absorbance spectrum obtained by PAS when compared to the optical absorption spectrum of mustard at the range of 300 to 670 nm. The maximum absorption peaks in the samples evaluated from calculating the first derivative of the absorbance spectra were found at 318, 345, and 535 nm (Hernandez et al.) [64].	Mexico
Curcuma curry mustard	The samples were placed in the photoacoustic cell without previous preparation. In the case of mustard, it was placed on filter paper.	280–700	Xe lamp $P = 700$ W (chopper, 17 Hz)	290–540 318, 345, and 535	First derivative		Mexico

TABLE 1: Continued.

Specimen	Experimental criterion	Spectral region λ (nm)	Source (power (W)) and modulation frequency (Hz)	Region or centers absorbing (CA) λ (nm)	Mathematical analysis	Significant findings/results	Country
Chili pasilla peppers (<i>Capsicum annuum</i> L.)	Pasilla chili peppers were studied in three different stages: green, red, and dried.	300–800	Xe lamp $P = 1000$ W (chopper, 17 Hz)	330, 354, and 367	None	The photoacoustic signal was directly proportional with the wavelength. Absorbance spectra qualitatively show that the green stage is richer in flavonoids and that decrease and degrade as the peppers ripen (Barrientos-Sotelo et al.) [65].	Mexico
Malting barley seeds	The seeds were photosensitized by soaking them for one hour in methylene blue.	400–700	Xenon lamp $P = 700$ W (chopper, 17 Hz)	575	Statistical analysis	By photoacoustic spectroscopy, it is possible to obtain the optical absorption coefficient of barley seeds at different conditions: in natural color and dyed with methylene blue. Also, it is possible to define the optical range where the samples are optically opaque or optically transparent (Pérez Reyes et al.) [66]. Both varieties show distinct maxima absorption peaks, which correspond to zero values in the first derivative of β (optical absorption coefficient). For the blue maize grain, maximum absorption peaks were observed at (348, 502, 623, and 671) nm. In the case of the yellow maize grain, maximum absorption peaks were observed at 392 nm and 505 nm (Molina et al.) [50].	Mexico
Maize grains (<i>Zea mays</i> L.)	Grains were obtained from the central part of the ear of corn for each variety; blue maize and yellow maize were used.	325–800	Xe lamp $P = 700$ W (chopper, 17 Hz)	348, 502, 623, 671, etc.	First derivative		Mexico

TABLE 1: Continued.

Specimen	Experimental criterion	Spectral region λ (nm)	Source (power (W)) and modulation frequency (Hz)	Region or centers absorbing (CA) λ (nm)	Mathematical analysis	Significant findings/results	Country
Dutch-processed cocoa powder	Grating chocolate samples was the only preparatory step required.	300–650	Xe lamp $P = 1000$ W (chopper, 17 Hz)	No peaks	Standard deviations, correlation	The obtained spectrum features no characteristic peaks in the investigated wavelength range. There is a trend of decreasing PA signal with increasing wavelength based on the shape of spectrum (Dóka et al.) [67]. β decreases with increasing wavelength, being reported the highest absorbance band in a range of 350–450 nm. Significant statistical differences were found between the photoacoustic signals obtained from each variety of beans at 408 nm (Sanchez-Hernandez et al) [68]. The spectrum reported by the authors presented the highest absorbance band in a range of 325–400 nm (Molina et al.) [48].	Hungary, Netherlands
Beans (<i>Phaseolus vulgaris</i> L.)	The varieties used were cultivated during the spring-summer agricultural cycles of the years 2002, 2001, 2006, 2002, and 2006 in different regions of Mexico	350–750	Xe lamp $P = 700$ W (chopper, 17 Hz)	350–450	Variance analysis		Mexico
Maize (<i>Zea mays</i> L.) grains	Corn adjusted to a size: diameter and thickness of 6 and 3 mm, respectively. The fruit of seven apricots were examined at 80 % of their commercial maturity, and sample volume was of 0.25 cm ³ .	325–800	Xe lamp $P = 700$ W (chopper, 17 Hz)	350	Analysis of the variance, first derivative		Mexico
Lyophilized apricots (<i>Prunus armeniaca</i> L.)		—	Xe lamp $P = 1000$ W 17 Hz	470, 450	Standard deviations, correlation	PAS appears to be the most favourable technique to determine total carotenoid content, among others (Dóka et al.) [69].	Hungary Croatia Netherlands Belgium

TABLE 1: Continued.

Specimen	Experimental criterion	Spectral region λ (nm)	Source (power (W)) and modulation frequency (Hz)	Region or centers absorbing (CA) λ (nm)	Mathematical analysis	Significant findings/results	Country
"Tortillas"	The samples were homogenized in color and sizes, ordering the measurement, same side of the "tortilla".	350–700	Xe lamp $P = 700$ W (chopper, 17 Hz)	360–400	Analysis of variance and model of Paulet and Chambroon (1979)	The authors indicate that PAS was able to find the optical absorption coefficients (β) of colors of different tortillas from the photoacoustic signals amplitude and using the Rosencwaig and Gersho model. PAS is simple to use, requires only a small quantity of sample for analysis, and involves a minimum preparation (Hernández et al.) [55]. PAS was considered as a potential diagnostic tool for the characterization of the seeds, and it was possible to find the optical absorption coefficient β for maize seeds. In addition, conventional reflectance measurements (obtained with the integrating sphere) were performed to validate PAS absorption measurements. The results show that the absorbance spectra and reflection data of the seed samples are complementary (Hernández-Aguilar et al.) [70].	Mexico
Maize (<i>Zea mays</i> L.)	The seeds were homogenized in terms of size, shape, and color and dimensions adjusted to the size of the PA cell (6 mm, diameter).	320–700 620–700	Xe lamp $P = 700$ W and modulated (chopper, 17 Hz)	350–390 Metil red: 450–590	Model of Rosencwaig and Gersho test Tukey		Mexico

TABLE 1: Continued.

Specimen	Experimental criterion	Spectral region λ (nm)	Source (power (W)) and modulation frequency (Hz)	Region or centers absorbing (CA) λ (nm)	Mathematical analysis	Significant findings/results	Country
Coffee grains (adulterated)	The beans were roasted (210°C) during a time of 6 to 7 min. The adulteration was carried out, adding beans and barley.	300–800	Xe arc lamp $P = 1000$ W (chopper, 17 Hz)	300–450 700–800	Derivatives and differences	The photoacoustic technique allows spectroscopic studies of adulterated coffee from a direct analysis of solid samples of coffee powder, barley soya, and beans. Significant differences are observed, in terms of form, between 300 and 450 nm, where the behaviour of the carotenes and β -carotenes change as the adulterant (bean) is added. Similarly, the region of 700 to 800 nm corresponding to the absorption of the alkaloid “caffeine,” is also attenuated (Salcedo et al.) [71].	Colombia
Dried pastas	Pastas prepared with different amounts of eggs were studied	400–550	Xe lamp $P = 1000$ W (chopper, 17 Hz)	470	Correlation Regression	PAS can be proposed as a new analytical tool for a rapid screening/control of the total carotenoid concentration in pastas (Dóka et al.) [72].	Hungary, Netherlands Croatia

TABLE 1: Continued.

Specimen	Experimental criterion	Spectral region λ (nm)	Source (power (W)) and modulation frequency (Hz)	Region or centers absorbing (CA) λ (nm)	Mathematical analysis	Significant findings/results	Country
Dyes in commercial products: brilliant blue (B), sunset yellow (S), and tartrazine (T)	Solutions of gelatine powder (peach and lemon flavors, dissolved in hot water) and juice powder (citrus fruit flavor, dissolved in water,) were used.	350–750 350–550 350–600	Xe arc lamp $P = 800$ W (chopper, 20 Hz)	600–680 380–490 430–540 620, 510, 452	Deconvolution from Gaussian	Photoacoustic spectroscopy allowed the simultaneous determination of brilliant blue, sunset yellow, and tartrazine as binary mixtures in gelatin and juice powders, with a very good agreement between the values determined by using first derivative spectrophotometry. The PAS technique can be applied for the determination of the selected dyes in commercial food products (Coelho et al.) [16]. Differences between the photoacoustic spectra of the infected seed were found. Superior PA spectral curve was for the sample (treated), intermediary PA spectral curve is for sample (with fungus scraps), and inferior PA spectral curve is for sample (fungus infected). Characteristics peaks and bands were observed in the range from 650 to 900 nm ascribed to organic compounds with carboxylates and amines (functional groups) forming the typical metabolic structures of the fungus (Rezende et al.) [73].	Brazil
Acai (<i>Euterpe oleracea</i>) seeds	<i>C. gloeosporioides</i> fungus-infected acai seed samples were used as small pastilles 6 mm in diameter and 1 mm in thickness to standardize its form.	250–1000	Xe arc lamp $P = 150$ W	300–350 650–900	Fit to the data when they were obtained as a function of frequency		Brazil

TABLE 1: Continued.

Specimen	Experimental criterion	Spectral region λ (nm)	Source (power (W)) and modulation frequency (Hz)	Region or centers absorbing (CA) λ (nm)	Mathematical analysis	Significant findings/results	Country
Maize (<i>Zea mays</i> L.)	The seeds used were of the following colors: white, yellowish, and bluish.	600–710 500–750	Xe lamp (chopper, 17 Hz)	650	Statistical analysis	PAS technique demonstrated to be a useful for the study of the effects in liquid chlorophyll of seedling leaves which came from irradiated maize seeds. The bluish-colored seed had the highest optical absorption coefficient and a negative laser light response, when it was treated before sowing (Hernández-Aguilar et al.) [74]. Photoacoustic spectrum decreases as a function of the frequency, and differences are obtained in the spectra of the deteriorated and nondeteriorated grain, where the authors reported lower optical absorption in the young seed when compared with the older one due to deterioration in the older seed because of the presence of fungi or bacteria during storage, and this fact produces dark regions and, as a consequence, a higher optical absorption (Pacheco et al.) [51].	Mexico
Wheat grains (<i>Triticum aestivum</i> L.)	Wheat seeds from different productive cycles and measured area of 4×6 mm were used without prior preparation.	350–800	Xe lamp (chopper, 17 Hz)	350	None		Mexico

TABLE 1: Continued.

Specimen	Experimental criterion	Spectral region λ (nm)	Source (power (W)) and modulation frequency (Hz)	Region or centers absorbing (CA) λ (nm)	Mathematical analysis	Significant findings/results	Country
Wheat	Two seed conditions were used: treated with methylene blue and untreated.	600–700	Xe lamp $P = 1000$ W (chopper, 17 Hz)	650	Statistical analysis	The PA spectroscopy was demonstrated as a suitable technique to study the optical absorption coefficient β of wheat seeds with and without photosensitizer (Hernández-Aguilar et al.) [75]. The PA method was demonstrated as a technique capable of studying the effect caused by irradiation (diode laser radiation at 650 nm) of maize seeds. PA signals were related in the range of 471 to 478 nm with β -carotene and lutein, the natural pigments present in the seedling leaf of maize (Hernández-Aguilar et al.) [76]. Statistical differences were found between certain ranges of wavelength of the spectra of each type of coffee. The PAS technique allows a spectroscopic analysis of organic opaque samples (Delgado et al.) [77]. The distilled water is transparent between the wavelengths 326 to 920 nm. The strong absorption peak was found at the wavelength 226, 289, and 974 nm (Kapil et al.) [78].	Mexico
Maize (<i>Zea mays</i> L.)	Maize seeds were irradiated by a diode laser.	400–500	Xe lamp $P = 1000$ W (chopper, 17 Hz)	471–478	Statistical analysis		Mexico
Coffee	Organic and conventional green coffee beans were used.	300–800	Xe arc lamp $P = 1000$ W	432–718, 725–740, 743–772	Derivative subtraction and ANOVA		Colombia
Water	PA spectrum were recorded under the laboratory conditions ($T = -10^\circ\text{C}$, $P = 3.5105$ Pa).	200–1100	Xe arc lamp $P = 500$ W	226, 244, 289, 302, 326, 744, 844, 920, 974	None		India

TABLE 1: Continued.

Specimen	Experimental criterion	Spectral region λ (nm)	Source (power (W)) and modulation frequency (Hz)	Region or centers absorbing (CA) λ (nm)	Mathematical analysis	Significant findings/results	Country
Corn (seedlings)	Irradiated seeds presowing with laser diode.	600–700	Xe lamp 1000 W (chopper, 17 Hz)	650, 680	Statistical analysis	Significant statistical differences were found in the amplitude of the photoacoustic signal when seedling leaves from irradiated seeds were measured, comparing the points corresponding to chlorophylls "a" and "b," i.e., at 680 and 650 nm (Hernández et al.) [79]. The amplitude of the PA signal contained several absorption centers; in this case, those corresponding to the chlorophyll pigments were identified. To identify them more clearly, the criterion of the second derivative was used (Delgado et al.) [80]. PA spectra show two characteristic bands: the first one (centered at 285 nm) is due to aromatic amino acids in sorghum flour, while another, close to 335 nm, is due to the flavonoids and phenolics acid present in the pericarp of sorghum flour. The PA signal decreases with increasing wavelength across the entire spectral range studied (Dóka et al.) [53].	Mexico
Coffee	The coffee roasting was done in a temperature range between 200 and 210°C.	510–775	Halogen lamp $P = 1000$ W	630 and 670	Second derivative		Colombia Mexico
Red sorghum (<i>Sorghum bicolor</i> L.) flours	Grains were surface-sterilized by washing and stirring them in a 5% aqueous solution of sodium hypochlorite, later the grains were dried.	250–550	Xe lamp 300 W (chopper, 16 Hz)	285, 335	Correlation		Hungary Netherlands

TABLE 1: Continued.

Specimen	Experimental criterion	Spectral region λ (nm)	Source (power (W)) and modulation frequency (Hz)	Region or centers absorbing (CA) λ (nm)	Mathematical analysis	Significant findings/results	Country
Water, hexagonal ice, and snow	Snow (surface hoar) was prepared in the laboratory by injecting warm moist air plus water vapor in a cold chamber.	200–1100	Xe arc lamp $P = 300$ W	320, 971–974	None	PA spectrum of distilled water shows a strong absorbance in the ultraviolet UV region below 320 nm and another strong absorbance maxima at the wavelengths 971–974 nm, in the near infrared NIR region. Between the wavelengths 320–922 nm, distilled water is transparent. In general, the overall PA signal strength is greater in ice as compared to snow (Kapil et al.) [81]. Indicated the presence of three bands at ~ 220 , 250–280 and 330–370 nm in good agreement with conventional optical absorption spectrum attributed to the flavonoid type of biomolecules called quercetin (Lima and Filho) [56]. The authors show that PA spectroscopy is a suitable nondestructive technique for distinguishing pathogens of different genera and species. This technique proved useful for differential diagnosis of various seed-borne pathogens of wheat and rice (Gupta et al.) [82].	India
Mango	None	200–400	Xe arc lamp $P = 1000$ W	220, 250–280, 330–370	None		Brazil
Wheat and rice (pathogens)	Spores were extracted from the infected seeds.	200–800	High-pressure Xe lamp $P = 300$ Watt	232, 292, 372, 552, 652, 272, etc.	None		India

TABLE 1: Continued.

Specimen	Experimental criterion	Spectral region λ (nm)	Source (power (W) and modulation frequency (Hz))	Region or centers absorbing (CA) λ (nm)	Mathematical analysis	Significant findings/results	Country
Milk (fresh and oxidized)	The whole milk powder of different compositions (composition: 27% fat, 26% protein, 5% water, 36% lactose, and 6% ash) was used and was oxidized by exposing it to UV radiation and heat in the presence of air.	250–500	Xe lamp 300 W (20 Hz)	290 320–360	Correlation	The authors indicated that PAS is a method for routine and rapid assessment of peroxide value in oxidized whole milk powder. Absorbent peaks were found at 290 nm associated with the presence of aromatic amino acids in the milk powders. Spectral changes by oxidation were in 320–360 nm (Dóka et al.) [41]. The optical absorbance spectra reveal the presence of flavonoids in the pericarp which are sensitive to the action of alkaline cooking and which are characterized by an absorbance band between 400 and 450 nm that provide the characteristic coloring yellowish to these biopolymers (Hernandez et al.) [83].	Hungary Netherlands
Pericarp of maize (<i>Zea Mays</i> L.)	The material evaluated was obtained of maize grain nixtamalized.	300–700	Xe lamp	400–450	Spectrum differences		Mexico

TABLE 1: Continued.

Specimen	Experimental criterion	Spectral region λ (nm)	Source (power (W)) and modulation frequency (Hz)	Region or centers absorbing (CA) λ (nm)	Mathematical analysis	Significant findings/results	Country
Pericarp of maize (<i>Zea Mays</i> L.)	Cooked corn was used from which the pericarp was extracted to evaluate it.	300–700	Xe lamp (chopper, 17 Hz)	300–350 375–450	Spectrum differences	Absorbance spectrum in the region of 300–800 nm in these films is constituted by the superposition of two absorbent centers: one corresponding to the absorption in the UV region of 300–350 nm for cellulose in the epidermis and the other in the region of 375–450 nm corresponding to the pigments present in the pericarp that are sensitive to an alkaline medium (Hernández et al.) [84]. The unknown amount of foreign whey powder can then be determined from a previously made calibration curve by PAS. So, is useful for detection of adulterated milk by whey powder (Dóka et al.) [40]. Demonstrated that the PAS as potential technique to identify samples adulterated with lead tetraoxide (Dóka et al.) [43].	Mexico
Skimmed milk powder and whey powder	Pure skimmed milk and whey powders; mixtures were made at 5, 7.5, 10, 15, and 20%.	300–600	Xe Lamp $P = 450$ W Modulation Frequency, 30 Hz	370	Subtraction correlation		Hungary Netherlands
Pb_3O_4 adulterant in ground sweet red paprika (<i>Capsicum annuum</i>)	The amount of Pb_3O_4 in mixture was 0.5, 1, 2, and 2.5 g.	320–700	Xe lamp 300 W (chopper, 54 Hz)	545	None		Hungary Netherlands

TABLE 1: Continued.

Specimen	Experimental criterion	Spectral region λ (nm)	Source (power (W)) and modulation frequency (Hz)	Region or centers absorbing (CA) λ (nm)	Mathematical analysis	Significant findings/results	Country
Paprika (<i>Capsicum annuum</i>) seasoning products of paprika	Pericarps of red, yellow, and green ripe paprika were dried and made powder to be evaluated.	200–800	Xenon arc lamp $P = 1 \text{ KW}$	220–550 540	Histogram	The spectrum of yellow paprika reveals in the visible region four absorptions, two maxima at 411 and 435 nm and two shoulders at about 442 and 483 nm. The maximum at 411 nm can be attributed to the absorption of capsorubin, whereas the predominance of the yellow-colored carotenoids in diverse concentrations determines the maximum at 435 nm (zeaxanthin and cryptoxanthin) and the absorption at 442 nm (β -carotene, zeaxanthin, and lutein). The red pigments capsorubin and capsanthin are responsible for the absorption at 540 nm (Vinha and Haas) [85]. Points out that the PAS technique has possibilities to evaluate the changes due to irradiation in egg powders (Dóka et al.) [42].	Germany
Eggs	Egg powders irradiated by ^{60}Co (0, 2.5, 5, 10, and 20 kGy).	240–530	Xe lamp 300 W (chopper, 56 Hz)	275, 480	Correlation		

TABLE 1: Continued.

Specimen	Experimental criterion	Spectral region λ (nm)	Source (power (W)) and modulation frequency (Hz)	Region or centers absorbing (CA) λ (nm)	Mathematical analysis	Significant findings/results	Country
Strawberries	Strawberries of different stages of maturity were used and selected according to their size and color, ranging from white (unripe) to dark red (overripe).	250–750	Xe arc lamp $P = 1000$ W 47, 107, and 190 Hz Light intensity = $139 \text{ W} \cdot \text{m}^{-2}$	510 278	Fitted curve	The authors demonstrate the potential of photoacoustic spectroscopy in the assessment of the maturity of strawberries using the spectral ratio of anthocyanin and protein bands. It is worth noting that it is a direct and nondestructive technique that might be extended to other horticultural crops (Bergevin et al.) [57]. The absorbance peaks at 442, 467, and 498 nm were assigned to bixin in solution, whereas the peak at about 260 nm was mainly due to the absorbance of soybean oil (Haas and Vinha) [86].	Canada
Annatto	Extracts of pigments were obtained by applying soybean oil or acetone as solvent.	200–1200	High-pressure Xe arc lamp $P = 1000$ W	260 442, 467, and 498	Fitted curve	Indicated discrimination of different flours based on origin, color, and grain size is possible; they suggested its usefulness for quality control purposes (Favier et al.) [52].	Germany
White bread flour, rye flour, soya flour, and dried pea flour	Samples of different colours were used: white, yellow, green, and brown.	350–700	Xenon lamp	370, 385, 410, and 475	None	The authors demonstrated that PA measurements (range visible light) on milk protein concentrates are capable of determining Fe content in the form of ferrogluconate (Dóka et al.) [39].	Netherlands Hungary
Milk protein	Milk protein concentrates containing ferrogluconate at 27, 136, 1230, and 12000 ppm were used.	300–700	Xe lamp $P = 1600$ W (chopper, 30 Hz)	348, 380, and 552	Model Rosencwaig and Gersho		Hungary

TABLE 1: Continued.

Specimen	Experimental criterion	Spectral region λ (nm)	Source (power (W)) and modulation frequency (Hz)	Region or centers absorbing (CA) λ (nm)	Mathematical analysis	Significant findings/results	Country
Corn (<i>Zea mays</i> L.)	Specimens were exposed to different concentrations of aluminum.	350–800	Xe arc lamp $P = 1000$ W 20 Hz	680	None	It was found that the most of the spectral differences lie in the region dominated by the chlorophyll band, with a maximum at 680 nm (Marquezini et al.) [87]. The photoacoustic spectrum of bean leaves was decreased with the use of herbicides. When the leaves were immersed in paraquat, the ratio of the photoacoustic signals, PA67S/PA475, decreased significantly. Benzointrile and diuron also decreased the intensity of the photoacoustic spectrum. The changes induced by benzointrile were less obvious than those induced by diuron. (Szigeti et al.) [88]. PA spectra of tablets of milk powder showed one peak at 280 nm corresponding to the absorption of proteins and a smaller band in the visible (400–500 nm) that might be assigned to milk carotenoids (Nsoukpog-Kossi et al.) [38].	Brazil
Bean plants (<i>Phaseolus vulgaris</i> L. cv. Fori GS)	Bean leaves were treated with herbicides.	380–720	High-pressure Xe lamp $P = 450$ W Modulation frequency of 22 Hz	475, 675	Statistic analysis		Hungary
Milk powder	The PA measurements were performed at room temperature $T = 298^\circ\text{K}$.	200–630	Xe lamp 1000 W (chopper, 20–1000 Hz)	280	None		Canada

TABLE 1: Continued.

Specimen	Experimental criterion	Spectral region λ (nm)	Source (power (W)) and modulation frequency (Hz)	Region or centers absorbing (C/A) λ (nm)	Mathematical analysis	Significant findings/results	Country
Skimmed milk, partly skimmed milk (2% fat), whole milk (3,25% fat), and other milk products	Cheddar cheese was placed in the photoacoustic cell in the form of a small disc 14 mm in diameter and 1 mm thick. For the other products, a small quantity was put in filling the cell.	250–440	Xe arc lamp $P = 1000$ W	Fat absorption band: 250–260 protein peaks 280	Subtraction of spectrum	The authors demonstrated the possibility of using photoacoustic spectroscopy for milk product analysis (Martel et al.) [30].	Canada
<i>Glycine max</i>	The sample used was an intact leaf cut in the form of discs of 5 mm diameter.	300–800	Xe arc lamp $P = 1000$ W MF = 25 Hz	450, 680	Phase-resolved	It was proposed that photoacoustic spectroscopy is an important tool for the investigation of insoluble plant components. The author reported the spectrum of the leaf with the characteristic absorbance bands of the waxy cuticle, carotenoids, and chlorophyll (Nery et al.) [89].	Brazil
Green coffee	Coffee beans freshly ground and roasted and compacted into a disk-shaped sample chamber in the PA cell holder were used.	340–610	Xe lamp $P = 400$ W 30 Hz	360 nm	None	Photoacoustic spectroscopy was proposed as possible nondestructive alternative for in situ assessment of water-soluble compounds in green or roasted coffee beans (Reis et al.) [90].	Brazil

TABLE 1: Continued.

Specimen	Experimental criterion	Spectral region λ (nm)	Source (power (W)) and modulation frequency (Hz)	Region or centers absorbing (C.A) λ (nm)	Mathematical analysis	Significant findings/results	Country
Seedlings of maize mutants	Samples were cut immediately before placing them in a photoacoustic cell.	300–800	Xe lamp $P = 450$ W 32 Hz	320	Deconvolution	Photoacoustic spectroscopy was proposed as a simple, direct, nondestructive alternative for both qualitative and quantitative assessment of plant mutations. It is a method important to the resources available to the plant geneticist (Lima et al.) [91]. The results indicated coincidences in the spectra obtained with all the techniques used, coinciding in all with the wavelength of the maximum peak of the signal (Li et al.) [92]. The photoacoustic absorbance spectra presented absorbent centers at 545 and 675 nm, which were related to anthocyanins and chlorophylls (Veeranjaneyulu and Das) [93].	Brazil
Flower petals Blue larkspur Red poppy petal	None.	380–750	MF = 500 Hz	380–420 and 500–650 400–580	Scattered transmission Diffuse reflectance Transmission		China
Leaves (species of <i>Euphorbia</i>)	The twigs of these plants were cut under water, washed in distilled water, and the leaves were dried (purple pigmentation in leaves).	400–740	Spectrometer model 6001 (EG & G) Modulation frequency = 40 Hz	545, 675	Average		India

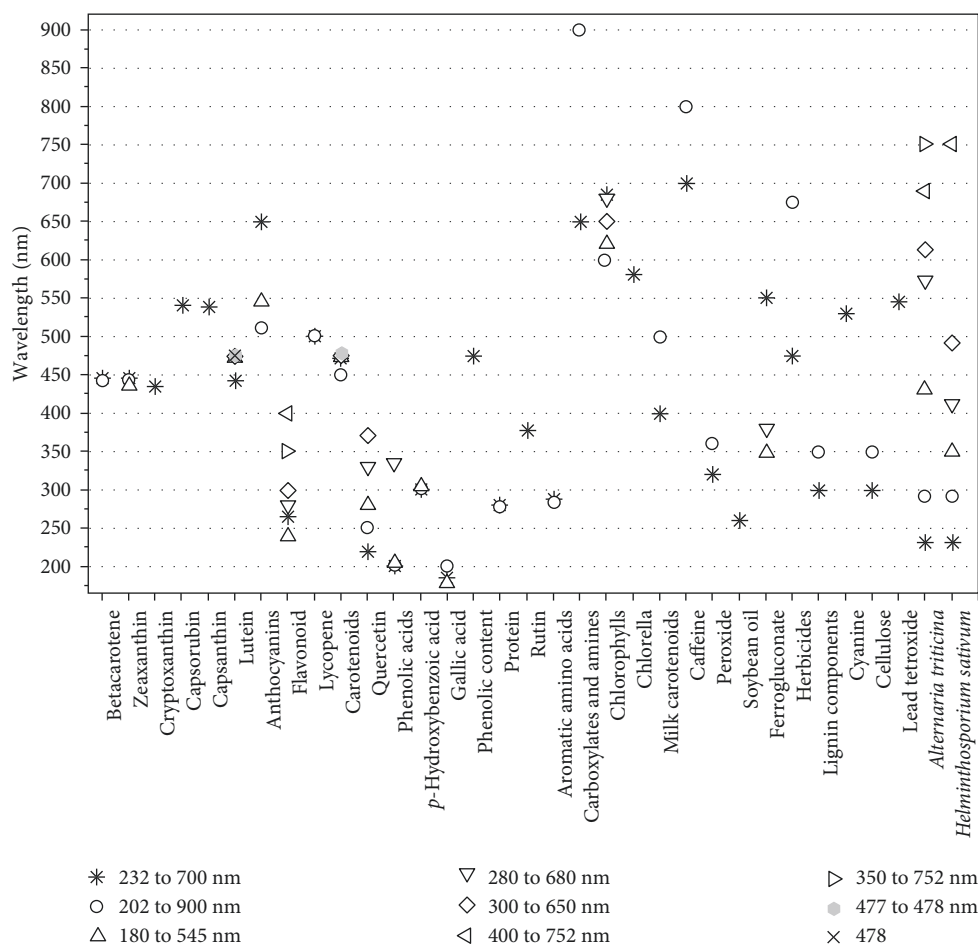
TABLE I: Continued.

Specimen	Experimental criterion	Spectral region λ (nm)	Source (power (W)) and modulation frequency (Hz)	Region or centers absorbing (CA) λ (nm)	Mathematical analysis	Significant findings/results	Country
Wheat lignin	Twigs of plants were cut under water, washed in distilled water, and the fresh wheat stems (culms) were obtained from mature, presenescent plants raised in growth chambers. Small sections of wood and field-dried culm were washed.	250–450	Xe lamp $P = 1000$ W Modulation frequency = 150 Hz	350	None	It was proposed that photoacoustic spectroscopy is an important tool for the investigation of insoluble plant components. Absorbance bands in the 300 to 400 nm region may be attributable to chemically modified or degraded lignin components resulting from natural aging of the polymer. Chemical modification of lignin is known to occur when lignocellulosic materials are exposed to near-UV light (Gould) [94]. The authors related the chlrella component at the wavelength of 580 nm, and the highest absorbance peak of the obtained spectrum was found at 680 nm (Cahen et al.) [33]. The author demonstrated that the major absorbing components in the spinach are the chlorophylls. The chlorophylls are similar to the haemoproteins and contain a porphyrin ring, this being chelated to magnesium at the ring center (Adams et al.) [34].	USA.
Lettuce (chloroplast membranes)	The chloroplast suspension was adsorbed on cotton wool and measurement.	400–720	Xe arc lamp $P = 450$ W 770 and 72 Hz	580, 680	Normalized		Israel
Spinach	Spinach leaf of 10 mm in diameter were cut and mounted on the support plate.	250–700	Xe Lamp $P = 1000$ W	450, 650	Differentiation		England

TABLE 1: Continued.

Specimen	Experimental criterion	Spectral region λ (nm)	Source (power (W) and modulation frequency (Hz))	Region or centers absorbing (CA) λ (nm)	Mathematical analysis	Significant findings/results	Country
Green leaf	—	—	—	—	—	Rosencwaig found Soret band at 420 nm, the carotenoid band structure between 450 and 550 nm, and the chlorophyll band between 600 and 700 nm [29]. PAS can reduce the amount of material required and could reduce the time required for the identification of plant species (Rosencwaig and Hall) [32].	USA
Marine algae	—	—	—	—	—	Two maxima peaks are found: the first is due to cyanine (530 nm) absorption in the flower, and the second at 340 nm is due to some other ultraviolet-absorbing compound in the red rose petal. In the blackeyed susan, the base of the flower petal is rich in ultraviolet- absorbing flavanol glucosides. The technique can give useful information about photochemistry (Harshbarger and Robin) [30].	USA
Black-eyed susan Red rose petals	—	200–800	Xe Lamp $P = 4200\text{ W}$	340, 530	None		

λ : wavelength; MF: modulation frequency, CA: centers absorbing, P : power, Xe: xenon, β : optical absorption coefficient, nm: nanometers, PA: photoacoustic, PAS: photoacoustic spectroscopy.



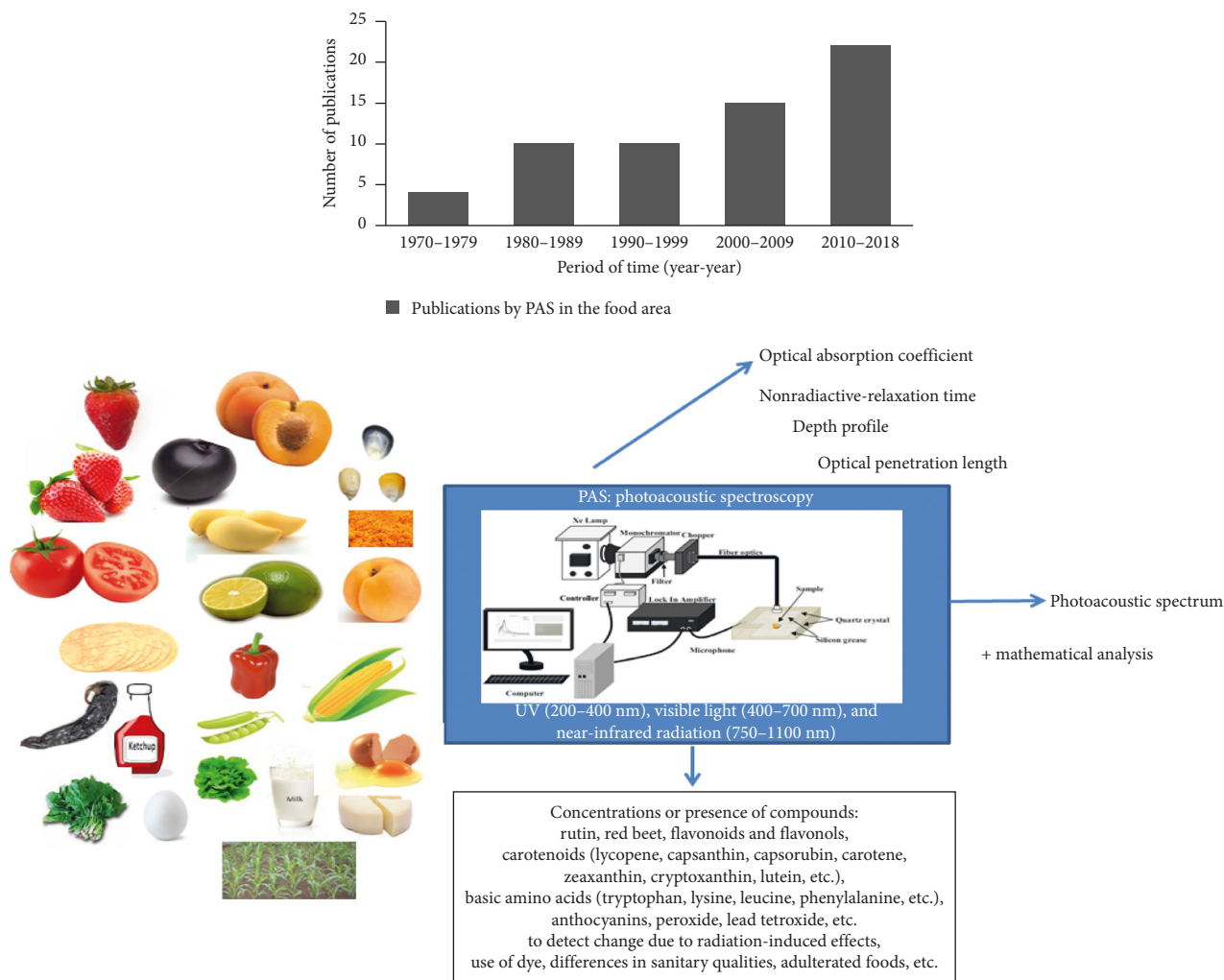


FIGURE 2: Publications per year of PAS technique, to obtain optical absorbance spectra in food, according to the present literature review.

consume better quality of foodstuff. Among the main features of the photoacoustic spectroscopy are the size of sample required is very small, due to the small volume of the cell; no special sample preparation is required; it reduces the number of analysis steps; it is a green method with less use of chemical substances, and it is nondestructive. Over the time, it has been observed that the applications of photoacoustic spectroscopy are increasing in the food area.

Disclosure

The authors alone are responsible for the content and writing of the paper.

Conflicts of Interest

The authors declare that there are no conflicts of interest regarding the publication of this paper.

Acknowledgments

The authors are grateful for the support of the National Polytechnic Institute through the projects SIP, EDI, and

COFFA. Claudia Hernández-Aguilar thanks the collaboration of educational institutions and research centers that have been allowed to collaborate in research with her for more than ten years: Colegio de Postgraduados-Montecillo, Texcoco, and Cinvestav, through the Department of Physics in particular to Esther Ayala, for his assistance and support during the learning and use of photoacoustic spectroscopy in the laboratories of Cinvestav, Mexico. Thanks are due to all for sharing the research path towards the transdisciplinarity. The present research and publication was funded by means of the projects (SIP 20181534 and SIP 20181645) supported by the Instituto Politécnico Nacional.

References

- [1] C. H. Aguilar, A. Dominguez Pacheco, A. Cruz-Orea, R. Ivanov, C. A. Carballo, and R. Z. Bautista, "Laser in agriculture," *International Agrophysics*, vol. 24, no. 4, pp. 407–422, 2010.
- [2] FAO, *High Level Expert Forum-How to Feed the World in 2050, Global agriculture towards 2050, Office of the Director, Agricultural Development Economics Division Economic and Social Development Department Viale*

- delle Terme di Caracalla, 00153 Rome, Italy, 2009a, http://www.fao.org/fileadmin/templates/wsfs/docs/Issues_papers/HLEF2050_Global_Agriculture.pdf.
- [3] FAO, *High Level Expert Forum-How to Feed the World in 2050, The technology challenge*, Office of the Director, Agricultural Development Economics Division Economic and Social Development Department Viale delle Terme di Caracalla, 00153 Rome, Italy, 2009b, http://www.fao.org/fileadmin/templates/wsfs/docs/Issues_papers/HLEF2050Technology.pdf.
- [4] J. A. Foley, "Can we feed the world and sustain the planet?," *Scientific American*, vol. 305, no. 5, pp. 60–65, 2011.
- [5] FORESIGHT, *El futuro de los alimentos y la agricultura*, Resumen ejecutivo. Oficina del Gobierno para la Ciencia, Londres, UK, 2011.
- [6] C. M. Pittelkow, X. Liang, B. A. Linquist et al., "Productivity limits and potentials of the principles of conservation agriculture," *Nature*, vol. 517, no. 7534, pp. 365–368, 2015.
- [7] L. D. Cunningham-Sabo, S. M. Davis, K. M. Koehler et al., "Food preferences, practices, and cancer-related food and nutrition knowledge of southwestern American Indian youth," *Cancer: Interdisciplinary*, vol. 78, no. 7, pp. 1617–1622, 1996.
- [8] M. Wiseman, "The second world cancer research fund/American institute for cancer research expert report. Food, nutrition, physical activity, and the prevention of cancer: a global perspective: nutrition society and BAPEN medical symposium on nutrition support in cancer therapy," *Proceedings of the Nutrition Society*, vol. 67, no. 3, pp. 253–256, 2008.
- [9] L. Torres-Sánchez, M. Galván-Portillo, S. Lewis et al., "Dieta y cáncer de mama en Latinoamérica," *Salud pública de México*, vol. 51, pp. s181–s190, 2009.
- [10] P. Greenwald, "From carcinogenesis to clinical interventions for cancer prevention," *Toxicology*, vol. 166, no. 1-2, pp. 37–45, 2001.
- [11] I. Palomo, R. Moore-Carrasco, G. Carrasco, P. Villalobos, and L. Guzmán, "El consumo de tomates previene el desarrollo de enfermedades cardiovasculares y cáncer: antecedentes epidemiológicos y mecanismos de acción," *Idesia (Arica)*, vol. 28, no. 3, pp. 121–129, 2010.
- [12] A. Sierra and D. Romero, "Contaminación y degradación de los alimentos," *Revista Mexicana de Ciencias Políticas y Sociales*, vol. 36, no. 146, 1991.
- [13] M. E. R. Corredor and B. A. M. De Pascual, *Los compuestos químicos en los alimentos desde la perspectiva de la seguridad alimentaria*. Murcia: consejería de Sanidad. Dirección General de Salud Pública, Servicio de Seguridad Alimentaria y Zoonosis. RIMBLAS C prevención de riesgos, Murcia: consejería de Sanidad y Consumo. RIVERO, JM (1994), Análisis histórico de los plaguicidas de síntesis en España, Murcia, Spain, Tercer Sy edition, 2004.
- [14] D. D. Bicanic, "On the photoacoustic, photothermal and colorimetric quantification of carotenoids and other phytonutrients in some food: a review," *Journal of Molecular Structure*, vol. 993, no. 1–3, pp. 9–14, 2011.
- [15] Y. He, L. Tang, X. Wu, X. Hou, and Y. I. Lee, "Spectroscopy: the best way toward green analytical chemistry?," *Applied Spectroscopy Reviews*, vol. 42, no. 2, pp. 119–138, 2007.
- [16] T. M. Coelho, E. C. Vidotti, M. C. Rollemberg et al., "Photoacoustic spectroscopy as a tool for determination of food dyes: comparison with first derivative spectrophotometry," *Talanta*, vol. 81, no. 1-2, pp. 202–220, 2010.
- [17] F. M. de Oliveira, J. B. Mokochinski, Y. R. Torres, H. S. D. Santa, and P. P. González-Borrero, "Photoacoustic spectroscopy applied to the direct detection of bioactive compounds in *Agaricus brasiliensis* mycelium," *Journal of Biological Physics*, vol. 44, no. 1, pp. 93–100, 2018.
- [18] A. D. Kaur and U. Gupta, "The review on spectrophotometric determination of synthetic food dyes and lakes," *Gazi University Journal of Science*, vol. 25, no. 3, pp. 579–588, 2012.
- [19] C. N. Scotter, "Non-destructive spectroscopic techniques for the measurement of food quality," *Trends in Food Science and Technology*, vol. 8, no. 9, pp. 285–292, 1997.
- [20] P. E. Hockberger, "A history of ultraviolet photobiology for humans, animals and microorganisms," *Photochemistry and Photobiology*, vol. 76, no. 6, pp. 561–579, 2002.
- [21] F. A. James, "The creation of a Victorian myth: the historiography of spectroscopy," *History of Science*, vol. 23, no. 1, pp. 1–24, 1985.
- [22] M. A. Sutton, "Essay review: spectroscopy, historiography and myth: the Victorians vindicated," *History of Science*, vol. 24, no. 4, pp. 425–433, 1986.
- [23] A. Rosencwaig, "Photoacoustic spectroscopy of biological materials," *Science*, vol. 181, no. 4100, pp. 657–658, 1973a.
- [24] A. Rosencwaig, "Photoacoustic spectroscopy, new tool for investigation of solids," *Analytical Chemistry*, vol. 47, no. 6, pp. 592A–604a, 1975.
- [25] E. Marín, "Escuchando la luz: breve historia y aplicaciones del efecto fotoacústico," *Latin-American Journal of Physics Education*, vol. 2, no. 2, p. 17, 2008.
- [26] E. P. Lai, B. L. Chan, and M. Hadjmohammadi, "Use and applications of photoacoustic spectroscopy," *Applied Spectroscopy Reviews*, vol. 21, no. 3, pp. 179–210, 1985.
- [27] A. Rosencwaig, "Photoacoustic spectroscopy of solids," *Optics Communications*, vol. 7, no. 4, pp. 305–308, 1973b.
- [28] T. H. Maugh, "Photoacoustic spectroscopy: new uses for an old technique," *Science*, vol. 188, no. 4183, pp. 38–39, 1975.
- [29] W. R. Harshbarger and M. B. Robin, "Opto-acoustic effect, revival of an old technique for molecular spectroscopy," *Accounts of Chemical Research*, vol. 6, no. 10, pp. 329–334, 1973.
- [30] R. Martel, C. N. N'Soukpoe-Kossi, P. Paquin, and R. M. Leblanc, "Photoacoustic analysis of some milk products in ultraviolet and visible light," *Journal of Dairy Science*, vol. 70, no. 9, pp. 1822–1827, 1987.
- [31] C. S. Sunandana, "Physical applications of photoacoustic spectroscopy," *Physica Status Solidi (a)*, vol. 105, no. 1, pp. 11–43, 1988.
- [32] A. Rosencwaig and S. S. Hall, "Thin-layer, chromatography and photoacoustic spectrometry," *Analytical Chemistry*, vol. 47, no. 3, pp. 548–549, 1975.
- [33] D. Cahen, S. Malkin, and E. I. Lerner, "Photoacoustic spectroscopy of chloroplast membranes; listening to photosynthesis," *FEBS Letters*, vol. 91, no. 2, pp. 339–342, 1978.
- [34] M. J. Adams, B. C. Beadle, A. A. King, and G. F. Kirkbright, "Analytical photoacoustic spectrometry. Part II. Ultraviolet and visible photoacoustic spectra of some inorganic, biochemical and phytochemical samples," *Analyst*, vol. 101, no. 1204, pp. 553–561, 1976.
- [35] C. Buschmann and H. Prehn, "In vivo studies of radiative and non-radiative de-excitation processes of pigments in *Raphanus* seedlings by photoacoustic spectroscopy," *Photobiochemistry and Photobiophysics*, vol. 2, pp. 209–215, 1981.

- [36] C. Buschmann and H. Prehn, "In vivo photoacoustic spectra of raphanus and tradescantia leaves taken at different chopping frequencies of the excitation light," *Photo-biochemistry and Photobiophysics*, vol. 5, pp. 63–69, 1983.
- [37] E. P. O'Hara, R. D. Tom, and T. A. Moore, "Determination of the in vivo absorption and photosynthetic properties of the lichen *acarospora schleicheri* using photo acoustic spectroscopy," *Photochemistry and Photobiology*, vol. 38, no. 6, pp. 709–715, 1983.
- [38] C. N. N'Soukpoe-Kossi, R. Martel, R. M. Leblanc, and P. Paquin, "Kinetic study of Maillard reactions in milk powder by photoacoustic spectroscopy," *Journal of Agricultural and Food Chemistry*, vol. 36, no. 3, pp. 497–501, 1988.
- [39] O. Dóka, J. Kispéter, and A. Lörincz, "Potential value of photoacoustic spectroscopy for determining iron content of milk protein concentrates," *Journal of Dairy Research*, vol. 58, no. 4, pp. 453–460, 1991.
- [40] O. Dóka, D. Bicanic, and R. Frankhuizen, "Photoacoustic study of heated binary mixtures containing whey and skimmed-milk powders," *Zeitschrift für Lebensmitteluntersuchung und-Forschung A*, vol. 208, no. 1, pp. 1–5, 1999.
- [41] O. Dóka, Z. Ajtony, D. Bicanic, and R. Koehorst, "Assessing the extent of degradation in the UV radiation and heat-catalyzed oxidized whole milk powder: the UV photoacoustic and diffuse reflectance spectroscopies versus the peroxide value," *Applied Spectroscopy*, vol. 54, no. 9, pp. 1405–1408, 2000.
- [42] O. Doka, J. Kispeter, and D. Bicanic, "The photoacoustic assessment of ⁶⁰Co irradiation induced effects in egg powders: results in the uv and visible," *Instrumentation Science and Technology*, vol. 25, no. 4, pp. 297–306, 1997.
- [43] O. Dóka, D. Bicanic, and L. Szöllösy, "Rapid and gross screening for Pb3O4 adulterant in ground sweet red paprika by means of photoacoustic spectroscopy," *Instrumentation science and technology*, vol. 26, no. 2-3, pp. 203–208, 1998.
- [44] D. Bicanic, J. Swarts, S. Luterotti, P. Helander, V. Fogliano, and M. Anese, "Optothermistor as a breakthrough in the quantification of lycopene content of thermally processed tomato-based food: verification versus absorption spectrophotometry and high-performance liquid chromatography," *Journal of Agricultural and Food Chemistry*, vol. 53, no. 9, pp. 3295–3299, 2005.
- [45] D. Bicanic, in *Instrumental Laser Techniques Based on the Photothermal Phenomena and their Applications for the Characterization of Food Melanoidins in Food and Health*, Vol. 85, Laboratory of Biophysics, Wageningen, Netherlands, 2003.
- [46] A. Domínguez-Pacheco, C. Hernández-Aguilar, and A. Cruz-Orea, "Photoacoustic determination of non-radiative relaxation time of absorbing centers in maize seeds," *International Journal of Thermophysics*, vol. 38, no. 7, p. 111, 2017.
- [47] C. H. Aguilar, A. Domínguez-Pacheco, A. Cruz-Orea, and R. Zepeda-Bautista, "Depth profiles in maize (*Zea mays* L.) seeds studied by photoacoustic spectroscopy," *International Journal of Thermophysics*, vol. 36, no. 5-6, pp. 891–899, 2015.
- [48] R. R. Molina, C. H. Aguilar, A. D. Pacheco, A. Cruz-Orea, and M. A. Canseco, "Alternative method to characterize corn grain by means of photoacoustic spectroscopy," *International Journal of Thermophysics*, vol. 34, no. 8-9, pp. 1540–1548, 2013.
- [49] O. Dóka, A. Brunori, R. Schmidt, D. Bicanic, and G. Végvári, "Rutin in buckwheat grain meal determined by UV photoacoustic spectroscopy and HPLC," *Nova Biotechnologica et Chimica*, vol. 16, no. 1, pp. 61–67, 2017.
- [50] R. R. Molina, C. H. Aguilar, A. D. Pacheco, A. Cruz-Orea, and J. L. Bonilla, "Characterization of maize grains with different pigmentation investigated by photoacoustic spectroscopy," *International Journal of Thermophysics*, vol. 35, no. 9-10, pp. 1933–1939, 2014.
- [51] A. D. Pacheco, C. H. Aguilar, A. C. Orea et al., "Evaluation of wheat and maize seeds by photoacoustic microscopy," *International Journal of Thermophysics*, vol. 30, no. 6, pp. 2036–2043, 2009.
- [52] J. P. Favier, J. Buijs, A. Miklos, A. Lörincz, and D. Bicanic, "Photoacoustic characterization of different food samples Photoakustische Charakterisierung von verschiedenen Lebensmitteln," *Zeitschrift für Lebensmittel-Untersuchung und Forschung*, vol. 199, no. 1, pp. 59–63, 1994.
- [53] O. Dóka, D. D. Bicanic, M. H. Dicko, and M. A. Slingerland, "Photoacoustic approach to direct determination of the total phenolic content in red sorghum flours," *Journal of Agricultural and Food Chemistry*, vol. 52, no. 8, pp. 2133–2136, 2004.
- [54] R. Takai, K. Kanazawa, K. Murai et al., "The determination of water contents in various powdered food by photoacoustic spectroscopy (PAS)," *Nippon Shokuhin Kogyo Gakkaishi*, vol. 36, no. 3, pp. 189–194, 1989.
- [55] C. H. Aguilar, F. A. Domínguez-Pacheco, A. Cruz-Orea et al., "Optical absorption coefficient of different tortillas by photoacoustic spectroscopy," *African Journal of Biotechnology*, vol. 11, no. 92, pp. 15916–15922, 2012.
- [56] R. J. D. S. Lima and J. S. Filho, "Carotenoids and flavonoids identification in brazilian tropical fruit and vegetables using photoacoustic technique," *Journal de Physique IV (Proceedings)*, vol. 125, pp. 51–53, 2003.
- [57] M. Bergevin, C. N. N'Soukpoé-Kossi, D. Charlebois, R. M. Leblanc, and C. Willemot, "Assessment of strawberry maturity by photoacoustic spectroscopy," *Applied Spectroscopy*, vol. 49, no. 3, pp. 397–399, 1995.
- [58] G. P. Pardo, A. D. Pacheco, S. A. Tomás, A. Cruz Orea, and C. H. Aguilar, "Characterization of aged lettuce and chard seeds by photothermal techniques," *International Journal of Thermophysics*, vol. 39, no. 10, p. 110, 2018.
- [59] M. L. Neto, K. L. Agra, J. S. Filho, and F. E. Jorge, "TDDFT calculations and photoacoustic spectroscopy experiments used to identify phenolic acid functional biomolecules in Brazilian tropical fruit in natura," *Spectrochimica Acta Part A: Molecular and Biomolecular Spectroscopy*, vol. 193, pp. 249–257, 2018.
- [60] S. C. Corzo-Ruiz, F. Hernández-Rosas, M. L. Alvarado-Noguez, J. Hernandez-Rosas, and A. Cruz-Orea, "Photoacoustic Spectroscopy applied to the juice and rind characterization of *Citrus latifolia* with different quality of samples," *Superficies y Vacío*, vol. 31, no. 1, pp. 1–5, 2018.
- [61] B. E. Zendejas-Leal, V. R. Barrientos-Sotelo, R. Cano-Casas, M. L. Alvarado-Noguez, J. Hernández-Rosas, and A. Cruz-Orea, "Photoacoustic monitoring of absorption spectrum during the dehydration process of pasilla chili pepper," *International Journal of Thermophysics*, vol. 39, no. 7, p. 80, 2018.
- [62] C. L. Rodríguez-Páez, A. Carballo-Carballo, R. Rico-Molina et al., "The optical absorption coefficient of maize grains investigated by photoacoustic spectroscopy," *International Journal of Thermophysics*, vol. 38, no. 1, p. 11, 2017.

- [63] C. H. Aguilar, F. A. D. Pacheco, A. C. Orea, and R. I. Tsonchev, "Thermal effects of laser irradiation on maize seeds," *International Agrophysics*, vol. 29, no. 2, pp. 147–156, 2015.
- [64] C. H. Aguilar, A. Domínguez-Pacheco, A. Cruz-Orea et al., "Anticancer food: photoacoustic spectroscopy, the SciTech," *Journal of Science and Technology*, vol. 4, no. 1, pp. 40–45, 2015.
- [65] V. R. Barrientos-Sotelo, R. Cano-Casas, A. Cruz-Orea, F. Hernández-Rosas, and J. Hernández-Rosas, "Photoacoustic characterization of green, red and dehydrated *Capsicum annuum* l. variety pasilla," *Food Biophysics*, vol. 10, no. 4, pp. 481–486, 2015.
- [66] M. C. Pérez Reyes, C. Hernandez-Aguilar, A. Dominguez-Pacheco, A. Cruz-Orea, and E. Moreno Martínez, "The optical absorption coefficient of barley seeds investigated by photoacoustic spectroscopy and their effects by laser Bio-stimulation," *International Journal of Thermophysics*, vol. 36, no. 9, pp. 2389–2400, 2015.
- [67] O. Dóka, D. Bicanic, and R. Kulcsár, "Direct estimate of cocoa powder content in cakes by colorimetry and photoacoustic spectroscopy," *International Journal of Thermophysics*, vol. 35, no. 12, pp. 2206–2214, 2014.
- [68] G. Sanchez-Hernandez, C. Hernandez-Aguilar, A. Dominguez-Pacheco, A. Cruz-Orea, M. C. J. Perez-Reyes, and E. M. Martinez, "The optical absorption coefficient of bean seeds investigated using photoacoustic spectroscopy," *International Journal of Thermophysics*, vol. 36, no. 5-6, pp. 835–843, 2015.
- [69] O. Dóka, E. Prágai, D. Bicanic, R. Kulcsár, and Z. Ajtony, "Colorimetry and photoacoustic spectroscopy as a suitable tool for determination of fat-free cocoa solids in dark chocolates," *European Food Research and Technology*, vol. 236, no. 6, pp. 963–968, 2013.
- [70] C. H. Aguilar, A. Cruz-Orea, R. Ivanov et al., "The optical absorption coefficient of maize seeds investigated by photoacoustic spectroscopy," *Food Biophysics*, vol. 6, no. 4, pp. 481–486, 2011.
- [71] A. J. G. Salcedo, F. G. Delgado, and F. Z. Rincón, "Determination of adulterants in ground roasted coffee using photoacoustic technique," *Revista Colombiana de Física*, vol. 44, no. 3, 2012.
- [72] O. Dóka, D. Bicanic, J. G. Buijnsters, R. Spruijt, S. Luterotti, and G. Végvári, "Exploiting direct and indirect methods for the estimation of the total carotenoid concentration in dried pastas," *European Food Research and Technology*, vol. 230, no. 6, pp. 813–819, 2010.
- [73] D. V. Rezende, O. A. C. Nunes, and A. C. Oliveira, "Photoacoustic study of fungal disease of acai (*Euterpe oleracea*) seeds," *International Journal of Thermophysics*, vol. 30, no. 5, pp. 1616–1625, 2009.
- [74] C. H. Aguilar, A. Dominguez-Pacheco, A. Cruz-Orea et al., "Laser irradiation effects on field performance of maize seed genotypes," *International Agrophysics*, vol. 23, pp. 327–332, 2009.
- [75] C. H. Aguilar, M. Mezzalama, N. Lozano et al., "Optical absorption coefficient of laser irradiated wheat seeds determined by photoacoustic spectroscopy," *The European Physical Journal Special Topics*, vol. 153, no. 1, pp. 519–522, 2008.
- [76] C. H. Aguilar, A. C. Carballo, A. Cruz-Orea, R. Ivanov, and A. Domínguez-Pacheco, "The carotenoid content in seedlings of maize seeds irradiated by a 650 nm diode laser: qualitative photoacoustic study," *The European Physical Journal Special Topics*, vol. 153, no. 1, pp. 515–518, 2008.
- [77] F. G. Delgado, F. Z. Rincón, and J. A. O. Vela, "Coffee certification criterion using the photoacoustic technique," *Microelectronics Journal*, vol. 39, no. 11, pp. 1331–1332, 2008.
- [78] J. C. Kapil, P. K. Satyawali, and D. N. Sethi, "VIS-NIR overtone bands of snow: photoacoustic spectroscopy," *Cold Regions Science and Technology*, vol. 43, no. 3, pp. 164–176, 2005.
- [79] C. H. Aguilar, A. Cruz-Orea, R. Ivanov, E. S. M. Martínez, and A. Michtchenko, "Photoacoustic spectroscopy applied to the study of the influence of laser irradiation on corn seeds," *In Journal de Physique IV, (Proceedings)*, vol. 125, pp. 853–855, 2005.
- [80] F. G. Delgado, J. A. Herrera-Cuartas, J. D. Duque-Ocampo, and H. Ariza-Calderón, "Estudio de la pigmentación de café orgánico con diferentes grados de humedad usando espectroscopía fotoacústica," *Revista Colombiana de Física*, vol. 37, no. 1, p. 114, 2005.
- [81] J. C. Kapil, S. K. Joshi, and A. K. Rai, "In situ photoacoustic investigations of some optically transparent samples like ice and snow," *Review of Scientific Instruments*, vol. 74, no. 7, pp. 3536–3543, 2003.
- [82] V. Gupta, A. Kumar, G. K. Garg, and A. K. Rai, "Photoacoustic spectroscopy for identification and differential diagnosis of *T. indica* with other seed-borne pathogens of wheat and rice," *Instrumentation Science and Technology*, vol. 29, no. 4, pp. 283–293, 2001.
- [83] R. A. M. Hernandez, A. Calderón, A. Cruz-Orea, F. S. Sinencio, S. A. Tomas, and G. Gonzalez de la Cruz, "Estudio de la influencia del Ca (OH) 2 en las películas de pericarpio de maíz nixtamalizado mediante técnicas fototérmicas," *Superficies y Vacío*, vol. 8, pp. 80–85, 1999a.
- [84] R. A. M. Hernández, A. Calderón, A. Cruz-Orea, S. A. Tomas, F. S. Sinencio, and G. P. Rodriguez, "Caracterización óptica de centros absorbentes en películas biopoliméricas obtenidas de pericarpio de maíz," *Superficies y Vacío*, vol. 8, pp. 89–93, 1999b.
- [85] C. A. Vinha and U. Haas, "Qualitative and semiquantitative analysis of dried fruit and seasoning products of paprika using photoacoustic spectroscopy," *Journal of Agricultural and Food Chemistry*, vol. 45, no. 4, pp. 1273–1277, 1997.
- [86] U. Haas and C. A. Vinha, "Qualitative and semiquantitative analysis of annatto and its content in food additives by photoacoustic spectrometry," *Analyst*, vol. 120, no. 2, pp. 351–354, 1995.
- [87] M. V. Marquezini, N. Cella, E. C. Silva et al., "Photoacoustic assessment of the in vivo genotypical response of corn to toxic Aluminium," *Analyst*, vol. 115, no. 3, pp. 341–343, 1990.
- [88] Z. Szigeti, E. M. Nagel, C. Buschmann, and H. K. Lichtenthaler, "In vivo photoacoustic spectra of herbicide-treated bean leaves," *Journal of Plant Physiology*, vol. 134, no. 1, pp. 104–109, 1989.
- [89] J. W. Nery, O. Pessoa, H. Vargas et al., "Photoacoustic spectroscopy for depth-profile analysis and herbicide monitoring in leaves," *Analyst*, vol. 112, no. 11, pp. 1487–1490, 1987.
- [90] F. D. A. M. Reis, C. A. S. Lima, O. Pessoa, H. Vargas, J. G. Cortez, and A. M. G. Azevedo, "Water soluble components in coffee beans: photoacoustic assessment," *Journal of Food Science*, vol. 51, no. 3, p. 849, 1986.
- [91] C. A. Lima, H. Vargas, C. L. Cesar, M. B. Lima, L. M. Prioli, and W. J. Da Silva, "Non-destructive assessment of chlorophyll-deficient mutants of maize (*Zea mays* L.) by

- photoacoustic spectroscopy," *Plant Science*, vol. 38, no. 1, pp. 47–51, 1985.
- [92] X. Li, K. H. Brücher, W. Görtz, and H. H. Perkampus, "PA-spectroscopic investigation on flower petals," *Le Journal de Physique Colloques*, vol. 44, no. C6, p. 137, 1983.
- [93] K. Veeranjanyulu and V. S. R. Das, "Photoacoustic spectroscopy—leaf absorption spectra," *Journal of Experimental Botany*, vol. 33, no. 3, pp. 515–519, 1982.
- [94] J. M. Gould, "Characterization of lignin in situ by photoacoustic spectroscopy," *Plant Physiology*, vol. 70, no. 5, pp. 1521–1525, 1982.
- [95] C. S. Mangolim, C. Moriwaki, A. C. Nogueira et al., "Curcumin- β -cyclodextrin inclusion complex: stability, solubility, characterisation by FT-IR, FT-Raman, X-ray diffraction and photoacoustic spectroscopy and food application," *Food Chemistry*, vol. 153, pp. 361–370, 2014.
- [96] C. Haisch, "Photoacoustic spectroscopy for analytical measurements," *Measurement Science and Technology*, vol. 23, no. 1, article 012001, 2011.
- [97] T. Schmid, "Photoacoustic spectroscopy for process analysis," *Analytical and Bioanalytical Chemistry*, vol. 384, no. 5, pp. 1071–1086, 2006.
- [98] A. K. Rai and J. P. Singh, "Perspective of photoacoustic spectroscopy in disease diagnosis of plants: a review," *Instrumentation Science and Technology*, vol. 31, no. 4, pp. 323–342, 2003.
- [99] H. Singh, S. K. Joshi, S. Rathore, T. Joshi, M. G. H. Zaidi, and A. K. Rai, "Optical and thermal properties of Poly bisphenol-A carbonate: photoacoustic study," *Instrumentation Science and Technology*, vol. 31, no. 4, pp. 377–383, 2003.
- [100] H. Singh, E. Rojas-Lima, F. A. Dominguez-Pacheco, C. Hernández-Aguilar, L. M. Hernández-Simón, and A. Cruz-Orea, "Kolmogorov-Smirnov test for statistical characterization of photopyroelectric signals obtained from maize seeds," *International Journal of Thermophysics*, vol. 40, no. 1, p. 4, 2018.

Review Article

The Quality Control of Tea by Near-Infrared Reflectance (NIR) Spectroscopy and Chemometrics

Ming-Zhi Zhu ^{1,2,3,4}, Beibei Wen,^{1,2,3,4} Hao Wu,⁵ Juan Li,¹ Haiyan Lin,² Qin Li,³ Yinhua Li,² Jianan Huang ^{1,2,3} and Zhonghua Liu ^{2,3,4}

¹Key Laboratory of Tea Science of Ministry of Education, Hunan Agricultural University, Changsha 410128, China

²Hunan Provincial Key Laboratory of Crop Germplasm Innovation and Utilization, Hunan Agricultural University, Changsha 410128, China

³National Research Center of Engineering Technology for Utilization of Functional Ingredients from Botanicals, Hunan Agricultural University, Changsha 410128, China

⁴Collaborative Innovation Centre of Utilization of Functional Ingredients from Botanicals, Hunan Agricultural University, Changsha 410128, China

⁵Key Laboratory of Tea Plant Biology of Henan Province, College of Life Science, Xinyang Normal University, Xinyang 464000, China

Correspondence should be addressed to Jianan Huang; jian7513@sina.com and Zhonghua Liu; larkin-liu@163.com

Received 29 June 2018; Revised 24 October 2018; Accepted 12 November 2018; Published 2 January 2019

Guest Editor: Sarfaraz Ahmed Mahesar

Copyright © 2019 Ming-Zhi Zhu et al. This is an open access article distributed under the Creative Commons Attribution License, which permits unrestricted use, distribution, and reproduction in any medium, provided the original work is properly cited.

Tea is known to be one of the most popular beverages enjoyed by two-thirds of the world's population. Concern of variability in tea quality is increasing among consumers. It is of great significance to control quality for commercialized tea products. As a rapid, noninvasive, and nondestructive instrumental technique with simplicity in sample preparation, near-infrared reflectance (NIR) spectroscopy has been proved to be one of the most advanced and efficient tools for the control quality of tea products in recent years. In this article, we review the most recent advances and applications of NIR spectroscopy and chemometrics for the quality control of tea, including the measurement of chemical compositions, the evaluation of sensory attributes, the identification of categories and varieties, and the discrimination of geographical origins. Besides, challenges and future trends of tea quality control by NIR spectroscopy are also presented.

1. Introduction

Tea is known to be one of the most popular beverages enjoyed by two-thirds of the world's population [1]. In 2017, 5.68 million tons of tea were produced all over the world, in which 2.55 million tons were produced in China. The tea quality is influenced by various factors, such as cultivars, picking standard, tea processing technology, storage condition, and time. Concern of variability in tea quality is increasing among consumers. It is of great significance to control quality for commercialized tea products [2].

The tea quality is determined by its major active components, including polyphenols, caffeine, and free amino acids. These compounds not only endow tea with

unique qualities of color, aroma, and taste but also contribute various health benefits for the human body [3]. Tea polyphenols account for 18~36% of dry weight in tea leaves, and the astringent and bitter taste of tea is mainly contributed by tea polyphenols. Tea catechins (flavan-3-ols) are the major ingredients in tea polyphenols. Tea catechins include (–)-epigallocatechin gallate (EGCG), (–)-epicatechin gallate (ECG), (–)-epigallocatechin (EGC), (–)-epicatechin (EC), (–)-gallocatechin gallate (GCG), (–)-gallocatechin (GC), and (+)-catechin (C), among which EGCG is the most abundant component [4]. The consumption of EGCG has been proved to have therapeutic effects for multiple diseases, such as cancer, metabolic syndrome, obesity, and cardiovascular and neurodegenerative diseases [5, 6]. The anticancer

property of EGCG appears to involve the suppression of angiogenesis, induction of apoptosis, altered expression of cell-cycle regulatory proteins, and activation of killer caspases [7, 8]. The suppression of angiogenesis by EGCG is associated with the change in various miRNA expressions, the inhibition of the VEGF (vascular endothelial growth factor) family, etc. [9]. The beneficial health effects of EGCG are presumed to be related with its antioxidative property. Another possible mechanism is through the direct binding of EGCG to target proteins, leading to the regulation of signal transduction pathways, transcription factors, DNA methylation, mitochondrial function, and autophagy [10]. Caffeine is another major functional component in tea and provides the bitter taste for tea [11, 12]. Caffeine has the therapeutic effects for various diseases, including metabolic syndrome, type 2 diabetes, liver diseases, and cardiovascular and cerebrovascular diseases [13, 14]. Free amino acids provide umami taste for the tea infusion. Among free amino acids, theanine accounts for approximately 50% of the total free amino acids in tea leaves [15]. Theanine not only offers a brisk flavor and an attractive aroma but also alleviates the astringency and bitterness caused by polyphenols and caffeine. Several studies have proved that theanine has significant health and cognitive benefits by influencing stress levels and learning efficiency [16].

Besides the chemical components, tea quality is influenced by various factors, including the sensory attributes, classification, and geographical origins [17–19]. Multiple analytical approaches have been used for the quality control, such as colorimetric measurements, high-performance liquid chromatography (HPLC), high-performance liquid chromatography coupled with mass spectrometry (HPLC-MS), gas chromatography (GC), and gas chromatography coupled with mass spectrometry (GC-MS) [20–30]. However, these methods not only are expensive, time-consuming, and destructive but also need specialists for the operation and cannot be applied for online applications. Therefore, near-infrared reflectance (NIR) spectroscopy, a rapid, noninvasive, and nondestructive instrumental technique with simplicity in sample preparation, has been developed and applied for the quality control of tea in recent years [19]. NIR spectroscopy is a spectroscopic method using the near-infrared region of the electromagnetic spectrum ranging from 750 nm to 2500 nm ($14,300\sim 4000\text{ cm}^{-1}$). An NIR spectrometer is usually composed of a light source, a monochromator, a sample presentation interface, and a detector. The NIR radiation can be absorbed, transmitted, or reflected after interaction with samples. The feedback of spectral stretching and bending of the chemical bonds (O–H, N–H, and C–H) can be captured by utilizing different measurement modes of NIR equipment. Therefore, the specific absorption of organic compounds in the NIR region can represent their chemical composition [31, 32]. *Anharmonicity* and *Fermi resonance* determine the occurrence and spectral properties, such as the frequency and intensity of NIR absorption bands. However, NIR absorption bands are typically broad and overlapping, which severely restricts the sensitivity in the classical spectroscopic sense. The original spectral data of NIR spectroscopy usually require pattern

recognition methods for accurate analysis by removing the disturbance of the noise, variability, uncertainties, and unrecognized features. Nevertheless, NIR spectroscopy is characterized by high penetration depth. This property allows direct analysis of strongly absorbing or even highly scattering samples, such as turbid liquids or solids, without further pretreatments [32].

Generally, the whole procedures of NIR spectroscopy include spectral data acquisition, data preprocessing, spectral data preprocessing, calibration models building with a set of samples, and models validating using a set of independent samples [33]. A typical NIR spectrum of tea is shown in Figure 1 [34]. The preprocessing of spectral data should be used for eliminating the noise and baseline shift from the background and instrument [33]. The commonly used preprocessing methods in tea analysis include standard normal variate (SNV), multiplicative scatter correction (MSC), and Savitzky–Golay (SG) smoothing [35, 36]. Various variables selection methods, such as synergy interval partial least squares (Si-PLS) and successive projections algorithm (SPA), are used for the screen of useful variables [37]. Multiple unsupervised and supervised pattern recognition methods have been used for the qualitative analysis (the discrimination of tea categories, varieties, and geographical origins) and quantitative analysis (the determination of chemical components in tea and optimization of processing conditions). These pattern recognition methods include principal component analysis (PCA), artificial neural network (ANN), linear discriminant analysis (LDA), support vector machine (SVM), soft independent modeling of class analogy (SIMCA), partial least squares (PLS), and backpropagation artificial neural network (BP-ANN) (Table 1) [33].

In this article, we review the most recent advances and applications of NIR spectroscopy and chemometrics for the quality control of tea, including the measurement of chemical compositions, the evaluation of sensory attributes, the identification of categories and varieties, and the discrimination of geographical origins.

2. The Application of NIR Spectroscopy in Tea

2.1. Chemical Composition. The major compositions in tea include polyphenols, catechins, caffeine, free amino acids, and moisture. These compositions are closely relevant to the overall quality of tea, and they thus are the key indexes of tea quality. The monitoring of these compositions contents in tea is critical for the quality control [54]. NIR spectroscopy has been successfully used for the prediction of major compositions contents in tea in recent years. Nonetheless, only one or several components were simultaneously measured by NIR spectroscopy in previous studies [55, 56]. Lee et al. firstly determined the contents of nine individual catechins and caffeine by NIR spectroscopy. These nine catechins include EGCG, (–)-epigallocatechin-3-(3''-O-methyl) gallate (EGCG-3Me), EGC, ECG, EC, C, GCG, GC, and gallic acid. The calibration models for EGCG, EGC, ECG, EC, C, total catechins, and caffeine exhibited accurate prediction, with high r^2 (coefficient of determination in the

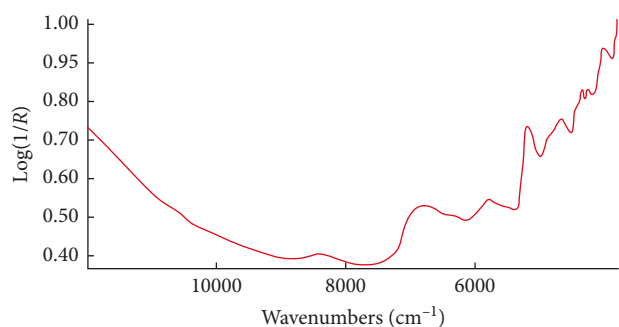


FIGURE 1: A typical absorbance ($\log(1/R)$) spectrum of tea in the wavenumbers from 12,000 to 3800 cm^{-1} [34].

prediction set, >0.9) and RSP (the ratio of standard deviation of reference data to SEP (C) in the external validation set, >4.1) values [38]. In addition, Zareef et al. used Fourier transform near-infrared reflectance (FT-NIR) spectroscopy for the simultaneous prediction of four compositions in black tea including amino acids, caffeine, theaflavins, and water extract. For quantitative analysis of these components, four kinds of chemometrics algorithms including PLS, Si-PLS, genetic algorithm PLS (GA-PLS), and backward interval PLS (Bi-PLS) were used for the establishment of prediction models. The results showed that GA-PLS was suitable for the quantitative analysis of amino acids and water extract and Bi-PLS was the best method for the quantification of caffeine and theaflavins (TFs) [39].

Tea usually can be divided into six categories in China, and more than 100 famous tea varieties or brands exist in China. However, a common model is lacking for simultaneously evaluating various quality parameters of various teas. Recently, Wang et al. developed a common across-category FT-NIR model for simultaneous determination of polyphenols, caffeine, and free amino acids in various Chinese teas, including green tea, black tea, oolong tea, and dark tea. Baseline offsets, random noise, and biases were removed, and characteristic signals were enhanced by a hybrid method, which combines MSC and first-order derivative and SG. Two variable selection methods, random frog (RF) and competitive adaptive reweighted sampling (CARS), were used for selecting key variables for PLS calculation. Both enhanced RF-PLS and CARS-PLS models simplified the model complexity, enhanced the model performance, and gave satisfactory prediction precision. NIR coupled with enhanced cross-category models thus has the potential for the simultaneous prediction of the major ingredients in various Chinese teas [35].

The determination of total polyphenols in tea by using NIR spectroscopy has been studied in detail. However, most of these research studies were performed in research laboratories. Furthermore, these research studies mainly used commercial NIR instruments, which are nonspecific, expensive, and sensitive to environmental variation, and they are thus not suitable for online detection in tea industrial usage. The new trend of tea quality monitoring is to supervise the whole production line so as to ensure the high quality and consistency of tea products [40, 41]. Qi et al.

developed a portable and low-cost optical visible and near-infrared reflectance (VIS-NIR) spectroscopy system, including a light source, a backscattering fiber probe, a grating system equipped with a slit, a detector, and a computer supported with data acquisition and control software. The genetic algorithm-synergy interval partial least squares (GA-Si-PLS) algorithm was used for monitoring the total polyphenols content in tea, and coefficients of variation (CVs) were $<5\%$ for most of the samples. This optical sensors system thus possessed great potential for the real-time and online monitoring of tea quality in processing enterprises [40]. In addition, summer-autumn tea leaves are the raw material of instant black tea products. The oxidation of the summer-autumn tea extract is a critical treatment for the production of instant black tea products, and the total polyphenols content is the key index for the oxidation degree. Pan et al. developed an *in situ* monitoring installation, including an oxidation system of the tea extract and VIS-NIR spectroscopy system, to monitor the total polyphenols content during tea oxidation. The ACO-PLS (ant colony optimization-partial least squares) algorithm was extremely suitable for the modeling of this monitoring installation, and CVs for most of the samples were less than 10%. This monitoring installation thus was a promising tool for *in situ* monitoring of tea oxidation [41].

NIR hyperspectral imaging has also been used for the prediction of chemical compositions in tea. Compared with NIR spectroscopy, NIR hyperspectral imaging could simultaneously obtain spectral and spatial information by the integration of spectroscopy and digital imaging. The componential and constructional characteristics of a sample could be acquired by the spectrum for each pixel and the gray scale image for each narrow band. Texture information is another significant image feature. It is more similar to human visual perception, which facilitates the direct identification of complex features in the sample [42, 57]. Deng et al. predicted the moisture content in Longjing tea leaves with NIR hyperspectral imaging. The property of continuous texture near the veins was validated according to the variable rates of water loss in the mesophylls and vein cells. Then, the three-dimensional Gabor filter (TDGF) algorithm and its corresponding filter bank were used for describing the textures of tea leaves. The overall metrics showed that the combination of spectrum and TDGF textures facilitated PLS regression modeling to predict the moisture content of Longjing tea [42].

2.2. Sensory Attributes. Sensory attributes of tea include color, taste, aroma, and appearance, which are the key factors of tea quality as well as indicators of commercial values. Traditional methods for evaluating the sensory attributes rely basically on experienced panels, also known as tea tasters. However, the results of traditional sensory evaluation are purely subjective, which are easily affected by experience, gender, mental state, physical condition, and other factors. Therefore, objective methods are the principal concern for the evaluation of tea sensory attributes. The NIR spectroscopy is an ideal solution for the rapid, accurate, and

TABLE 1: Overview of NIR spectroscopy for the quality control of tea.

Commodity	Attributes	Methods	Wavelength scanned	Spectral pretreatment	Calibration models	Results	No. of samples	References
Tea leaves	Caffeine, catechin (gallic acid, GC, EGC, C, EGCG, EC, GCG, ECG)	NIR	400~2500 nm	Win ISI Score	MPLS	r^2 for caffeine: 0.97; GA: 0.85; GC: 0.78; EGC: 0.95; C: 0.91; EGCG: 0.97; EC: 0.95; GCG: 0.85; ECG: 0.94	665	[38]
Black tea	Amino acids, caffeine, theaflavins, water extract	FT-NIR	4000~10,000 cm^{-1}	SNV, MSC	PLS, Si-PLS, GA-PLS, Bi-PLS	Using GA-PLS, R_p for amino acids: 0.9498; water extract: 0.8785; using Bi-PLS, R_p for caffeine: 0.9232; theaflavins: 0.924	95	[39]
Black, dark, oolong, and green tea	Total polyphenols, caffeine, free amino acids	FT-NIR	4000~10,000 cm^{-1}	MSC combined with first-order derivative and SG smoothing	PLS1, PLS2, RF-PLS, CARS-PLS	CARS-PLS (R_p^2) achieved best predictive performance for total polyphenols: 0.994; caffeine: 0.986; free amino acids: 0.993	145	[35]
Green tea	Total polyphenols	VIS-NIR	300~1000 nm	SNV	PLS, Si-PLS, CARS-Si-PLS, GA-Si-PLS	Prediction set (R_p) for PLS: 0.8043; Si-PLS: 0.8804; GA-Si-PLS: 0.8859; CARS-Si-PLS: 0.8753	50	[40]
Tea extract	Total polyphenols	VIS-NIR	300~1000 nm	SNV	PLS, Si-PLS, GA-PLS, CARS-PLS, ACO-PLS	Prediction set (RMSEP) for PLS: 0.7659; Si-PLS: 0.8766; GA-PLS: 0.8993; CARS-PLS: 0.8897; ACO-PLS: 0.8853	85	[41]
Longjing tea leaves	Moisture content	NIR hyperspectral imaging	874.41~1733.91 nm	Smoothing filter (3 * 3 window) MNF rotation, 2D filter LoG (Laplacian of Gaussian)	PCPLS1-9, SPA-PLS	r^2 for PCPLS1-9: 0.9491, 0.8826, 0.9531, 0.8905, 0.9548, 0.9105, 0.9713, 0.9071, and 0.9610; SPA-PLS: 0.9216	30	[42]
“Biluochun” green tea	Sensory attributes	FT-NIR	4000~10,000 cm^{-1}	SNV	Si-PLS, PCA, BPN, BP-AdaBoost	BP-AdaBoost model revealed its superior performance, $R_p = 0.7717$	70	[37]
Black tea	Color sensory quality	VIS-NIR	200~1100 nm	SNV	GA-BPANN	$R_p = 0.8935$	127	[18]
Black tea	Theaflavin, thearubigin	NIR	1000~1799 nm	MSC, SG 1st derivative, Min/Max, SNVT	PLS, Si-PLS, Si-CARS-PLS, Si-CARS-ELM, Si-CARS-SVM, Si-CARS-ELM-AdaBoost	ELM-AdaBoost was used for the validation, $R_p^2 = 0.893$	78	[43]

TABLE 1: Continued.

Commodity	Attributes	Methods	Wavelength scanned	Spectral pretreatment	Calibration models	Results	No. of samples	References
Green tea	Lutein, Chl-b, Chl-a, Phe-b, Phe-a, β -carotene	VIS-NIR	400~2498 nm	ANOVA	PLS, SPA, MLR	MLR gave superior prediction (R_p^2) for lutein: 0.975; Chl-b: 0.973; Chl-a: 0.993; Phe-b: 0.919; Phe-a: 0.962; β -carotene: 0.965	135	[44]
White tea and albino tea	Tea polyphenols, free amino acids, moisture, ash contents	FT-NIR	4000~12,400 cm^{-1}	MSC, SNV, SG smoothing, KND, 1st and 2nd derivatives	DPLS, DA	DPLS: 98.48; DA: 100	70	[45]
Green, yellow, white, black, and oolong tea	Region of interest	VIS-NIR	589, 635, 670, 783 nm	SNV	LDA, Lib-SVM, ELM	Lib-SVM was the best model, $r^2 = 98.39\%$	206	[46]
Green, yellow, white, black, and pu-erh tea	—	NIR	950~1760 nm	SG smoothing, standard deviation, SNV	PCA, MDS, t-SNE, ISOMAP, SVM-ECOC	SVM-ECOC model provided a classification accuracy of $97.41 \pm 0.16\%$	6	[19]
Iron Buddha tea	Total polyphenols	VIS-NIR	800~2500 nm	SNV	PLS (LS-SVM and BPNN)	Classification accuracies: LS-SVM: 95.0%; BPNN: 97.5%	180	[47]
Pu-erh tea	Metabolomics analysis	NIR	3600~12,500 cm^{-1}	OPUS 7.2 software from Bruker Optics	PCA, PLS, HCA, PLS-DA	PLS model showed nearly complete fit and excellent predictive capability ($r^2 = 0.967$; $Q^2 = 0.93$)	17	[48]
Green tea (Anji-white)	—	NIR	4000~12,000 cm^{-1}	Smoothing, 2nd derivative, SNV	OCPLS, SIMCA	With SNV preprocessing, OCPLS provided sensitivity of 0.886 and specificity of 0.951; SIMCA provided sensitivity of 0.886 and specificity of 0.938 and achieved best classification performance	248	[36]
Green tea	Catechin, EC, EGC, ECG, EGCG, GCG	NIR	1050~2500 nm	1st derivative	PLS, BP-ANN, SVM	Accuracy (%): PLS: 100.000; BP-ANN: 95.455; SVM: 98.485	220	[49]
Green tea	—	NIR	4000~9000 cm^{-1}	2nd derivative, SNV	OVR-PLSDA, OVO-PLSDA, PLSDA-softmax, ES-PLSDA	Total accuracy (%): OVR-PLSDA: 64.68; OVO-PLSDA: 84.94; PLSDA-softmax: 92.99; ES-PLSDA: 93.77	1540	[50]

TABLE 1: Continued.

Commodity	Attributes	Methods	Wavelength scanned	Spectral pretreatment	Calibration models	Results	No. of samples	References
Black tea	Caffeine, water extract, total polyphenols, free amino acids	NIR	4000~12,500 cm ⁻¹	SNV, MSC, Min/Max	PLS	(1) <i>R</i> in the prediction set for caffeine: 0.955; water extracts: 0.962; total polyphenols: 0.954; free amino acids: 0.927 (2) Identification accuracy (%): 94.30	140	[51]
Green and black tea	—	NIR	3800~14,000 cm ⁻¹	1st derivative, SG smoothing	SIMCA, PLSDA, SPA-LDA	Classification accuracy (%): SIMCA: 88.00; PLSDA: 92.00; SPA-LDA: 100	82	[52]
Oolong tea	—	NIR	4000~12,000 cm ⁻¹	SNV, 2nd derivative, smoothing	PLSDA	The sensitivity of PLSDA model for raw data: 0.971; SNV: 1.000; 2nd derivative: 0.886; smoothing: 0.971	570	[53]
Oolong tea	Polyphenols, alkaloids, protein, volatile and nonvolatile acids, aroma compounds	NIR and NMR	3300~12,500 cm ⁻¹	SNV, 2nd derivative, SG smoothing	PCA, PLSDA	Discrimination accuracy (%) for NMR + NIR data: 86.20~95.80; NMR data: 68.20~78.70; NIR data: 80.00~89.30	90	[17]

Abbreviations: ACO, ant colony optimization; ANOVA, one-way analysis of variance; Bi-PLS, backward interval PLS; BP-ANN, backpropagation artificial neural network; BPNN, backpropagation neural network; C, (+)-catechin; CARS-PLS, competitive adaptive reweighted sampling-partial least squares; Chl-a, chlorophyll a; Chl-b, chlorophyll b; EC, (-)-epicatechin; ECG, (-)-epicatechin gallate; EGC, (-)-epigallocatechin; EGCG, (-)-epigallocatechin gallate; ELM, extreme learning machine; ES, ensemble strategy; NIR, near-infrared reflectance; FT-NIR, Fourier transform near-infrared reflectance; GA, genetic algorithm; GC, (-)-gallo catechin; GCG, (-)-gallo catechin gallate; ISOMAP, isometric mapping; KND, Karl Norris derivative filter; LDA, linear discriminant analysis; PLS, partial least squares; PLSDA, partial least squares discriminant analysis; Lib-SVM, library support vector machine; MDS, multidimensional scaling; Min/Max, min/max normalization; MLR, multiple linear regression; MNE, minimal noise fraction; MPLS, modified partial least squares; MSC, multiplicative scattering correction; NMR, nuclear magnetic resonance; OCP, one-class partial least squares; OVO-PLSDA, one-versus-one-partial least squares discriminant analysis; OVR-PLSDA, one-versus-rest-partial least squares discriminant analysis; PCA, principal component analysis; Phe-a, pheophytin a; Phe-b, pheophytin b; *Q*², cross-validated correlation coefficient; *r*², coefficient of determination in the prediction set; *R*_p, correlation coefficient in the prediction set; *R*_p², determinate coefficient; RF-PLS, random frog-partial least squares; SG smoothing, Savitzky-Golay smoothing; SIMCA, soft independent modeling of class analogy; Si-PLS, synergy interval partial least squares; SNV, standard normal variate; SNVT, standard normal variate transformation; SPA-LDA, successive projections algorithm associated with linear discriminant analysis; SVM, support vector machine; SVM-ECOC, error-correcting output code (ECOC) model containing support vector machine (SVM); t-SNE, t-distributed stochastic neighbor embedding; VIS-NIR, visible and near-infrared reflectance; —, not mentioned.

noninvasive sensory evaluation of tea [18]. Jiang and Chen used FT-NIR spectroscopy for predicting the sensory properties of green tea infusion. The Si-PLS algorithm was applied for the selection of significant spectral regions, and the modified BP-AdaBoost algorithm was used for calibrating the models. The BP-AdaBoost algorithm showed its superiority in modeling, with the R_p (the correlation coefficient in the prediction set) of 0.7717, RPD (the ratio performance deviation in the prediction set) of 1.59, R_c (the correlation coefficient in the calibration set) of 0.8554, and RMSECV (the root mean square error of cross-validation) of 5.0305. Thus, the FT-NIR spectroscopy technique proved to be a rapid, accurate, and noninvasive analytical method for the evaluation of sensory quality in green tea. Nonetheless, tea sensory properties should be individually characterized by NIR spectroscopy [37].

Qin et al. investigated the feasibility for predicting the color sensory attribute in black tea by using VIS-NIR spectroscopy. The spectra information and color information were acquired for the modeling. Spectra information-based models obtained better performance than color parameters-based models. The excellent performance for predicting the color sensory quality was acquired by genetic algorithm-backpropagation artificial neural network (GA-BPANN) models, with the R of 0.8935 and the root mean square error of 0.392 in the prediction set [18]. Furthermore, TFs and thearubigins (TRs) are the major pigments that determine the color and brightness of black tea infusion. During the fermentation process, the color of black tea leaves changes remarkably from green to red and then to brown. When the TRs/TFs ratio is approximately equal to 10 : 1, the fermentation process of black tea reaches the optimum point, and the most beautiful color was produced in tea infusion. The TRs/TFs ratio thus is a critical parameter for evaluating the fermentation degree and sensory quality characteristics of black tea. Dong et al. used NIR spectroscopy for the prediction of the TRs/TFs ratio value during the Congou black tea fermentation process. The combination of Si-PLS and CARS could effectively select the characteristic wavelength variables related to the TRs/TFs ratio, with a variable compression ratio up to 98.6%. Based on these characteristic variables, an extreme learning machine (ELM) combined with an adaptive boosting (AdaBoost) algorithm (ELM-AdaBoost) was used for constructing the prediction model. The prediction performance of the SI-CARS-ELM-AdaBoost model was higher than that of other nonlinear models including extreme learning machine (ELM), SVM, linear models, and full-spectrum PLS model. The rapid and accurate prediction of the TRs/TFs value was acquired during fermentation, with a determinate coefficient (R_p^2) of 0.893, relative standard deviation (RSD) below 10%, RPD above 3, and root mean square error of prediction (RMSEP) of 0.0044 [43]. Similarly, Li et al. found that color of green tea had close correlations with the contents of six lipid-soluble pigments, including chlorophyll a, chlorophyll b, lutein, β -carotene, pheophytin a, and pheophytin b. VIS-NIR spectroscopy was used for rapid and simultaneous determination of six lipid-soluble pigments in green tea.

Based on multiple linear regression (MLR) with the characteristic wavelengths, the quantitative models of the six pigments showed excellent performance, with R_p^2 of 0.975, 0.973, 0.993, 0.919, 0.962, and 0.965, respectively [44]. The color sensory quality of tea thus could be evaluated or controlled by the rapid determination of pigments with NIR spectroscopy [43, 44].

By conducting Pearson's correlation analysis between chemical components and taste score, Chen et al. found that eight ingredients (water extracts, total polyphenols, total catechins, caffeine, free amino acids, TFs, theaflavin-3-gallate, and theaflavin-3'-gallate) in the black tea were the main contributors to the taste quality, while gallic acid, EGCG, EC, and theaflavin-3,3'-digallate had weak correlations with taste quality. Then, the FT-NIR spectroscopy system coupled with the backpropagation-AdaBoost (BP-AdaBoost) algorithm was used for simultaneous prediction of taste quality and these eight taste-related compounds content in black tea. BP-AdaBoost models showed superior predictions for taste quality and taste-related compounds content in black tea, with the $R_p > 0.76$, and the RMSEP $< 1.7\%$ for all models [45].

2.3. Classification and Authentication. Tea usually can be divided into six categories, including green tea (unfermented), white tea (slightly fermented), yellow tea (partly fermented), oolong tea (semifermented), black tea (fully fermented), and dark tea (postfermented). Rapid and feasible classification of two or three tea categories has been achieved by NIR spectroscopy [58, 59]. Recently, NIR hyperspectral imaging has also been used for the tea classification. Ning et al. used VIS-NIR hyperspectral imaging for the classification of five Chinese tea categories, including green, black, oolong, yellow, and white teas. Hyperspectral data were extracted within the range of 400~1000 nm wavelength from a total of 206 tea samples. Four dominant wavelengths (589, 635, 670, and 783 nm) were selected as spectral features, and textural features were extracted by the gray-level cooccurrence matrix (GLCM) at these four dominant wavelengths. The classification models of library support vector machine (Lib-SVM), LDA, and ELM were constructed based on spectral features, full spectra, textural features, and data fusion. The model of Lib-SVM based on data fusion or full spectra was the best model, with the correct classification rate of 98.39% [46]. Nonetheless, the applications of VIS-NIR hyperspectral imaging described above only cover five types of teas. Furthermore, tea characteristics measured by VIS-NIR spectral imaging (400~1000 nm) dominated by physical characteristics and the pigments. Compared with VIS-NIR spectral imaging, the NIR spectral imaging provides more detailed chemical information, which offers a better classification system. NIR hyperspectral imaging (950~1760 nm) has also been used for the classification of six different commercial tea products, including green, black, oolong, yellow, white, and pu-erh teas. Before data modeling, the NIR imaging data should be preprocessed to reduce the disturbances of light scattering caused by the uneven and inhomogeneous leaf surface. By

using the data visualization method of t-distributed stochastic neighbor embedding (t-SNE), the six commercial tea products could be effectively divided into three categories based on the extent of processing: minimal processing, oxidation, and fermentation. A multiclass error-correcting output code (ECOC) model containing SVM binary learners was further constructed for the tea classification according to the product type. The ECOC-SVM model provided excellent classification accuracy up to 97.41% for the six commercial tea products [19].

The NIR technology has also been used for the authentication of tea storage periods. Xiong et al. used the VIS-NIR imaging system (405~970 nm) to classify the Iron Buddha tea based on the storage period (years of 2004, 2007, 2011, 2012, and 2013). The classification accuracies of 97.5% and 95.0% were acquired by using backpropagation neural network (BPNN) and least squares-support vector machine (LS-SVM) models [47]. Similarly, Wang et al. used NIR spectroscopy for the storage period classification of pu-erh raw tea, which has been stored for 1~10 years. Obvious difference between new and aged pu-erh raw teas was found, and 85% of the samples could be identified without any false-positive result. However, the remaining 15% samples could not be successfully clustered into the right year of production, and they also could not be clustered into the wrong year either [48].

2.4. Geographical Origins. The tea qualities of different geographical origins are somewhat jagged, due to the disparity of geographical and natural conditions (altitude, climate, soil, microelement, etc.), tea cultivars, cultivation traditions, and processing procedures. The same kind of tea from different geographical origins might vary dramatically in prices and quality [17]. Therefore, almost all of the famous teas are labeled with their origins, such as Anji-white tea, Anxi-Tieguanyin tea, and Yingde-black tea [36, 53]. However, some merchants fraudulently falsify the geographical origins of tea for illegal profits. It is urgent to enforce quality control against various counterfeits [53]. NIR spectroscopy has been successfully used for determining the geographical origin of various teas in recent years. Anji-white tea, one of the most famous green teas, has been documented as a protected geographical indication product in China. 167 representative Anji-white tea samples were gathered from the original producing areas, and non-Anji-white tea samples with similar appearances were collected from unprotected producing areas in China. NIR spectroscopy coupled with SIMCA or one-class partial least squares (OCPLS) was used for the geographical origin discrimination of these samples. Based on the SNV preprocessing, the sensitivity and specificity were 0.886 and 0.938 for SIMCA and 0.886 and 0.951 for OCPLS, respectively. Although it is hard to achieve the exhaustive analysis of all types of potential counterfeits, NIR spectrometry coupled with SNV-OCPLS and SNV-OCPLS models could rapidly detect most of the non-Anji-white teas in the Chinese market [36]. Besides, Zhuang et al. used the NIR spectroscopy to classify the green tea from two geographical origins. 100%

identification accuracies in training and testing were acquired by the classification model of PLS [49]. Although NIR spectroscopy coupled with chemometrics algorithms has been used for the discrimination of tea geographical origins, the discrimination is usually limited to small scale [49, 60]. However, the class number of teas has increased significantly in recent years. For instance, Longjing tea, a top-quality green tea in China, has more than 20 geographical origins. A substantial difference in price exists among these geographical origins. More complex large-class-number classification would pose new challenges to the traditional pattern recognition, due to increasing data complexity and class overlapping, and degraded model generalization performance. Fu et al. proposed a novel ensemble strategy (ES) to solve the problem of large-class-number classification. ES combined the one-versus-one (OVO) and one-versus-rest (OVR) strategies to design a set of classifiers with reduced class numbers. The pattern recognition of ES, OVO, OVR, and softmax function was compared to discriminate the geographical origins of 25 Longjing tea samples by using NIR spectroscopy and partial least squares discriminant analysis (PLSDA). The highest total accuracy was acquired by ES-PLSDA with the value of 0.9377, while the total accuracies of OVO-PLSDA, OVR-PLSDA, and PLSDA-softmax were 0.8494, 0.6468, and 0.9299, respectively. ES pattern recognition thus achieved improved performance in large-class-number classification [50].

The geographical origins of black teas have been discriminated by NIR spectroscopy. Ren et al. constructed an NIR spectroscopy for rapidly determining the geographical origins of black tea. Different geographical origins including Anhui, Hubei, and Yunnan in China, India, Kenya, Sri Lanka, and Burma were remarkably recognized by a factorization method, with an accuracy rate of 94.3%. Meanwhile, the contents of major constituents in black tea including water extracts, caffeine, total polyphenols, and free amino acids were predicted well by the PLS algorithm, with the correlation coefficient (R) values of 0.962, 0.955, 0.954, and 0.927, respectively, in the calibration set [51]. Furthermore, Diniz et al. used NIR spectroscopy for simultaneous classification of tea samples according to their geographical origins (Brazil, Argentina, or Sri Lanka) and varieties (green or black). The successive projections algorithm associated with the linear discriminant analysis (SPA-LDA) was used for the variable selection, and its recognition accuracy was compared with that of SIMCA and partial least squares-discriminant analysis (PLS-DA). Argentinean green tea, Brazilian green tea, Argentinean black tea, Brazilian black tea, and Sri Lankan black tea were successfully discriminated by the SPA-LDA model with 100% classification accuracy, while SIMCA and PLS-DA models were not able to achieve 100% classification accuracy. Although simultaneous classification of teas according to their geographical origins and varieties was successfully realized by the SPA-LDA model, a larger testing of tea samples must be implemented to guarantee any generalization of the proposed methodology [52].

Tieguanyin tea is one of the most famous oolong teas. It is a protected geographical indication product in China. The

geographical origin of Tieguanyin tea is restricted to Anxi County, a small town in Fujian Province of China. 450 representative samples of Tieguanyin tea were collected from Anxi County, which is the original production area of Tieguanyin tea. Another 120 counterfeits with a similar appearance were gathered from nonprotective areas in China. NIR spectroscopy coupled with PLSDA was used for the geographical origin discrimination of these samples. The sensitivity and specificity of the PLSDA model based on SNV transformation reached 0.93 and 1.00, respectively. NIR spectrometry combined with the SNV-PLSDA model thus could discriminate the geographical origins of Tieguanyin tea rapidly [53]. Recently, the combinational analysis of NIR spectroscopy and proton nuclear magnetic resonance (^1H NMR) has been used for distinguishing 90 Tieguanyin tea samples, which were collected from three different growing places (Xiandu, Xianghua, and Xiping towns) in the Fujian Province of China. ^1H NMR spectroscopy could offer the structure and content information of compounds in samples, which is complementary to the NIR data [61, 62]. The ^1H NMR spectroscopy provided accurately qualitative information of 26 components (polyphenols, amino acids, and saccharides) in Tieguanyin tea. Compared with NIR (80.0~89.3% of accuracy) or NMR (68.2~78.7% of accuracy) analysis alone, a better discrimination accuracy of geographical origins of oolong tea could be achieved by combining the NIR and NMR data (86.2~95.8% of accuracy). The combination of NIR and NMR approaches could be used as an effective way to identify the geographical origin of tea. More Tieguanyin tea collected from more original producing areas or even different tea varieties could be included to validate the effectiveness of this combined method in the future works [17].

3. Conclusion and Prospects

As a rapid, nondestructive, and inexpensive technique, NIR spectroscopy has been extensively applied for analyzing multiple aspects of tea quality control in recent years, such as chemical compositions, sensory attributes, classification, authentication, and geographical origins. It is anticipated that NIR spectroscopy may progressively become a routine method for the tea quality control and expand to the food safety field of tea [63]. However, some challenges still impede the pervasive application of NIR spectroscopy for the quality control of tea. Although the performance of the NIR spectrometer has been significantly improved in recent years by increasing the sensitivity and reducing the background noise, improving accuracy and ensuring stability of the NIR spectrometer are still required. Innovative calibrations and prediction models with higher accuracy should be developed. More robust calibrations should be constructed for the simultaneous analysis of various teas and multiple quality attributes by using larger sample sets. Moreover, it is difficult for beginners and nonresearchers to select and optimize the appropriate algorithms and models. Intelligent software packs, which could select the optimal algorithms and models automatically from various algorithms and models, should be developed for the more widespread

commercial application of NIR spectroscopy. In addition, NIR spectroscopy offers the exciting prospect potentially for real-time and online monitoring of the whole progress of tea production. The whole monitoring of tea production by NIR spectroscopy could objectively measure the chemical compositions and sensory attributes, detect unwanted problems immediately, and assure the quality of the final products.

Disclosure

Ming-Zhi Zhu and Beibei Wen are the co-first authors.

Conflicts of Interest

The authors declare that they have no conflicts of interest.

Authors' Contributions

Ming-Zhi Zhu and Beibei Wen contributed equally to this work.

Acknowledgments

This work was supported by China Postdoctoral Science Foundation (2018M632962).

References

- [1] E. H. Xia, H. B. Zhang, J. Sheng et al., "The tea tree genome provides insights into tea flavor and independent evolution of caffeine biosynthesis," *Molecular Plant*, vol. 10, no. 6, pp. 866–877, 2017.
- [2] K. W. Ng, Z. J. Cao, H. B. Chen, Z.-Z. Zhao, L. Zhu, and T. Yi, "Oolong tea: a critical review of processing methods, chemical composition, health effects, and risk," *Critical Reviews in Food Science and Nutrition*, vol. 5, pp. 1–24, 2017.
- [3] M. Z. Zhu, N. Li, M. Zhao, W. Yu, and J. L. Wu, "Metabolomic profiling delineate taste qualities of tea leaf pubescence," *Food Research International*, vol. 94, pp. 36–44, 2017.
- [4] A. Chowdhury, J. Sarkar, T. Chakraborti, P. K. Pramanik, and S. Chakraborti, "Protective role of epigallocatechin-3-gallate in health and disease: a perspective," *Biomedicine & Pharmacotherapy*, vol. 78, pp. 50–59, 2016.
- [5] M. P. Kapoor, M. Sugita, Y. Fukuzawa, and T. Okubo, "Physiological effects of epigallocatechin-3-gallate (EGCG) on energy expenditure for prospective fat oxidation in humans: a systematic review and meta-analysis," *Journal of Nutritional Biochemistry*, vol. 43, pp. 1–10, 2017.
- [6] R. Y. Gan, H. B. Li, Z. Q. Sui, and H. Corke, "Absorption, metabolism, anti-cancer effect and molecular targets of epigallocatechin gallate (EGCG): an updated review," *Crit Rev Food Sci Nutr*, vol. 58, no. 6, pp. 924–941, 2018.
- [7] M. S. Butt, R. S. Ahmad, M. T. Sultan, M. M. N. Qayyum, and A. Naz, "Green tea and anticancer perspectives: updates from last decade," *Critical Reviews in Food Science and Nutrition*, vol. 55, no. 6, pp. 792–805, 2015.
- [8] C. S. Yang and J. G. Hong, "Prevention of chronic diseases by tea: possible mechanisms and human relevance," *Annual Review of Nutrition*, vol. 33, pp. 161–181, 2013.
- [9] B. Rashidi, M. Malekzadeh, M. Goodarzi, A. Masoudifar, and H. Mirzaei, "Green tea and its anti-angiogenesis effects," *Biomedicine and Pharmacotherapy*, vol. 89, pp. 949–956, 2017.

- [10] H. S. Kim, M. J. Quon, and J. A. Kim, "New insights into the mechanisms of polyphenols beyond antioxidant properties; lessons from the green tea polyphenol, epigallocatechin 3-gallate," *Redox Biology*, vol. 2, pp. 187–195, 2014.
- [11] P. Nawrot, S. Jordan, J. Eastwood, J. Rotstein, A. Hugenholtz, and M. Feeley, "Effects of caffeine on human health," *Food Additives and Contaminants*, vol. 20, no. 1, pp. 1–30, 2003.
- [12] J. J. Luszczki, M. Zuchora, K. M. Sawicka et al., "Acute exposure to caffeine decreases the anticonvulsant action of ethosuximide, but not that of clonazepam, phenobarbital and valproate against pentetrazole-induced seizures in mice," *Pharmacological Reports*, vol. 58, no. 58, pp. 652–659, 2006.
- [13] D. E. Platt, M. Ghassibe-Sabbagh, P. Salameh et al., "Caffeine impact on metabolic syndrome components is modulated by a CYP1A2 variant," *Annals of Nutrition and Metabolism*, vol. 68, no. 1, pp. 1–11, 2016.
- [14] L. A. Beyer and M. L. Hixon, "Review of animal studies on the cardiovascular effects of caffeine," *Food and Chemical Toxicology*, vol. 118, pp. 566–571, 2018.
- [15] D. X. Wang, Q. Gao, T. T. Wang et al., "Theanine: the unique amino acid in the tea plant as an oral hepatoprotective agent," *Asia Pacific Journal of Clinical Nutrition*, vol. 26, no. 3, pp. 384–391, 2017.
- [16] M. Saeed, M. Naveed, M. Arif et al., "Green tea (*Camellia sinensis*) and L-theanine: medicinal values and beneficial applications in humans—a comprehensive review," *Bio-medicine and Pharmacotherapy*, vol. 95, pp. 1260–1275, 2017.
- [17] W. J. Meng, X. N. Xu, K. K. Cheng et al., "Geographical origin discrimination of Oolong tea (TieGuanYin, *Camellia sinensis* (L.) O. Kuntze) using proton nuclear magnetic resonance spectroscopy and near-infrared spectroscopy," *Food Analytical Methods*, vol. 10, no. 11, pp. 3508–3522, 2017.
- [18] O. Y. Qin, Y. Liu, Q. S. Chen et al., "Intelligent evaluation of color sensory quality of black tea by visible-near infrared spectroscopy technology: a comparison of spectra and color data information," *Spectrochimica Acta Part A-Molecular and Biomolecular Spectroscopy*, vol. 180, pp. 91–96, 2017.
- [19] P. Mishra, A. Nordon, J. Tschannerl, G. Lian, S. Redfern, and S. Marshall, "Near-infrared hyperspectral imaging for non-destructive classification of commercial tea products," *Journal of Food Engineering*, vol. 238, pp. 70–77, 2018.
- [20] D. D. Qi, A. Q. Miao, J. X. Cao et al., "Study on the effects of rapid aging technology on the aroma quality of white tea using GC-MS combined with chemometrics: in comparison with natural aged and fresh white tea," *Food Chemistry*, vol. 265, pp. 189–199, 2018.
- [21] J. Fiori, B. Pasquini, C. Caprini et al., "Chiral analysis of theanine and catechin in characterization of green tea by cyclodextrin-modified micellar electrokinetic chromatography and high performance liquid chromatography," *Journal of Chromatography A*, vol. 1562, pp. 115–122, 2018.
- [22] K. Fraser, S. J. Harrison, G. A. Lane et al., "Analysis of low molecular weight metabolites in tea using mass spectrometry-based analytical methods," *Critical Reviews in Food Science and Nutrition*, vol. 54, no. 7, pp. 924–937, 2014.
- [23] H. P. Lv, Y. Zhang, J. Shi, and Z. Lin, "Phytochemical profiles and antioxidant activities of Chinese dark teas obtained by different processing technologies," *Food Research International*, vol. 100, pp. 486–493, 2017.
- [24] G. Alaerts, J. Van Erps, S. Pieters et al., "Similarity analyses of chromatographic fingerprints as tools for identification and quality control of green tea," *Journal of Chromatography B*, vol. 910, pp. 61–70, 2012.
- [25] M. Goodarzi, P. J. Russell, and Y. V. Heyden, "Similarity analyses of chromatographic herbal fingerprints: a review," *Analytica Chimica Acta*, vol. 804, pp. 16–28, 2013.
- [26] M. Z. Zhu, X. Dong, and M. Q. Guo, "Phenolic profiling of *duchesnea indica* combining macroporous resin chromatography (MRC) with HPLC-ESI-MS/MS and ESI-IT-MS," *Molecules*, vol. 20, no. 12, pp. 22463–22475, 2015.
- [27] M. Z. Zhu, T. Liu, C. Y. Zhang, and M. Guo, "Flavonoids of Lotus (*Nelumbo nucifera*) seed embryos and their antioxidant potential," *Journal of Food Science*, vol. 82, no. 8, pp. 1834–1841, 2017.
- [28] T. Liu, M. Z. Zhu, C. Y. Zhang, and M. Guo, "Quantitative analysis and comparison of flavonoids in Lotus plumules of four representative Lotus cultivars," *Journal of Spectroscopy*, vol. 2017, Article ID 7124354, 9 pages, 2017.
- [29] M. Z. Zhu, N. Li, Y. T. Wang et al., "Acid/salt/pH gradient improved resolution and sensitivity in proteomics study using 2D SCX-RP LC-MS," *Journal of Proteome Research*, vol. 16, no. 9, pp. 3470–3475, 2017.
- [30] M. Z. Zhu, W. Wu, L. L. Jiao, P. F. Yang, and M. Q. Guo, "Analysis of flavonoids in Lotus (*Nelumbo nucifera*) leaves and their antioxidant activity using macroporous resin chromatography coupled with LC-MS/MS and antioxidant biochemical assays," *Molecules*, vol. 20, no. 6, pp. 10553–10565, 2015.
- [31] W. H. Su, H. J. He, and D. W. Sun, "Non-destructive and rapid evaluation of staple foods quality by using spectroscopic techniques: a review," *Critical Reviews in Food Science and Nutrition*, vol. 57, no. 5, pp. 1039–1051, 2017.
- [32] G. Reich, "Near-infrared spectroscopy and imaging: basic principles and pharmaceutical applications," *Advanced Drug Delivery Reviews*, vol. 57, no. 8, pp. 1109–1143, 2005.
- [33] Q. S. Chen, D. L. Zhang, W. X. Pan et al., "Recent developments of green analytical techniques in analysis of tea's quality and nutrition," *Trends in Food Science and Technology*, vol. 43, no. 1, pp. 63–82, 2015.
- [34] F. Zhao, H. T. Lin, J. F. Yang et al., "Online quantitative determination of Wuyi Rock Tea quality compounds by near infrared spectroscopy," *Transactions of the Chinese Society of Agricultural Engineering*, vol. 30, no. 2, pp. 269–277, 2014.
- [35] J. H. Wang, Y. F. Wang, J. J. Cheng et al., "Enhanced cross-category models for predicting the total polyphenols, caffeine and free amino acids contents in Chinese tea using NIR spectroscopy," *LWT-Food Science and Technology*, vol. 96, pp. 90–97, 2018.
- [36] L. Xu, P. T. Shi, X. S. Fu et al., "Protected geographical indication identification of a Chinese green tea (Anji-white) by near-infrared spectroscopy and chemometric class modeling techniques," *Journal of Spectroscopy*, vol. 2013, Article ID 501924, 8 pages, 2013.
- [37] H. Jiang and Q. S. Chen, "Chemometric models for the quantitative descriptive sensory properties of green tea (*Camellia sinensis* L.) using fourier transform near infrared (FT-NIR) spectroscopy," *Food Analytical Methods*, vol. 8, no. 4, pp. 954–962, 2015.
- [38] M. S. Lee, Y. S. Hwang, J. Lee, and M.-G. Choung, "The characterization of caffeine and nine individual catechins in the leaves of green tea (*Camellia sinensis* L.) by near-infrared reflectance spectroscopy," *Food Chemistry*, vol. 158, pp. 351–357, 2014.
- [39] M. Zareef, Q. S. Chen, Q. Ouyang et al., "Prediction of amino acids, caffeine, theaflavins and water extract in black tea using

- FT-NIR spectroscopy coupled chemometrics algorithms,” *Analytical Methods*, vol. 10, no. 25, pp. 3023–3031, 2018.
- [40] S. Qi, Q. Ouyang, Q. S. Chen, and J. Zhao, “Real-time monitoring of total polyphenols content in tea using a developed optical sensors system,” *Journal of Pharmaceutical and Biomedical Analysis*, vol. 97, pp. 116–122, 2014.
- [41] W. X. Pan, J. W. Zhao, Q. S. Chen, and L. Yuan, “*In situ* monitoring of total polyphenols content during tea extract oxidation using a portable spectroscopy system with variables selection algorithms,” *RSC Advances*, vol. 5, no. 75, pp. 60876–60883, 2015.
- [42] S. G. Deng, Y. F. Xu, X. L. Li, and Y. He, “Moisture content prediction in tea leaf with near infrared hyperspectral imaging,” *Computers and Electronics in Agriculture*, vol. 118, pp. 38–46, 2015.
- [43] C. W. Dong, J. Li, J. J. Wang et al., “Rapid determination by near infrared spectroscopy of theaflavins-to-thearubigins ratio during Congou black tea fermentation process,” *Spectrochimica Acta Part a-Molecular and Biomolecular Spectroscopy*, vol. 205, pp. 227–234, 2018.
- [44] X. L. Li, J. J. Jin, C. J. Sun, D. Ye, and Y. Liu, “Simultaneous determination of six main types of lipid-soluble pigments in green tea by visible and near-infrared spectroscopy,” *Food Chemistry*, vol. 270, pp. 236–242, 2019.
- [45] Q. S. Chen, M. Chen, Y. Liu et al., “Application of FT-NIR spectroscopy for simultaneous estimation of taste quality and taste-related compounds content of black tea,” *Journal of Food Science and Technology-Mysore*, vol. 55, no. 10, pp. 4363–4368, 2018.
- [46] J. M. Ning, J. J. Sun, S. H. Li, M. Sheng, and Z. Zhang, “Classification of five Chinese tea categories with different fermentation degrees using visible and near-infrared hyperspectral imaging,” *International Journal of Food Properties*, vol. 20, no. 2, pp. 1515–1522, 2017.
- [47] C. W. Xiong, C. H. Liu, W. J. Pan et al., “Non-destructive determination of total polyphenols content and classification of storage periods of Iron Buddha tea using multispectral imaging system,” *Food Chemistry*, vol. 176, pp. 130–136, 2015.
- [48] T. Wang, X. L. Li, H. C. Yang et al., “Mass spectrometry-based metabolomics and chemometric analysis of Pu-erh teas of various origins,” *Food Chemistry*, vol. 268, pp. 271–278, 2018.
- [49] X. G. Zhuang, L. L. Wang, Q. Chen, X. Wu, and J. Fang, “Identification of green tea origins by near-infrared (NIR) spectroscopy and different regression tools,” *Science China-Technological Sciences*, vol. 60, no. 1, pp. 84–90, 2017.
- [50] H. Y. Fu, Q. B. Yin, L. Xu et al., “Challenges of large-class-number classification (LCNC): a novel ensemble strategy (ES) and its application to discriminating the geographical origins of 25 green teas,” *Chemometrics and Intelligent Laboratory Systems*, vol. 157, pp. 43–49, 2016.
- [51] G. X. Ren, S. P. Wang, J. M. Ning et al., “Quantitative analysis and geographical traceability of black tea using Fourier transform near-infrared spectroscopy (FT-NIRS),” *Food Research International*, vol. 53, no. 2, pp. 822–826, 2013.
- [52] P. H. G. D. Diniz, A. A. Gomes, M. F. Pistonesi, B. S. F. Band, and M. C. U. de Araújo, “Simultaneous classification of teas according to their varieties and geographical origins by using NIR spectroscopy and SPA-LDA,” *Food Analytical Methods*, vol. 7, no. 8, pp. 1712–1718, 2014.
- [53] S. M. Yan, J. P. Liu, L. Xu et al., “Rapid discrimination of the geographical origins of an Oolong tea (Anxi-Tieguanyin) by near-infrared spectroscopy and partial least squares discriminant analysis,” *Journal of Analytical Methods in Chemistry*, vol. 2014, Article ID 704971, 6 pages, 2014.
- [54] B. N. Singh, A. K. S. Rawat, R. M. Bhagat, and B. R. Singh, “Black tea: phytochemicals, cancer chemoprevention, and clinical studies,” *Critical Reviews in Food Science and Nutrition*, vol. 57, no. 7, pp. 1394–1410, 2017.
- [55] Z. M. Guo, Q. S. Chen, L. P. Chen, W. Huang, C. Zhang, and C. Zhao, “Optimization of informative spectral variables for the quantification of EGCG in green tea using fourier transform near-infrared (FT-NIR) spectroscopy and multivariate calibration,” *Applied Spectroscopy*, vol. 65, no. 9, pp. 1062–1067, 2011.
- [56] V. R. Sinija and H. N. Mishra, “FT-NIR spectroscopy for caffeine estimation in instant green tea powder and granules,” *LWT-Food Science and Technology*, vol. 42, no. 5, pp. 998–1002, 2009.
- [57] F. Zhu, D. R. Zhang, Y. He, F. Liu, and D.-W. Sun, “Application of visible and near infrared hyperspectral imaging to differentiate between fresh and frozen-thawed fish fillets,” *Food and Bioprocess Technology*, vol. 6, no. 10, pp. 2931–2937, 2013.
- [58] J. W. Zhao, Q. S. Chen, X. Y. Huang, and C. H. Fang, “Qualitative identification of tea categories by near infrared spectroscopy and support vector machine,” *Journal of Pharmaceutical and Biomedical Analysis*, vol. 41, no. 4, pp. 1198–1204, 2006.
- [59] Q. S. Chen, J. W. Zhao, C. H. Fang, and D. Wang, “Feasibility study on identification of green, black and Oolong teas using near-infrared reflectance spectroscopy based on support vector machine (SVM),” *Spectrochimica Acta Part A-Molecular and Biomolecular Spectroscopy*, vol. 66, no. 3, pp. 568–574, 2007.
- [60] Q. S. Chen, J. W. Zhao, and H. Lin, “Study on discrimination of Roast green tea (*Camellia sinensis* L.) according to geographical origin by FT-NIR spectroscopy and supervised pattern recognition,” *Spectrochimica Acta Part a-Molecular and Biomolecular Spectroscopy*, vol. 72, no. 4, pp. 845–850, 2009.
- [61] M. Z. Zhu, G. L. Chen, J. L. Wu, N. Li, Z.-H. Liu, and M.-Q. Guo, “Recent development in mass spectrometry and its hyphenated techniques for the analysis of medicinal plants,” *Phytochemical Analysis*, vol. 29, no. 4, pp. 365–374, 2018.
- [62] M. Z. Zhu, T. Liu, and M. Q. Guo, “Current advances in the metabolomics study on Lotus seeds,” *Frontiers in Plant Science*, vol. 7, 2016.
- [63] F. Y. H. Kutsanedzie, Q. Chen, M. M. Hassan, M. Yang, H. Sun, and H. Rahman, “Near infrared system coupled chemometric algorithms for enumeration of total fungi count in cocoa beans neat solution,” *Food Chemistry*, vol. 240, pp. 231–238, 2018.